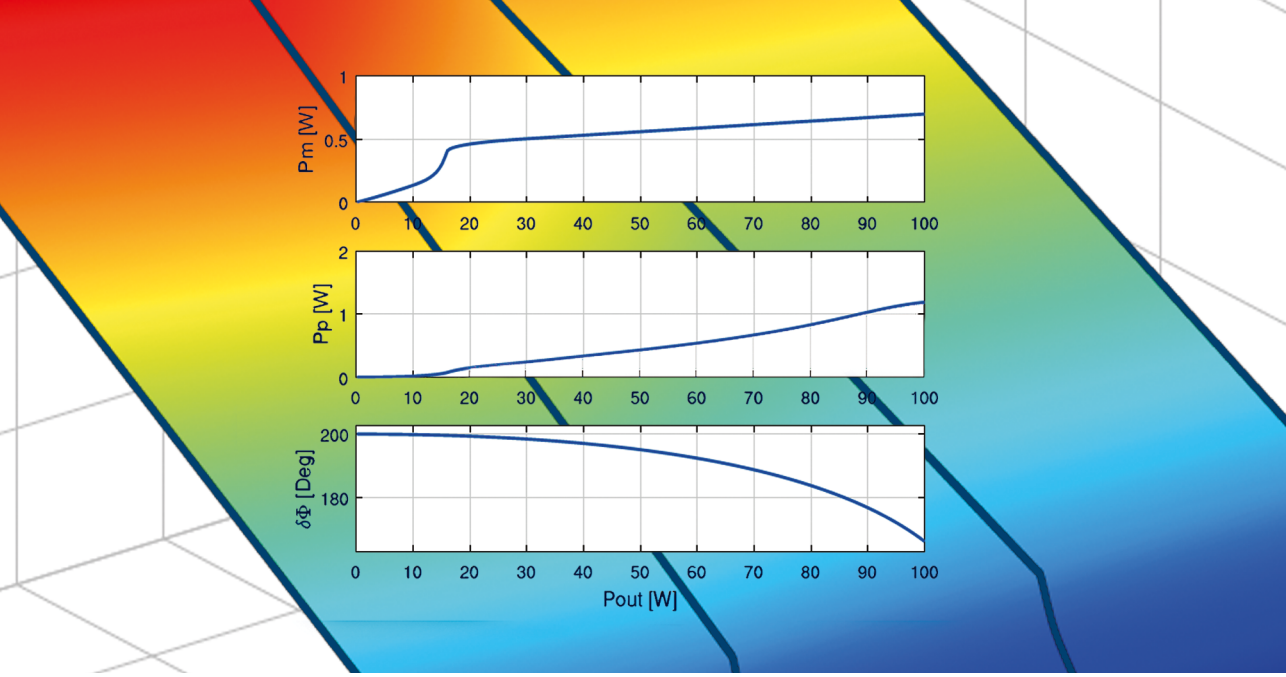

FAU Studien aus der Elektrotechnik 11

Giovanni Donati

Advanced Digital Predistortion Algorithms for modern Base-Station Front-Ends

A physically motivated approach

FAU UNIVERSITY PRESS

Giovanni Donati

Advanced Digital Predistortion Algorithms for modern Base-Station Front-Ends

FAU Studien aus der Elektrotechnik

Band 11

Herausgeber der Reihe:

Prof. Dr. Günter Roppenecker

Giovanni Donati

Advanced Digital Predistortion Algorithms for modern Base-Station Front-Ends

A physically motivated approach

Erlangen
FAU University Press
2017

Bibliografische Information der Deutschen Nationalbibliothek:
Die Deutsche Nationalbibliothek verzeichnet diese Publikation in der Deutschen Nationalbibliografie; detaillierte bibliografische Daten sind im Internet über http://dnb.d-nb.de abrufbar.

Verlag und Auslieferung:
FAU University Press, Universitätsstraße 4, 91054 Erlangen

Druck: docupoint GmbH

ISBN: 978-3-96147-080-8 (Druckausgabe)
eISBN: 978-3-96147-081-5 (Online-Ausgabe)
ISSN: 2363-8699
DOI: 10.25593/978-3-96147-081-5

Advanced Digital Predistortion Algorithms for modern Base-Station Front-Ends. A physically motivated approach.

Erweiterte
Digitale Vorverzerrungsalgorithmen für moderne
Front-Ends in Basisstationen.
Ein physikalisch motivierter Ansatz.

Der Technischen Fakultät der Friedrich-
Alexander-Universität Erlangen-Nürnberg
zur
Erlangung des Doktorgrades Dr.-Ing.
vorgelegt von

Giovanni Donati
aus Ravenna

Als Dissertation genehmigt
von der Technischen Fakultät
der Friedrich-Alexander-Universität Erlangen-Nürnberg
Tag der mündlichen Prüfung: 13.03.2017
Vorsitzende des Promotionsorgans: Prof. Dr.-Ing. Reinhard Lerch

Gutachter: Prof. Dr.-Ing. Georg Fischer
Prof. Dr.-Ing. Jan-Erik Müller

Abstract

Modern telecommunications systems are designed to fulfill very high requirements, imposed by the new standards, in order to support new high quality services and deal with the ever increasing bandwidth of the signals, high power efficiency and linearity. The key component of the transmit chain is the power amplifier, which is amplifying the signal to transmit so that a wide area of service can be covered. Power amplifiers are non-linear components. Therefore to meet high efficiency requirements they need to operate close to saturation which generates non-linear distortion on the output signal, resulting in high bit error rates and strong interference on the adjacent channels. Letting power amplifiers operate in their linear region results in very low efficiency, which in the power budget of base-stations translates into a very high amount of energy wasted. Digital Pre-Distortion (DPD) is the commonly used solution to overcome this problem. During the last years the improvements of telecommunication technologies have enabled multimedia mobile services that also set very large bandwidth requirements. Such requirements depend on the signal standards, allowing wideband transmissions. For instance Long Term Evolution (LTE) systems have adopted the Orthogonal Frequency Division Modulation (OFDM) transmission scheme. OFDM allows wide-band signal transmission and also copes with severe channel conditions. The drawback of using these techniques is that signals come with a high Peak To Average Power Ratio (PAPR). As a consequence, such signals assuming low power levels with a high probability over time are responsible for low average efficiency.
To meet all these requirements, dual-input Doherty power amplifiers (DPAs) with wideband terminations have been developed. Opening the input branches of the DPAs has introduced new degrees of freedom in terms of linearization and reconfiguration by proper digital steering.
In this work I have investigated the trade-offs between linearity, efficiency and linearization bandwidth, by digitally driving the DPA inputs separately. I have identified a linearization technique based on the physics of the devices, in an attempt to: i. reduce the hardware costs for the realization of the digital algorithms, ii. linearize the device by taking into account the requirements for very high efficiency, iii. show the reconfigurability of the device. An intelligent algorithm has been developed, based on such knowledge, to calibrate the DPD directly at the base-station, using the same digital hardware for the linearization.

Zusammenfassung

Moderne Telekommunikationssysteme werden konzipiert, um sehr hohe Anforderungen erfüllen zu können. Diese Anforderungen bestehen auf auferlegten Standards, welche durch neue und qualitativ hochwertige Dienstleistungen definieren wird. Dieses fordern große Signalbandbreiten, hohe Energieeffizienz und Linearität. Die Schlüsselkomponente der Sendekette ist der Leistungsverstärker, der das zu übertragende Signal verstärkt, um es über die Antenne abstrahlen zu können. Leistungsverstärker sind nichtlineare Komponenten und müssen in Sättigung betrieben werden, um hohe Effizienzen zu erreichen. Die Schlüsselkomponente des Sendesystems ist der Leistungsverstärker, der die Aufgabe hat das Sendesignal zu verstärken, damit ein großes Gebiet abgedeckt werden kann. Für eine hohe Effizienzausbeute müssen Leistungsverstärker in Sättigung betrieben werden.
Aufgrund des hohen nichtlinearen Verhaltens der Leistungsverstärker werden nichtlineare Verzerrungen im Ausgangssignal erzeugt. Diese Verzerrungen können zu hohen Bitfehlerraten im Empfangsystem führen und benachbarte Kanäle stören oder blockieren. Würden Leistungsverstärker nicht in Sättigung, sondern in ihrem linearen Bereich betrieben, würde die geringe Effizenz zu hohen Verlustleistungen führen. Um die Verzerrungen im Ausgangsignal zu entfernen werden Linearisierungstechniken wie die Digitale Vorverzerrung (DPD) verwendet.
In den letzten Jahren haben die Forschritte in der Telekommunikationstechnologie zu immer schnelleren mobilen Datendiensten geführt, welche hohe Signalbandbreiten benötigen.
Um die technologischen Anforderungen zu bedienen, wurden Standards wie Long Term Evolution (LTE) definiert, welche auf Orthogonal Frequency Division Modulation (OFDM) basieren und hohe Bandbreiten der Sendesignale erlauben. OFDM ermöglicht hohe Signalbandbreiten und kommt mit schlechten Kanälen zurecht. Der Nachteil dieses Ansatzes ist das hohe Peak to Average Power Ration (PAPR) des Sendesignals. Durch die kleine mittlere Leistung eines OFDM-Signals arbeitet ein gewöhnlicher Leistungsverstärker die meiste Zeit in einem ineffizienten Bereich. Dies führt zu einer geringen durchschnittlichen Gesamteffizienz des Verstärkers. Um den genannten Problemen zu begegnen wurde der Zweiwege-Basisband-Doherty (DPAs) entwickelt.
Durch den direkten Zugang zu den Verstärkerkernen des DPA, der durch das

Entfernen des Leistungssplitters erreicht wird, entstehen durch eine sorgfältig ausgewählte digitale Ansteuerung neue Möglichkeiten für die Linearisierung des DPAs insbesondere Breitbandbetrieb.
In dieser Arbeit wurde das Potential der digitalen Ansteuerung der einzelnen Verstärkerkerne ausgelotet. Basierend auf der physikalischen Grundlage des Verstärkers wurde eine Linearisierungtechnik entwickelt. Ziel war es die Hardwarekosten für die Realisierung der digitalen Algorithmen zu verringern, die Linearisierung das Gerätes unter Berücksichtigung sehr hoher Effizienzen und die Rekonfigurierbarkeit des Gerätes zu zeigen. Wir haben einen intelligenten Algorithmus entwickelt, der den Zwei-Wege-DPD Block direkt an der Basisstation identifizieren kann.

Aknowledgements

This thesis is the result of the period I have spent in Erlangen between 2012 and 2016. My time at the department of Electronics Engineering of the Friedrich Alexander University has changed my way of thinking and working. It has also left very nice memories in my mind and heart and I will bring these moments with me forever.
I would like to express my deepest gratitude to my supervisor and Doktorvater, Professor Georg Fischer for giving me the opportunity to do this Ph.D., accompanying and motivating me until the end of this journey. My next aknowledgement goes to Professor Robert Weigel, who welcomed me at his Electronics Engineering department and gave me the chance to be part of this big family.
I am very thankful to Nokia and particularly to Dr. Tilman Felgentreff, Mr. Hartmut Mueller and Mr. Helmut Heinz for their patience and support during the last years.
A very warm thought goes to my colleagues Christian Musolff, Giuseppe Gottardo, Daniel Popp, Thomas Plachter. Working with you and being part of the PA Team has been the most precious gift I could ask for.
I want to extend my gratitude to my friend and colleague Francesco Barbon, who brought me here in Erlangen and with whom I could always exchange ideas inside and outside the work environment.
Life at the department would not be the same without the organization of Aurelia Martinek, Gabriele Koehnen and Sylvia Hussong.
Thanks to Andreas Baenisch, Amr Zohny, Mohame Hamouda, Ahmed Gharib, Gabor Vinci and Sarah Linz and all the other colleagues that I cannot mention here.
In Erlangen I made many friends with whom I have spent a very nice time and that shared with me the Ph.D. way of life: Felix Held, Andrea Cavanna, Andrea Armaroli, Marina Leone, Stefano Sansotta, Fabrizio Sadafi.
Thanks also to my old friend Vahid Baharvand, that I left in Ravenna after the high school and ended up meeting again here.
A big thank you goes to my parents for always supporting me and being there for me.
This experience also led me to meet the most special person in the world, Sophie Piquerez. I had to finish this work to start a new big adventure with her, and to her I dedicate this thesis.

Acronyms

ACLR	Adjacent Channel Leakage Ratio
ACPR	Adjacent Channel Power Ratio
ADS	Advanced Design System
BO	Back-Off
BS	Base Station
CE	Circuit Envelope
CFR	Crest Factor Reduction
DAC	Digital to Analog Converter
DF	Drive Function
DLM	Dynamic Load Modulation
DPA	Doherty Power Amplifier
DPD	Digital Pre-Distortion
DUT	Device Under Test
ET	Envelope Tracking
EVM	Error Vector Magnitude
FIR	Finite Impulse Response
FPGA	Field Programmable Gate Array
GMP	Generalised Memory Polynomial
HB	Harmonic Balance

IM	intermodulation
LSA	”Least Squares Algorithm”
LTE	Long Term Evolution
LUT	Lookup Table
MP	Memory Polynomial
NMSE	Normalized Mean Square Error
OFDM	Orthogonal Frequency Division Multiplex
OPBO	Output Power Back-Off
PA	Power Amplifier
PAE	Power Added Efficiency
PAPR	Peak to Average Power Ratio
PBO	Power Back-Off
PSD	Power Spectral Density
PSO	Particle Swarm Optimization
RF	Radio Frequency
RLS	Recursive Least Squares
SISO	Single-Input Single-Output
SNR	Signal to Noise Ratio
SPC	Static Phase Correction
W-CDMA	Wideband Code Division Multiplex

Contents

Chapter 1

INTRODUCTION

1.1 Organization of this Work

This thesis is composed of seven chapters. Chapter 1 explains the structure of the thesis and gives a quick overview of the scenario where this research is focused. Chapter 2 gives an overview about the Doherty Power Amplifier (DPA) showing its characteristics and evolutions. Chapter 3 describes Digital Pre-Distortion (DPD) algorithms for classic power amplifiers, and linearization techniques for dual-input DPAs. The core of this thesis is then divided into three main chapters. Chapter 4 documents the analysis tools used through this thesis, the simulation environment and the datasets used for the analysis of the dual-input DPA available at our laboratory. Chapter 5 presents the analysis made on the dual-input DPA, explains the trade-offs met when tweaking the signals at the input of the amplifier stages inside the DPA configuration. This study led to a new identification technique for the linearizer which we have named Drive Function (DF). This chapter also shows the concept of the wideband pre-distorter, which opens new directions for future research. Chapter 6 proposes a new identification technique of the pre-distorter, based on an intelligent and biologically-inspired algorithm, to identify narrow band DF and linearize the dual-input DPA for the best performance.

1.2 Motivation

Modern telecommunications systems have to face high requirements dictated by the increasing performance demands of multimedia services and pervasive mobile internet-based applications. The number of users, or handsets, introduces the need to guarantee efficient ways to access the available frequency spectrum, by using efficient modulation techniques (Wideband Code Division Multiplex (W-CDMA), Orthogonal Frequency Division Multiplex (OFDM)). These techniques are increasing the Peak to Average Power Ratio (PAPR) of the signals to transmit. In this scenario, the Power Amplifier (PA) design must also be optimized in order to operate with the dynamic range of the modulated signals and deliver high output power and high efficiency. When evaluating the power budget of a Base Station (BS) (Figure 1.1) most of the power consumption is due to the PA and the circuitry supporting its operation. Given that PAs are nonlinear devices, the whole amplification process inside the BS is generating higher order harmonics and intermodulation products at the output of the power amplifier. The transmission formats just mentioned above are very sensitive to the nonlinear distortion caused by the device nonlinear effects. This is where the usual trade off between linearity and power efficiency is located. If we would simply back-off the input power to the PA to improve the linearity, we would end up using just a part of the efficiency budget available from the PA. This is where DPD comes into play. The high PAPR of the input signals creates the "space" to operate a linearization on the PA by finding the inverse characteristic of the device, and uses it to compensate for the nonlinearities by pre-distorting the input signal. From the standpoint of the design a very attractive PA architecture is the Doherty, which combines the operation of two active devices to extend the efficiency range. Just to have an idea about the typical achievable improvement obtained, we could compare the performance of the classic PA architectures with the ones obtained by using a Doherty power amplifier. Figure 1.2 shows the maximum achievable power efficiency by using common classes of amplifiers (class A, B, C), where the performances are depending on the conduction angle of the current inside the PA. The Doherty PA is already known since 1935, but became very attractive for the application in modern telecommunication systems because it can maintain high efficiency also when operating several dB in back-off [1]. Figure 1.3 highlights how the Doherty PA, in its most classic "flavor", can deliver high efficiency for an extended

range of output powers. For this reason it works very well with high PAPR signals. Another advantage of Doherty PAs is the extended efficiency bandwidth, which is classically ranging between 5 and 10%, but can be further extended by improving the design of the output power combiner. The scientific work and the algorithms described in this scientific work were conceived in this scenario, and lays down the basis for more advanced techniques to be developed in future research. Modern telecommunications systems must meet high performance and the linearization techniques will, in the future, need to involve more physical motivations to obtain the best performance and meet all the increasing requirements and reduce the complexity of the pre-distorter.

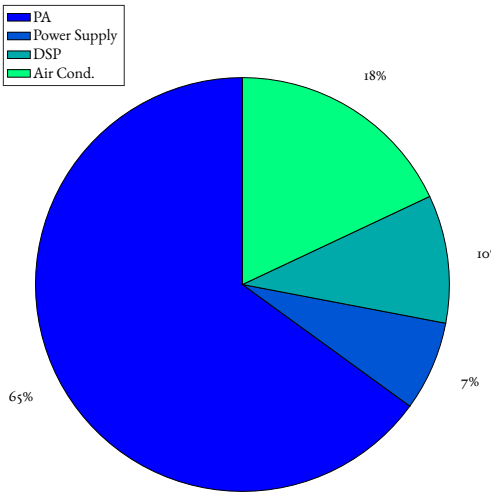

Figure 1.1: Typical Base-Station Front-End power budget.

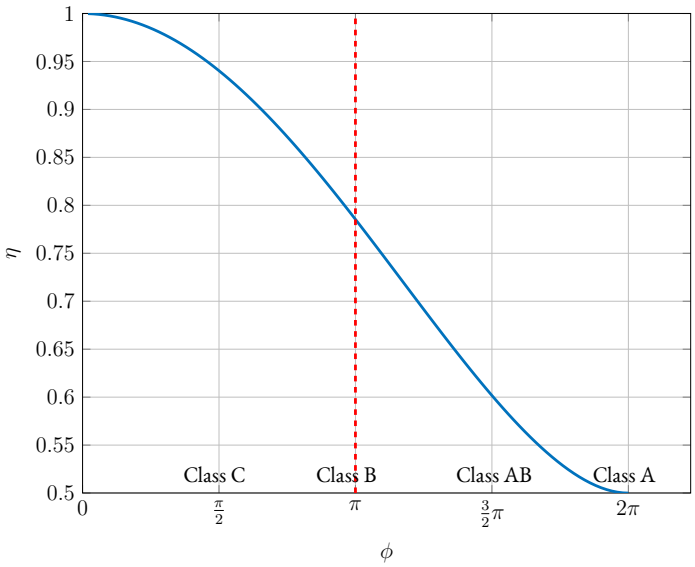

Figure 1.2: Relationship between conduction angle ϕ and PA efficiency.

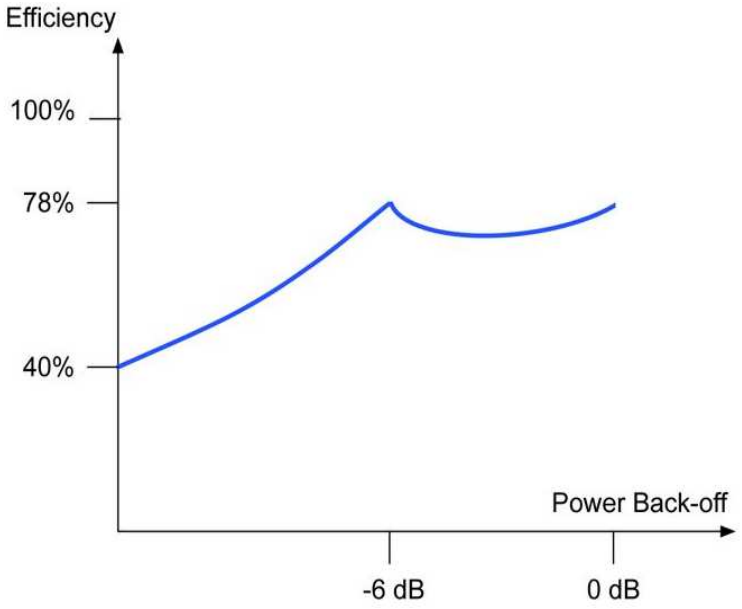

Figure 1.3: Typical Doherty efficiency curve.

Chapter 2

Doherty PA architectures

This chapter focuses on the DPA, and how it evolved, laying the ground for solutions used in this work.

2.1 Origins of the Doherty Power Amplifier

Amplifying an amplitude modulated Radio Frequency (RF) signal is not a very straightforward task; but rather raising issues in terms of linearity and Power Added Efficiency (PAE). The main effects of the amplification are a distortion of the envelope of the RF signal, and a low average efficiency depending on the signal's statistic. In order to avoid the distortion one could always decide to operate the PA by backing off the drive power by some dB s. By doing so, we are reducing the intensity of the nonlinear effects, but we are also moving the operating point of the PA away from the saturation and consequently from high efficiency. Modern communication standards, such as Long Term Evolution (LTE), are making use of signals with high PAPR (around 10 dB). Figure 2.1 shows the trade off mentioned above. The PAPR of a signal is defined as the ratio between the maximum and the average power of the modulated signal. In simple words, it just expresses the power gap between the peak and the average

power of the signal.

$$PAPR(\text{ dB }) = 10 * \log\left(\frac{max(PX)}{mean(PX)}\right) \tag{2.1}$$

Having an input signal with 10 dB of PAPR operates the PA, at exactly 10 dB in back-off, where the average efficiency achieved is 55.5% in this case. It is clear that applying techniques to reduce the peaks of the signal reduces also its dynamic range, allowing the PA to reach a higher efficiency (theoretically as close as possible to the maximum efficiency). In the case represented in 2.1, reducing the PAPR by 2 dB would increase the average PAE up to almost 70%. This is indeed a theoretical example, but it allows us envision how to tweak the parameters, also from the point of view of the signal, improving the efficiency of the whole system. The technique just introduced is named Crest Factor Reduction (CFR), and will be discussed later in this thesis (since it is not related to efficiency improvements due to the PA design).

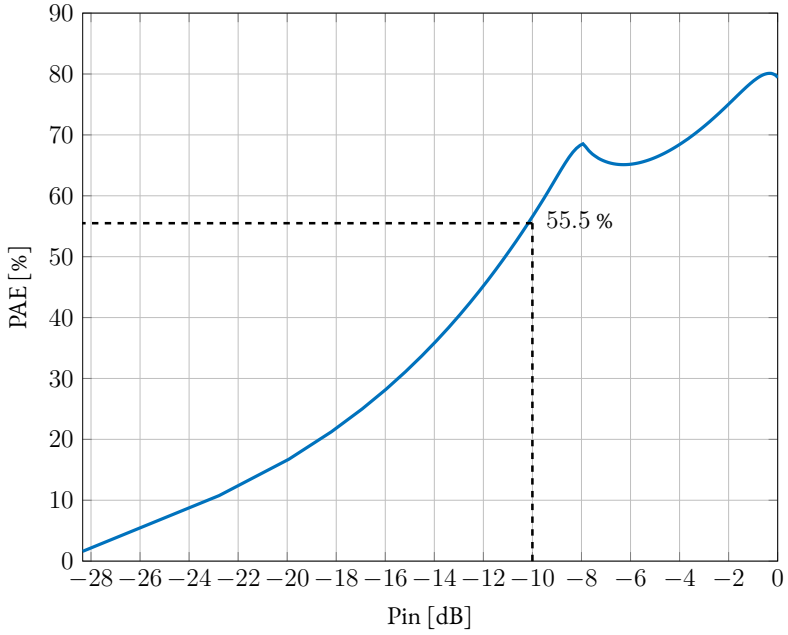

Figure 2.1: PAE vs PAPR in a DPA.

The main issue with classic PA designs is that they cannot deliver high efficiency

when signals with high PAPR are used, because there is no mechanism allowing the device to adapt the load to the particular working point. In order to deal with signals having such high PAPR, it was necessary to introduce a PA architecture capable of "modulating" the load according to the drive level led by the signal's dynamic range. The answer to this need was found in 1936 by W.H.Doherty.

2.2 Symmetric Doherty PA

Classically, efficiency enhancement is obtained by changing the conduction angle of the transistor current. A good explanation about the theory can be found in [2]. Given that we are mainly interested in the principle that leads to the advantage of the DPA architecture, so we start directly by evaluating the factors controlling the PAE, which represents the ability of the device to convert the energy of the power supply into the RF power for the transmitted signal. The PAE is expressed as the ratio between the RF power and the DC power. In classic PAs, the power added efficiency is increasing with the output power. This happens because in a classic approach the load impedance does not change. But, if we could dynamically change the value of the load, we would be able to obtain high efficiency also when the input power is backed-off. The DPA is based exactly on this principle, enhancing the average efficiency by conserving power. All of this is assured by an active load-pull mechanism happening at the output power combiner of the PA. In order to explain the concept we can consider the simple model introduced in [2] and represented in figure 2.2.

If we assume that the generator G_2 is off. In this situation the load resistance R_L is absorbing the current I_1 generated by G_1. The voltage present on the load is just depending on the current I_1 injected by G_1. When G_2 is turned on, it starts contributing to the total current on R_L, and the voltage present on the load resistor becomes:

$$V_L = R_L \left(I_1 + I_2 \right). \tag{2.2}$$

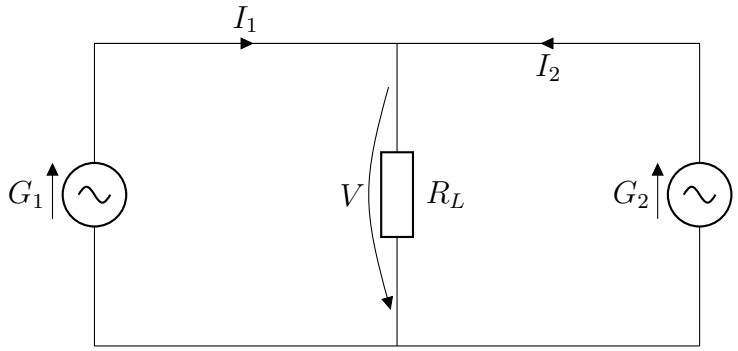

Figure 2.2: Doherty operation principle.

Each generator shares the same load, but senses a different impedance:

$$R_1 = R_L \left(1 + \frac{I_2}{I_2}\right) \tag{2.3}$$

$$R_2 = R_L \left(1 + \frac{I_1}{I_2}\right). \tag{2.4}$$

This means that the load seen by one of the active devices can be modulated by injecting current on the same load from another device. This theory can in general be applied also in the case of AC circuits, where the currents are represented by complex values:

$$Z_L = R_L \left(1 + \frac{I_1}{I_2}\right). \tag{2.5}$$

In that case, the value of the impedance seen by G_1 can be increased by injecting I_2 in phase with I_1, and decreased by setting the phase of I_2 in opposition with the phase of I_1. G_1 is called MAIN PA and G_2 is called PEAK PA. This principle is the base for the DPA architecture. As can be seen from equations 2.3 and 2.4, when the PEAK is activated, the load impedance is raised by increasing the drive level of the transistors. The obtained macro effect is that of maintaining maximum voltage swing on the drain of the MAIN PA and high PAE. In [2] it is also shown how the outputs of the two amplifiers stages are connected together

by a $\lambda/4$ line (see figure 2.3). This line is acting as an impedance inverter which is made in such a way that the resistive part of the load, seen by the MAIN PA, decreases when I_2 is increasing.

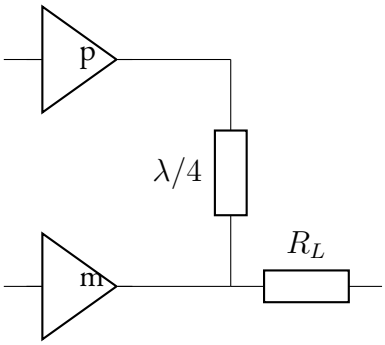

Figure 2.3: Simple Doherty scheme block.

We can say that the load seen by the MAIN PA is modulated by a quantity called load modulation factor (Γ):

$$\Gamma = \frac{I_2}{I_1} \tag{2.6}$$

so when both the transistors are active the impedances seen by each side are:

$$Z_M = \frac{R_{opt}}{2}(1 + \Gamma) \tag{2.7}$$

$$Z_P = \frac{R_{opt}}{2}(1 + \frac{1}{\Gamma}) \tag{2.8}$$

where $\frac{R_{opt}}{2}$ is the value assumed by the resistive part of the load impedance under the hypothesis of similar active devices. In particular, it is important the value of I_{max} for which MAIN and PEAK are designed. In general due to the nonlinearity of the active devices, a PA designer must always consider that higher harmonics are generated, therefore must be shortened to obtain the expected behavior of the output current. A more general scheme for studying the classic Doherty configuration is shown in figure 2.4.

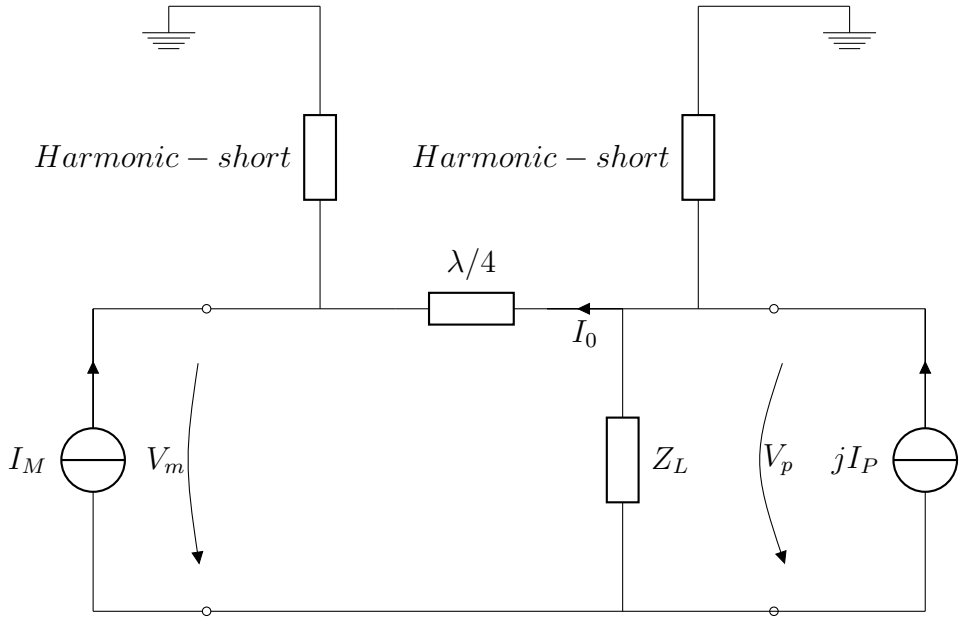

Figure 2.4: More generic model of DPA.

The input branches are in general connected together by putting $90°$ line on the branch of the PEAK, to compensate for the phase shift introduced by the $\lambda/4$ inverter, such that both device currents can be expressed as functions of the normalized input drive level v_{in}.

Having introduced the load modulation factor, the symmetric DPA architecture is realized by setting the following operating conditions:

$$\begin{cases} I_m = f_m(v_{in}) \\ I_p = f_p(v_{in}) \end{cases} \tag{2.9}$$

The assumption here is that the impedance of the two PA stages are pure linear

transconductances, as MAIN and PEAK are voltage controlled current sources:

$$\begin{cases} I_M = I_P & \Gamma = 1 \\ I_p = \begin{cases} f_p(v_{in}) = v_{in} I_P & 0.5 < v_{in} < 1 \\ = 0 & 0 < v_{in} < 0.5 \end{cases} & \\ Im = f_m(v_{in}) = v_{in} I_M & 0 < v_{in} < 1 \end{cases} \tag{2.10}$$

where I_M and I_P are the maximum current swings for MAIN and PEAK PAs. As a consequence of having a load modulation factor equal to one, and so having same maximum value for the two currents, we are also assuming that the lower half of the input voltage swing is used by the MAIN PA only, while the other half is used when both PEAK and MAIN are operating at the same time. This behavior is controlled by the parameter v_{bk} that is the drive level at which the PEAK starts operating. For the symmetric DPA studied, this value is 0.5 (half of the maximum drive level).

The analysis of the network at the terminals of the inverter can be expressed in matrix form:

$$\begin{bmatrix} V_p \\ I_p \end{bmatrix} = \begin{bmatrix} 0 & jZ_0 \\ 1/jZ_0 & 0 \end{bmatrix} \begin{bmatrix} V_m \\ I_m \end{bmatrix} \tag{2.11}$$

By analysing figure 2.4 we can obtain two important results:

$$V_p = jZ_0 I_m \tag{2.12}$$

$$V_m = Z_0 \left[\left(\frac{Z_0}{R} \right) I_m - I_p \right] \tag{2.13}$$

V_p, the voltage on the PEAK device is not depending from I_p, V_p, the output voltage of the MAIN PA is kept under the clipping level by the action of the current injected by the PEAK. Increasing I_p neutralizes the raise of V_m and keeps it under the saturation over the whole dynamic range [3]. The macroeffects obtained by this kind of design are that: the effect of the PEAK is not noticed at

the output of the PA whatever is the level of nonlinearity presented by $fp(v_{in})$ and, the output stays proportional to $fp(v_{in})$. The characteristic of the drive level defines the behavior of the PAE. Figure [2] shows that assuming that both devices operate in class B, we obtain the PAE formulas as:

$$\eta_{comp} = \frac{2v_{in}}{V_{max}} \left(\frac{\pi}{4}\right), 0 < v_{in} < V_{max} \tag{2.14}$$

$$\eta = \frac{\pi}{2} \frac{\left(\frac{v_{in}}{Vmax}\right).^2}{3\left(\frac{v_{in}}{V_{max}}\right) - 1}, 0.5 < v_{in} < V_{max} \tag{2.15}$$

in the low input drive, the PEAK does not contribute, so the maximum efficiency reached by the MAIN PA is just the one of a class B amplifier, which is $\frac{\pi}{4}$ (about 78%). When the PEAK kicks in, the efficiency has the maximum value delivered by the MAIN at $\frac{V_{max}}{2}$ and high efficiency is kept until the maximum drive level where it is again equal to the maximum achievable by a class B amplifier (figure 2.5).

For these reasons DPAs are very attractive for applications in BS technology, given their high efficiency versus dynamic range relationship. Since RF signals are nowadays presenting PAPR even higher than 6 dB , architectures different from the one just introduced are used, getting even more extension of the PAE range. A further improvement can be obtained by generalizing this architecture, and using asymmetric configurations for MAIN and PEAK.

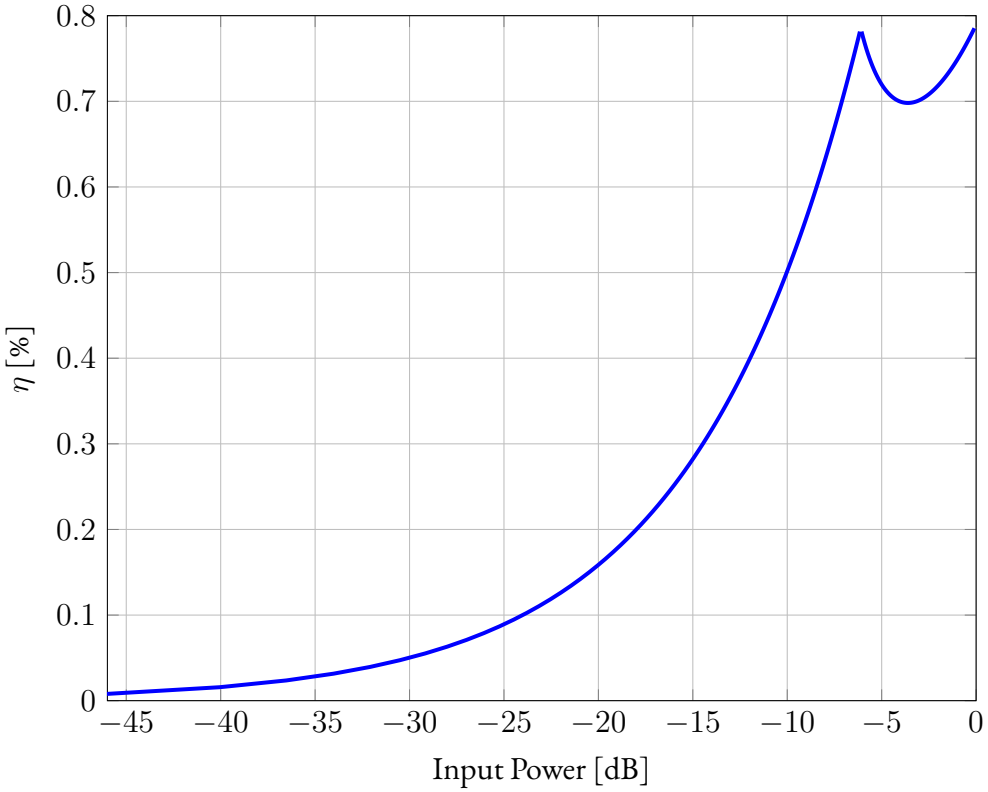

Figure 2.5: Input power vs PAE in a symmetric DPA.

2.3 Asymmetric Doherty PA

One can further improve the Power Back-Off (PBO) efficiency by choosing different classes of operation for the two active devices. If we configure, for instance, the MAIN PA in class B and the PEAK PA in class C we set a lower break point and the transistors will have different I_M and I_P, turning the parameter Γ into a design parameter. The behavior we are expecting from this architecture is similar to the one in figure 2.1. The working principle of this architecture is exactly the same as the one seen for the symmetric one, we have here the advantage of lowering the Back-Off (BO) point according to the specific design parameters. Many references about the design of this architecture can be found ([4], [5], [6]). The problem of both symmetric and asymmetric DPA is that, because

of the $\lambda/4$ adapter, the whole design is relatively narrowband. Improvements for the bandwidth are obtained by designing the right harmonic termination circuits: ([7], [8], [9], [10], [11]). During the last years, two PA topologies are becoming more and more interesting for wireless transmission systems. Those two architectures are the class F and the class J amplifiers (documented respectively in [12], [9]).

2.4 Class F and Class J Amplifiers

As mentioned in the section above, one of the major limitations of the classical DPA is the bandwidth limitation due to the inverter. Since the $\lambda/4$ adapter design is dependent on the particular carrier frequency, it does not perform well far from it. In a class F amplifier, the inverter is paired with a passive network tuned to provide an even order harmonics short of the drain voltage, allowing the load R_L to be seen only by the odd order harmonics. Theoretically, an infinite number of harmonics could be taken into account (the obtained voltage would be a square wave), but this is practically not easy to obtain. Any imperfection in the resonator network would lead to an improvement in the wideband behavior of the PA, but would also deliver worse efficiency due to the wrong harmonic impedance. In a real design no more than the third harmonic is included. Regarding the current, this is always assuming the form of the current generated by a class B PA. In a class J design, instead, one is controlling the reactive second harmonic termination. Class J can be interpreted as a "continuous Class-B" operation. The fractional bandwidth reachable by using this kind of amplifier configuration is about 33%. We can find many references about the usage of this PA classes in [9], [10], [8], [7], [12].

2.5 Dual Input Doherty PA

A further advance in Doherty design improving both efficiency and bandwidth at output PBO is represented by the dual input DPA architecture. Despite the advances described above, DPAs are still narrowband in relation to the requirements dictated by the new communication standards. The behavior of the inverter has still some dependence on the design frequency and a proper load mod-

ulation must be performed in order to overcome the frequency dependence at PBO. Depending on the statistic of the signal and so from its PAPR as stated in [13], there is a specific power ratio that is maximizing the output power and the efficiency of the PA. Separating the input branches of the DPA introduces the possibility to define the normalized back-off point ε_b as a design parameter permitting to maintain the efficiency at PBO over a wide fractional bandwidth. The formula of the output power obtained in [13], valid for the operation between back-off and maximum drive level is:

$$P_{out}(\varepsilon, \overline{f}, \theta) = \frac{I_{max1}^2 R_L}{8} \left[\varepsilon^2 + 2\varepsilon \cos\left(\frac{\pi \overline{f}}{2}\right) \cos(\theta) + k^2 \cos^2\left(\frac{\pi \overline{f}}{2}\right) \right] \tag{2.16}$$

where I_{max1} is the maximum current deliverable from the MAIN PA, ε is the normalized input drive level ($\varepsilon_b < \varepsilon < 1$), θ is the phase difference between MAIN and PEAK amplifier inputs, $\overline{f}$ is the fractional bandwidth and k is the optimized drive level of the PEAK PA that sets the efficiency bandwidth of the DPA. In addition [13] has also demonstrated the relationship determining the acceptable values for $\overline{f}$ through:

$$\frac{1 - \varepsilon_b}{1 + \varepsilon_b} \leq \sin\left(\frac{\pi \overline{f}}{2}\right) \tag{2.17}$$

Figure 2.6 shows how the choice of ε_b is decisive for determining the efficiency bandwidth. In addition, in [13] it was presented a closed formula for the phase relationship between MAIN and PEAK PA, where the dependency on the fractional bandwidth and the drive level of the PEAK is exploited:

$$\theta = \arccos\left(\frac{-k \cos\left(\frac{\pi \overline{f}}{2}\right)}{2\varepsilon}\right) \tag{2.18}$$

It is clear that the ability to control the input signals of the DPA architecture makes it possible to reach high efficiency at both maximum power and PBO, causing an active load modulation that assures high performance on an extended frequency range. The theory previously developed in [13] states that improving the efficiency bandwidth of the DPA architecture leads to a degree of

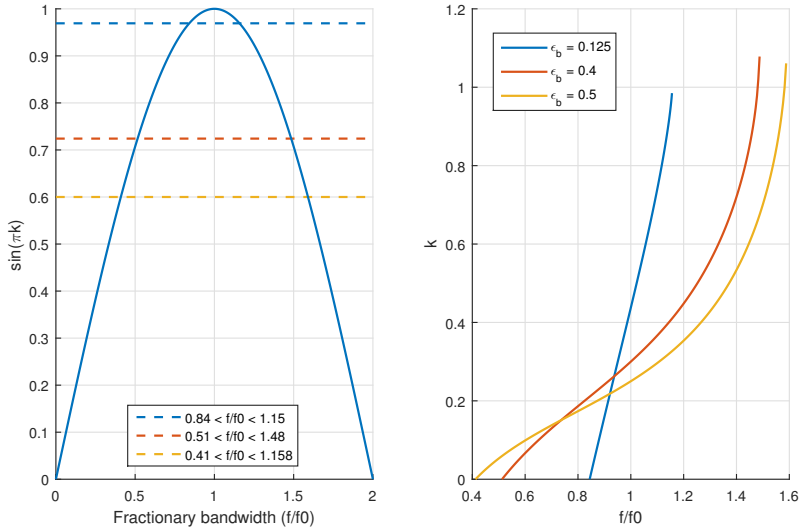

Figure 2.6: Dependency of the DPA bandwidth on the back-off point choice.

freedom in the reconfiguration of the PAE, depending on the particular frequency where the signal is residing. This is very important for modern BS where we are continuosly dealing with multi-standard signals and scenarios involving multi-band transmission.

Chapter 3

Linearization techniques for DPA

Classic predistortion techniques operate on Single-Input Single-Output (SISO) systems. Such algorithms involve the black box identification of the Device Under Test (DUT) adapting a behavioral model to its measured characteristics. In the case of DPAs we want to include more information in the predistortion algorithm in order to control its behavior according to its physic characteristics. Many techniques in the literature aim to improve linearity, efficiency and bandwidth of the DPA architectures, but to linearize such devices we need to apply novel digital approaches able to operate on multiple input systems.
This chapter gives an overview of the existing techniques for the linearization of DPAs.

3.1 Classic Linearization Approach

Linearization of RF devices was introduced already in the 20s, where the first feed-forward linearization was developed by Howard Black [14] at Bell Labs.
This technique was applied to multiplex telephone systems to remove the nonlinear effects introduced by consecutive amplification stages necessary to compensate cable losses on long distance connections.
In 1927 Black had then elaborated the concept of negative feedback [15], where the linearization is performed by feeding the output signal back to the input and subtracting it from the current input signal. This allowed to reach very high lin-

earization performance, while delivering a lower PA gain. An additional problem related to this technique is represented by the inability to handle wideband signals. As rule of thumb, the relation between the bandwidth (BW) and the delay introduced by the series of signal processing components and PA (Δt_s), must be about:

$$BW \leq \frac{1}{4\Delta t_s} \tag{3.1}$$

to introduce a significant correction inside the signal. This means that to linearize a PA fed with a 10 MHz signal we aim to have a total delay smaller than:

$$\Delta t_s \leq \frac{1}{4 \cdot 10\,\mathrm{MHz}} = 25\,\mathrm{ns} \tag{3.2}$$

and even less when signals have even higher bandwidth, for example, due to carrier aggregation.
A better solution is represented by predistortion linearizers which are simpler to implement and can handle signals with wide dynamic range and offer potential for wideband operation. The idea behind predistortion is quite simple and can be sketched as in figure 3.1.
The DUT presents a nonlinear gain, which in case of a PA means that for high input powers we will experience compression (due to the saturation of the PA) and distortion in the output signal [1]. Therefore, we need to apply higher input power to compensate for the compressive characteristic of the device. It is also important to recognize that in order to get a linear output characteristic we have to operate at power levels under the saturation power of the PA, otherwise, we would end up pushing the output power more into saturation and we would add more nonlinear effects on the output signal.

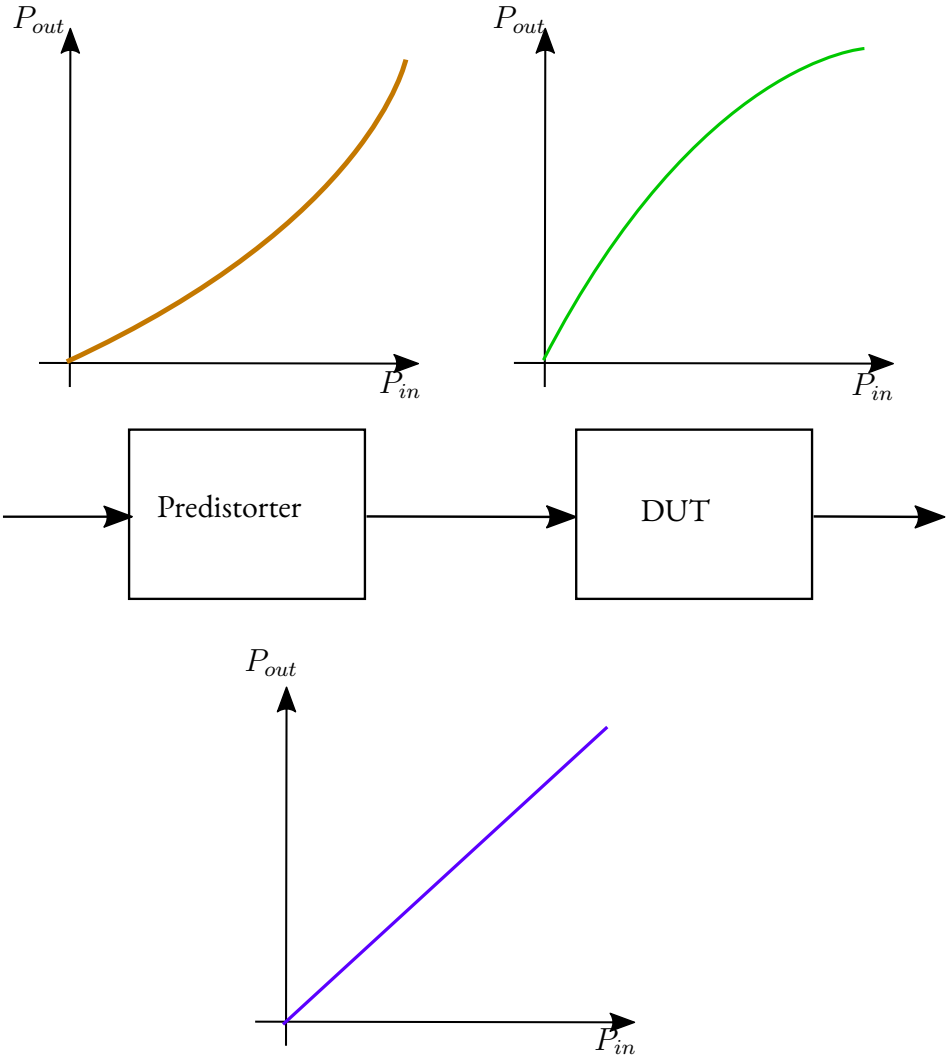

Figure 3.1: Basic DPD concept.

We can alternatively analyze predistortion in the frequency domain, where the function of the predistorter is to generate the same intermodulation (IM) products found at the output of the PA but with the phase inverted of 180^o so they cancel each other out. Modern PAs must allow for at least five times the bandwidth of the input signal in order to accommodate the action of the predistorter. They also have to be designed to accept higher input signals than

a commonly designed PA usually do. A strong gate drive may stimulate electromigration, thus an accelerated aging of the device is to be expected. Therefore DPD behavior must be properly designed and controlled.
The block taking care of the PA linearization is nothing more than a complex gain adjuster and can be implemented both in the analog and digital domains. In modern system, where digital circuits are used to compensate for imperfections in the analog domain, the predistorter is implemented on Field Programmable Gate Array (FPGA) based systems.
The core of such algorithms is the particular model used for the identification of the PA nonlinear behavior which is obtained by means of a black box modeling. The behavioral model of the system is mathematically expressing the relation between its input and output signals and does so mostly taking into account little or no physical *a priori* knowledge of the system. In addition, we should point out that nonlinear effects are better described in time domain in order to consider both transient and steady state phenomena [1].
One of the simplest models to represent static nonlinear effects is the baseband polynomial model:

$$y(t) = \sum_k a_k \left|x(t)\right|^{k-1} x(t) \tag{3.3}$$

where a_k are the model coefficients, $x(t)$ is the baseband signal at the input of the amplifier and k is the order of nonlinearity that we want to use in order to approximate the PA behavior. The basis function for such model is formed by the product between the baseband signal and the k_{th} power of its envelope, thus the nonlinear effects are confined only to this part of the equation. We generally say that the model is linear in the coefficients k which can be computed by using classic linear identification algorithms such as the Least Squares Algorithm (LSA) which is extensively explained in the literature [16].
The typical identification workflow is represented in figure 3.2. To identify the black box we first need a dataset containing samples from the input signals used for the identification, and the measured or simulated output of the PA. The data must be time-aligned, in order to compensate for the delay introduced by the PA, normalized to improve convergence and partitioned into three subsets (test, cross-check and validation). The second step involves the selection of DPD model to represent the nonlinear behavior of the device.

Usually at this step we also take care of regularization, a process that improves the convergence of the solution.
After choosing the model, we need to estimate the model coefficients by making use of the LSA. The process ends with the validation of the model which can be performed by calculating the Normalized Mean Square Error (NMSE):

$$NMSE = \frac{1}{N} \sum_{i} (x_i \cdot \Phi - y_i)^2 \tag{3.4}$$

which is obtained by comparing the model with the measurements. A low value of the NMSE corresponds to a good match between the behavioral model and the measurement of the real device. The process of the identification of such nonlinear devices is simple and with a relatively small number of steps, allows to obtain a model for the measured PA. To perform a linearization we need to invert this model and use it to predistort the input signal.
Two classic schemes to apply pre-distortion in real systems are the indirect learning (3.3) and the direct learning (3.4) approach. In the direct learning architecture an estimate of the relation between input and output of the system is estimated, before the pre-distortion of the input signal is performed by pre-inverting the identified PA characteristics.
The indirect learning procedure determines instead the post-inverse characteristic of the PA without making use of a pre-distorter. After the post-inverse is identified, its copy is positioned in front of the PA and the estimation block is disconnected. A comparison between those two approaches is presented in [17].
In order to better understand how the pre-distorter is obtained, we need first to choose a model and fit it to our DUT. The most relevant behavioral models used in this work, will be introduced in the next section.

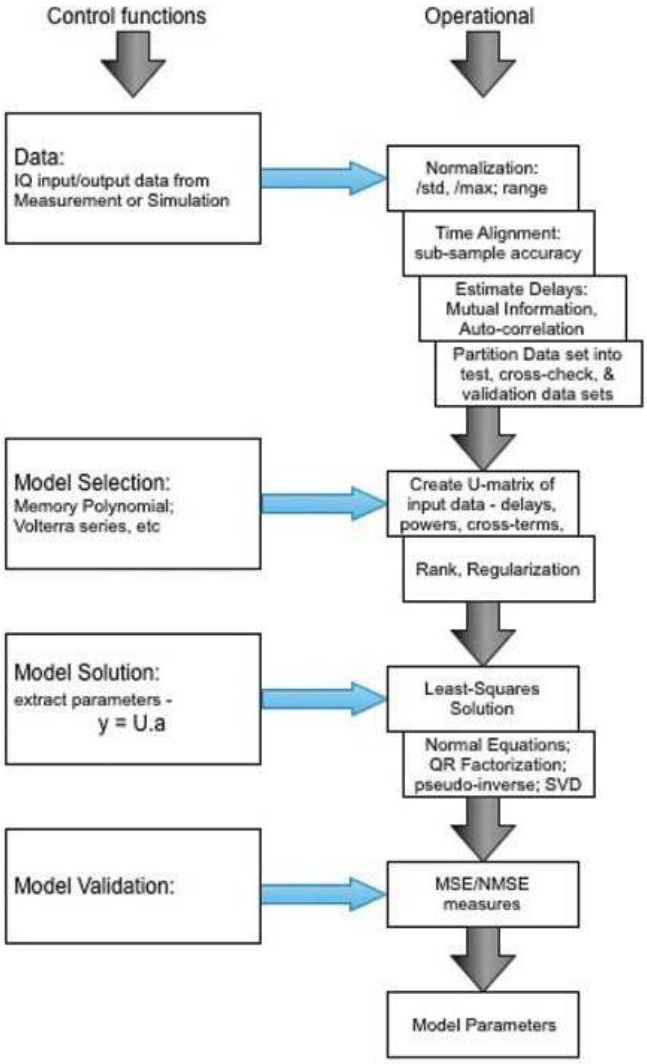

Figure 3.2: Classic workflow for PA model identification [1].

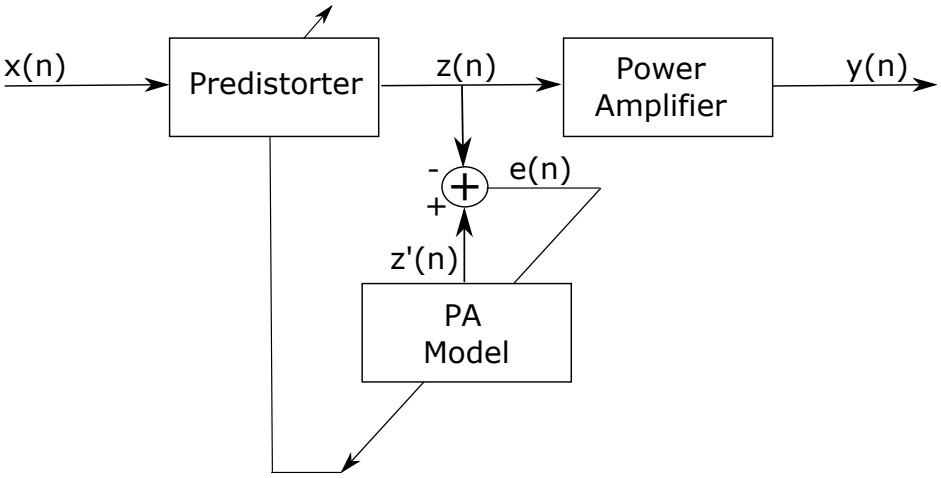

Figure 3.3: Indirect Learning Architecture.

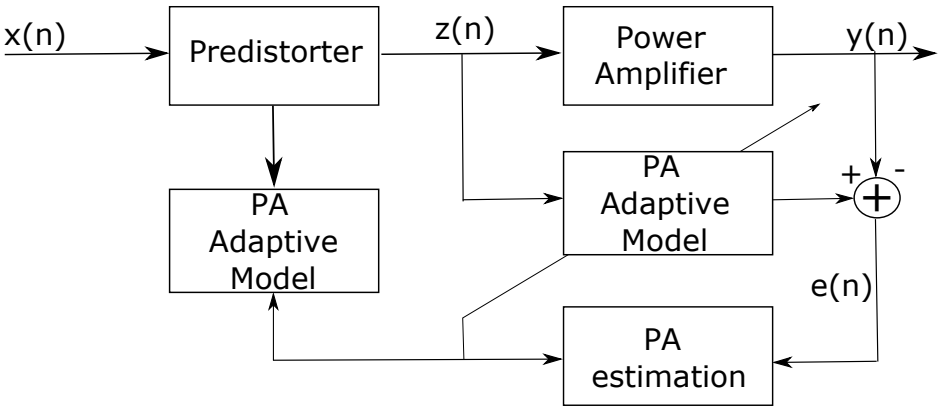

Figure 3.4: Direct Learning Architecture.

3.2 Classic DPD Models

In order to pre-distort a non-linear system we need to choose a non-linear behavioral model and find its post-inverse. Power amplifiers are showing two kinds of non-linearities, we can distinguish between static and dynamic non-linearities. The static non-linearities are generated by the static transfer characteristic of the PA (gain compression). Dynamic effects are generated by: memory inside the system introduced by passive (inductive, capacitive) components, thermal effects, charge trapping, bias and supply lines. An overview of these effects can be found in [1]. In this section we are going to introduce some of the most relevant behavioral models for PA, and their adaptation to dual input PAs.

3.2.1 Volterra Series Model

The general framework to mathematically describe nonlinear time variant phenomena is the Volterra series [18], elaborated by the italian mathematician Vito Volterra in 1887 as a tool to solve integral and differential equations. His theory was then adapted by Norbert Wiener to time-invariant nonlinear dynamic system, hypothesizing that these could be modeled using Volterra functionals. An exhaustive explanation of the Wiener model is given by Schetzen [19]. If we consider a simple polynomial:

$$y(t) = a_0 + \sum_{n=1}^{N} a_n u(t)^n \tag{3.5}$$

where $y(t)$ is the output signal of the nonlinear system, $u(t)$ is the input signal and a_n, with $n = 0, ..., N-1$, are the polynomial coefficients. From this formulation we see that the output of the system is depending on the input signal instantaneously. If we expand the polynomial as a Taylor series, in a specific point u_0 we obtain an equation of the form:

$$\begin{aligned} y(u(t)) = y(u)\Big|_{u=u_0} + \frac{1}{2!}\frac{dy}{du}\Big|_{u=u_0}(u-u_o) + \frac{1}{3!}\frac{d^2y}{du^2}(u-u_o)^2\Big|_{u=u_0} + ... \\ = a_0 + a_1 u + a2u^2 + ... \end{aligned} \tag{3.6}$$

This expansion can also be done by considering $y(t) = f(u, u_1, u_2, ..., u_n)$ as a function of past values of the input signal ($u = u(t)$, $u_1 = u(t-\tau_1)$, $u_2 = u(t-\tau_2)$, ...), obtaining the following multinomial series:

$$\begin{aligned} y(u(t)) = y(u)\Big|_{u=u_0} + \frac{1}{2!}\frac{dy}{du}\Big|_{u=u_0}(u-u_0) + \frac{1}{2!}\frac{dy}{du_1}\Big|_{u=u_0}(u_1-u_0) \\ + \frac{1}{3!}\frac{d^2y}{du^2}\Big|_{u=u_0}(u-u_0)^2 + \frac{1}{3!}\frac{d^2y}{du_1^2}\Big|_{u=u_0}(u_1-u_0)^2 \\ + \frac{1}{3!}\frac{d^2y}{dudu_1}\Big|_{u=u_0}(u-u_0)(u_1-u_0) + ... \end{aligned} \tag{3.7}$$

which is expressing the memory through the terms $(u_1 - u_0)$ and the so called Volterra cross-terms $(u-u_0)(u_1-u_0)$, generating the inter-modulation products of the nonlinear system.
The well known form of the continuous time Volterra series is obtained as an extension of the linear systems theory. The output of a linear dynamic system is described by the convolution between the input signal and the impulsive response ($h(t)$) of the system:

$$y(t) = \int_0^t h(t-\tau)\, u(\tau)\, \mathrm{d}\tau \tag{3.8}$$

Starting from the same polynomial model we have introduced in 3.5, we see that the nonlinearity is expressed by higher order terms. Substituting this model into the convolution product 3.8, we obtain the expression of the second order term for the Volterra series:

$$\int_{-\infty}^{\infty}\int_{-\infty}^{\infty} h_2(\tau_1, \tau_2)\, u(t-\tau_1)\, u(t-\tau_2)\, \mathrm{d}\tau_1 \mathrm{d}\tau_2 \tag{3.9}$$

and using the same procedure we obtain also the expression for the generic n-th order term:

$$\int_{-\infty}^{\infty}\int_{-\infty}^{\infty}...\int_{-\infty}^{\infty} h_n(\tau_1, \tau_2, ..., \tau_n)\, u(t-\tau_1)\, u(t-\tau_2)\, ...u(t-\tau_n)\, \mathrm{d}\tau_1 \mathrm{d}\tau_2 ... \mathrm{d}\tau_n \tag{3.10}$$

As we mentioned this model is containing all the nonlinear and memory effects we would expect from a dynamic nonlinear device. For instance with such model it is possible to explain the generation of inter-modulation products when the input signal is not a pure sinusoid but is composed by more than one frequency component.
Since the pre-distortion is operating on sampled data, we use a discrete version of the Volterra series:

$$\begin{aligned} y(t) &= \sum_{m_1=0}^{M} h_1(m_1)\, u(t-m_1) \\ &+ \sum_{m_1=0}^{M} \sum_{m_2=0}^{M} h_2(m_1, m_2)\, u(t-m_1)\, u(t-m_2) \\ &+ \sum_{m_1=0}^{M} \dots \sum_{m_n=0}^{M} h_n(m_1, \dots, m_n)\, u(t-m_1) \dots u(t-m_n) \\ &= \sum_{n=1}^{N} \sum_{m_1=0}^{M} \dots \sum_{m_n=0}^{M} h_n(m_1, \dots, m_n) \prod_{j=1}^{n} u(t-m_j) \end{aligned} \tag{3.11}$$

The terms h_n are called Volterra kernels, a set of coefficients representing the nonlinear filters taking into account inter-modulation products and memory. Volterra series are expressed as a linear superposition of nonlinear effects, since the model is linear in the parameters, the kernels can be computed using the classic linear identification algorithms.
The precision of Volterra series models, increases by taking into account more high order terms. Increasing the degree of the model, exponentially increases the number of coefficients necessary to the model making it computationally more costly. This is why, Volterra models were not so popular in past applications. Nowadays the computational power of computers is very high and efficient Volterra models, based on special pruning techniques, made possible to use them in linearization applications.
In response to the complexity of Volterra series in terms of kernel identification and implementation, many models have been developed as a simplification of Volterra series.
While a very good insight of Volterra series and techniques for its identification are given in [20], we are now going to introduce some models, derived from

the Volterra series, which are simpler to implement and are currently used in DPD applications: Polynomial model, Wiener model, Hammerstein model, Memory Polynomial (MP) model, Generalised Memory Polynomial (GMP) model, Lookup Table (LUT).

3.2.2 Polynomial Model

The polynomial model is the simplest way to model static nonlinearities, its discrete time version is:

$$y(n) = \sum_{p=0}^{P} a_p \cdot u(n)^p \tag{3.12}$$

where $u(n)$ and $y(n)$ are complex valued signals, $|u(n)|$ is the envelope of the complex input signal, n is the time index of the input and output sequences and P is the degree of the nonlinearity. The polynomial coefficients a_n are linear in the parameters, so they can be identified using classic linear approaches. Since the models are generally used in the complex baseband, we need a model making use of complex signals. By applying a simple baseband translation of the model we obtain the following form:

$$y(n) = \sum_{p=0}^{P} a_p u\left(n\right) \left|u\left(n\right)\right|^{p-1} \tag{3.13}$$

3.2.3 Memory Polynomial Model

The memory polynomial [21] is obtained by simply introducing delay terms for the input signal into the polynomial model. Considering the baseband version of the polynomial model, we can express the MP as:

$$y_{MP}(n) = \sum_{m=1}^{M} \sum_{p=0}^{P} a_n \cdot u\left(n\right) \cdot \left|u\left(n-m\right)\right|^{p-1} \tag{3.14}$$

where m accounts for the delay taps of the memory, expressed like in a common Finite Impulse Response (FIR) filter.

3.2.4 Wiener Model

The Wiener model can be derived from the Volterra series. It separates the static nonlinearity of device from the memory using the cascade of two sub-models: the static nonlinear part is represented by a static polynomial, while the dynamic part (memory) is abstracted by using a linear dynamic block realized with an FIR filter (figure 3.5). The relationship between input and output in a Wiener model is described as:

$$y_W(t) = \sum_{n=0}^{N} a_n \left[\sum_{m=1}^{M} h\left(\tau_m\right) u\left(t - \tau_m\right) \right]^n \tag{3.15}$$

In the Wiener model, the kernels $h(\tau_m)$ are incorporated inside the power series and are not linear in parameters. For this reason, in order to identify the kernels we need to use nonlinear optimization algorithms, and the model identification becomes more complex.

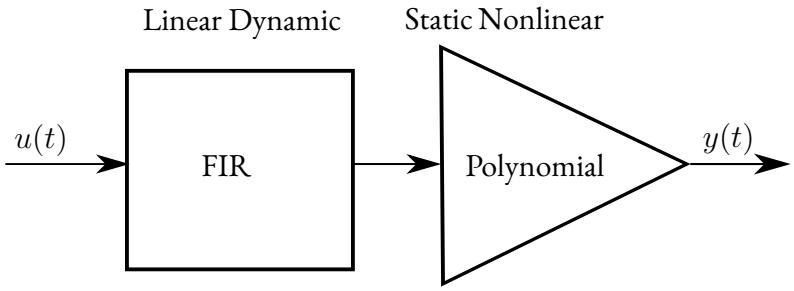

Figure 3.5: Wiener Model.

3.2.5 Hammerstein Model

The Hammerstein model is obtained from the Wiener model by exchanging the position of the nonlinear and dynamic block (figure 3.6). Doing so leads to a simpler equation:

$$y_H(t) = \sum_{m=1}^{M} h\left(\tau_m\right) \left[\sum_{n=0}^{N} a_n u^n \left(t - \tau_m\right) \right] \tag{3.16}$$

where the coefficients are linear in the parameters and can be identified using linear identification techniques. A comparison between Wiener and Hammerstein models can be found in [22].

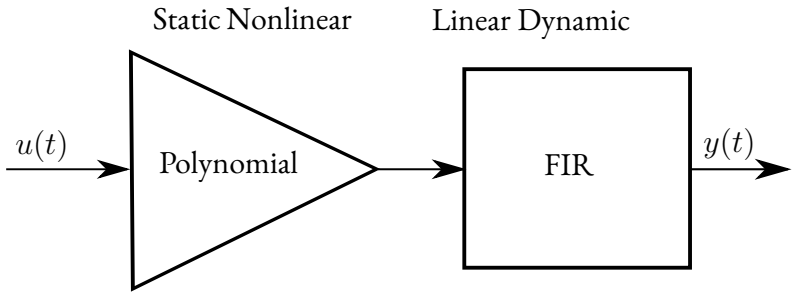

Figure 3.6: Hammerstein Model.

3.2.6 Generalised Memory Polynomial

The complexity involved in building Volterra models is mostly generated by the calculation of the kernels. When higher accuracy is required, more kernels have to be included inside the model and an exponentially higher number of parameters is involved in the identification process. The GMP was first presented in [23], its input output relation is similar to the one of Volterra series, but allows to include a smaller number of parameters:

$$\begin{aligned} y_{GMP}(t) = & \sum_{k=0}^{Ka-1} \sum_{l=0}^{La-1} a_{kl} x(n-l) \left|x(n-l)\right|^k \\ & + \sum_{k=1}^{Kb} \sum_{l=0}^{Lb-1} \sum_{m=1}^{Mb} b_{klm} x(n-l) \left|x(n-l-m)\right|^k \\ & + \sum_{k=1}^{Kc} \sum_{l=0}^{Lc-1} \sum_{m=1}^{Mc} b_{klm} x(n-l) \left|x(n-l+m)\right|^k \end{aligned} \tag{3.17}$$

The equation is composed of three sections: the modelling part for the aligned signal (coefficients Ka, La), signal and lagging envelope (coefficients Kb, Lb,

Mb) and signal and leading envelope (coefficients Kb, Lb, Mb). GMP is a cross-term model which presents coefficients in linear form, and can be solved with least-squares algorithms. Depending on parameters such as the sample rate and the signal's bandwidth, we might not require to use all the coefficients and we can further simplify the model. With this model it is possible to have higher pre-distortion performance with a limited number of coefficients.

3.2.7 Lookup Tables

LUTs [24], [25] are simply obtained by measuring the PA characteristic at specific input power levels. They can be formed, for instance, by a certain number of homogeneous input-output couples of the PA and can be used to calculate the inverse correction factor that linearizes the device. The accuracy of LUTs increases when there are more entries, and also when interpolation technique used to calculate the input values is appropriate. One of the problems generated by the usage of LUTs is that they generate both even and odd terms of nonlinearity, increasing the bandwidth of the predistorted signal much more than polynomial models do. This problem can be mitigated by defining the LUTs in a smarter way [26].

3.3 Dual-Input DPD Model

Currently not much scientific work is focusing on the linearization for Dual-Input DPA. This architecture is becoming very attractive for the application in BS front ends, and will be surely improved in the next future. The challenge of DPD in modern systems is that one of improving both linearity and efficiency over a large bandwidth.
Some analysis about the relationships between the input signals of the Dual-Input DPA, and the optimization of the phase relationships between the input branches of the DPA were proposed in [27], [28]. A first approach to the linearization of a dual input systems was proposed in 2011. This work was based on two previously proposed approaches targeting high PAE for systems using signals with high PAPR such as Envelope Tracking (ET) and varactor-based Dynamic Load Modulation (DLM). Figure 3.7 represents the architecture of

ET/DLM PAs, where in general V_{dd} is the envelope signal's voltage, x is the input signal and y is the output signal of the PA.

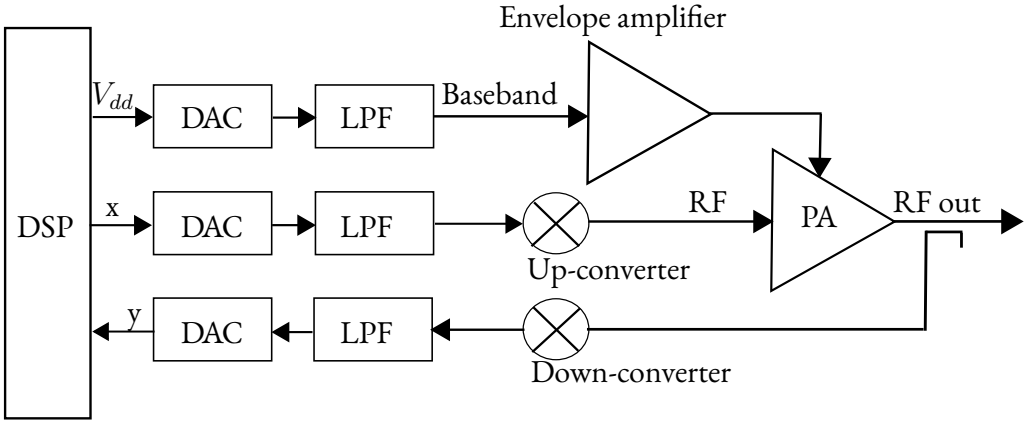

Figure 3.7: ET architecture scheme block.

Both ET and DLM are sharing the same architecture and they are both affected by the same basic problem; since the bandwidth of the envelope signal is bigger than the one of the amplified RF signal, DC/DC converters need to be wideband and introduce challenges into the design. Passing to a dual-input characteristic allows to achieve linearity and enhancement of the average PAE at the same time. The block diagram in figure 3.8 sketches the concept behind an high efficiency PA structure. The meaning behind the block scheme is that voltage and magnitude , x, $|x|$, and the envelope signal, v_c, are controlling the RF output signal, y, and the instantaneous PAE, η.

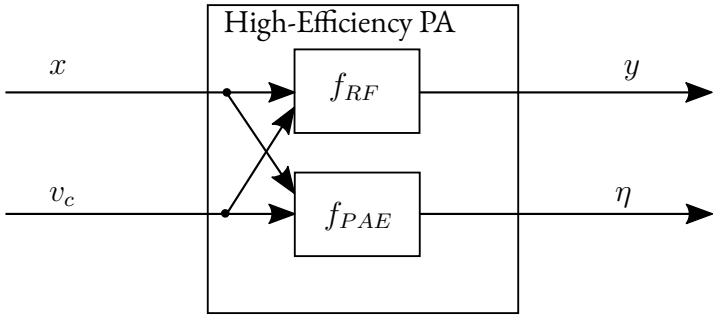

Figure 3.8: High efficiency PA architecture.

$$y = f_{\mathrm{RF}}\left(x, v_{\mathrm{c}}\right) \tag{3.18}$$

$$\eta = f_{\mathrm{PAE}}\left(|x|, v_{\mathrm{c}}\right) \tag{3.19}$$

Equations 3.18 and 3.19 have to be solved in order to obtain the maximum PAE and the desired output, $y_{desired}$ which has to be a linear version of the input signal x. The solution to such optimization problem translates into choosing the right combinations of x and v_c to maximize the efficiency cost function, given a wanted behavior of the output signal ($y_{desired}$). The solution proposed in [29] to solve this optimization problem can be resumed in two formulas:

$$x_{opt} = f_{RF}^{-1}\left(y_{desired}, v_c\right) \tag{3.20}$$

$$v_{c,opt} = \arg\max_{v_c} f_{PAE}\left(|x_{opt}|, v_c\right) \tag{3.21}$$

where f_{RF}^{-1} is the inverse PA characteristic and $y_{desired}$ is the wanted output signal. This approach was still based on a single input system and was extended to the dual input architecture in [30], represented in figure 3.9.

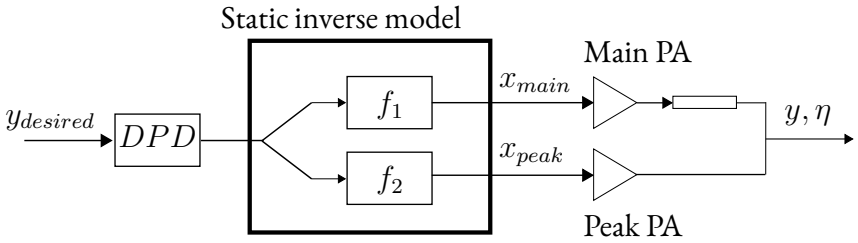

Figure 3.9: Dual Input DPD concept.

Comparing this architecture with the scheme in figure 3.8, we recognize that the static inverse model is composed by two static functions $f1$ and $f2$ which are determining the behavior of the digital splitter taking care of optimizing the PA efficiency. The relationship between input and output of the dual input DPA can be expressed, for instance, as a third order Volterra series:

$$
\begin{aligned}
& x_{main}(n) = f_{RF}^{-1}\left(y_{desired}(n), x_{peak}(n)\right) = \\
& + \sum_{m_1=0}^{M} \sum_{m_p=0}^{M_p} h_{m_1 m_p} y_{desired_{m1}} x_{peak,m_p} \\
& + \sum_{m_1=0}^{M} \sum_{m_2=m_1}^{M} \sum_{m_3=m_2}^{M} \sum_{m_4=0}^{M_p} \sum_{m_5=m4}^{M_p} \sum_{m_6=m_5}^{M_p} h_{m_1 m_2 m_3 m_4 m_5 m_6} \\
& y_{desired_{m_1}} y_{desired_{m_2}} y^*_{desired_{m_3}} x_{peak,m_4} x_{peak,m_5} x^*_{peak,m_6}
\end{aligned}
\tag{3.22}
$$

the formula in reality is a truncation of the Volterra series model with two input signals. It is ignoring symmetric terms thus has already a reduced complexity if compared with the full Volterra series expansion. In equation 3.22, the $*$ represents the conjugate operation, M is the depth of the memory accounted for the MAIN PA, M_p is the memory of the PEAK PA, $y_{desired_m}$ is the target output signal delayed of m samples and x_{peak_m} is the signal to the PEAK PA delayed by m samples.

This solution doesn't make use of an efficiency optimized static splitter, it is just using a dual input approach to earn a degree of freedom, allowing to reach high efficiency and linearity. This approach compensates residual errors in the identification phase, but the function used to derive the optimal RF input for the PEAK PA will still be affected by fitting errors.

The performance of this algorithm is documented in [30]. The algorithm was tested with a W-CDMA signal of 7 dB PAPR, setting the model parameters $M = 2$ and $M_p = 0$ an Adjacent Channel Leakage Ratio (ACLR) was about -45 dBc while the obtained average PAE was about 40%.

The dual input model introduced flexibility into the DPD, showing the advantage of separately driving the branches of the dual input DPA to gain a degree of freedom in the configuration of linearity and average efficiency. Despite that, this model still considers the model as a black box, and doesn't really take into account all the physical effects that generate non-linearity and need to be corrected. We must also point out the fact that this model is valid only in a narrowband approach.

In modern telecommunication systems, the design of PA is more challenging due to the requirements of linearity, average efficiency and bandwidth. It is important to deliver high average efficiency on a wide frequency range.

Chapter 4

Analysis Tools and Simulation Environment

In this chapter, we are introducing an innovative and revisited approach to the DPD. The device we have targeted is a dual-input DPA with a 300 MHz bandwidth located between 700 and 1000 MHz and a 35% fractional bandwidth. In order to build up our model we needed a dataset to study the behavior of the device and design an algorithm to efficiently pre-distort it. Our analysis was based on the complete DPA model (matching networks, IQ modulator and demodulator, combiner, accurate CREE transistor models) designed in Advanced Design System (ADS) from Keysight (figure 4.1). The analysis and study of the PA behavior has been performed mainly in two phases. In the first study phase, a simulation environment in ADS was used to perform harmonic balance simulations and extract the necessary parameters. In the second phase, we have switched to a circuit envelope simulation environment where we could keep track of the dynamic effects present in the system.

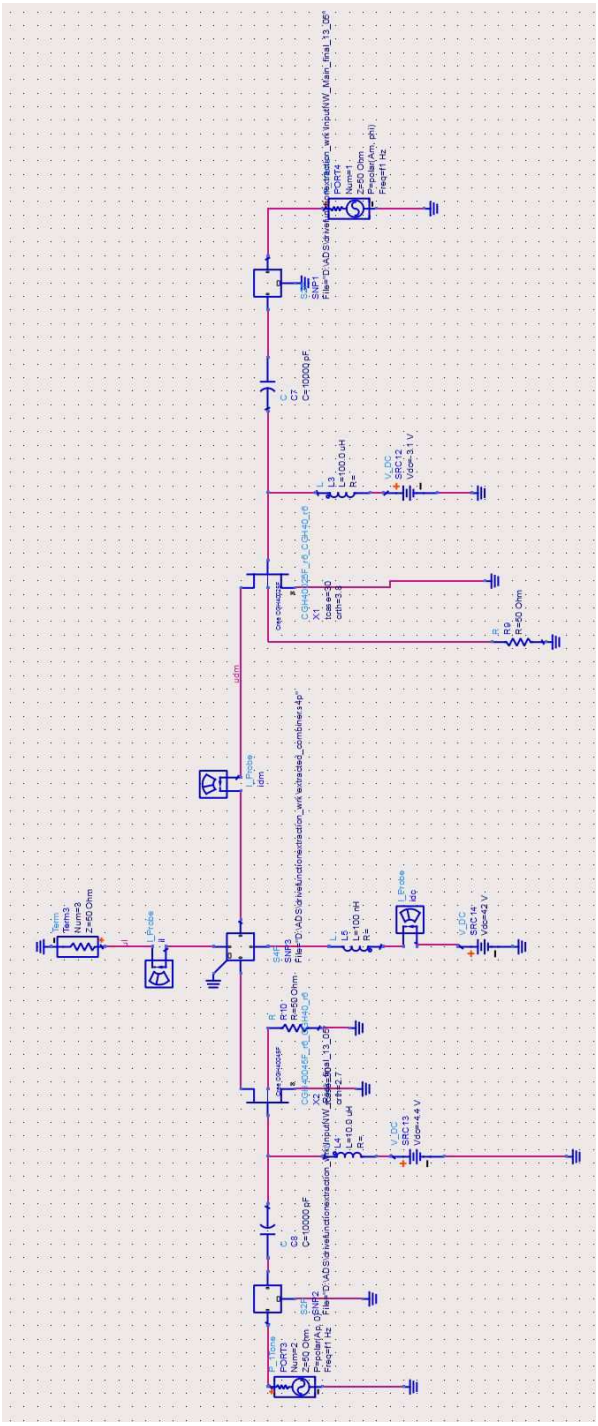

Figure 4.1: ADS model of the DPA.

4.1 Dual-input DPA Dataset

In section 2.5 we mentioned the importance of separately driving the inputs of a DPA in order to linearize it, and improving the average efficiency of the PA, at the same time. The DPA can be seen as a block with four inputs and three outputs, so it can be used to perform a system identification to obtain a linearity and efficiency optimized pre-distorter function. The input parameters contained in the dataset are:

- Pm : Input power to the MAIN PA, in Watts
- Pp : Input power to the PEAK PA, in Watts
- $\delta\Phi$: Phase difference between MAIN PA and PEAK PA inputs, in Degrees

We will refer to the combinations of input parameters (P_m, P_p, $\Delta\Phi$) as triplets. Previously we mentioned four parameters, including the carrier frequency F_c at which the simulation takes place, has to be set. An Harmonic Balance (HB) simulation has been performed at four different carrier frequencies (700, 800, 900 and 1000 MHz), sweeping the input parameters for a wide range of values. The HB simulation in ADS, involved in the experiments, sends the triplets as single tone RF signals, thus dynamic effects are avoided and the measured points are related to the only static part of the behavioral model. This is a mere "brute force" approach to test several combinations of the input parameters, that writes the respective output parameters into the dataset as:

- $Pout$: PA Output power PA
- η : PAE PA
- Φ_O : output absolute phase

The duration of each simulation was about one week, obtaining four datasets with about 9.000.000 points each. Starting from this dataset we could address the problem and we established a theoretical baseline to reach our scope. An example of the data from the dataset with carrier frequency of 900 MHz can be seen in figure 4.2, where the color is coding the efficiency with a resolution of about 2%.
Since HB with continuous wave measurements does not export dynamic effects, we used these tables just to identify the static behavior of the DPA. In order to see dynamic effects, we then switched to Circuit Envelope (CE) simulation environment.

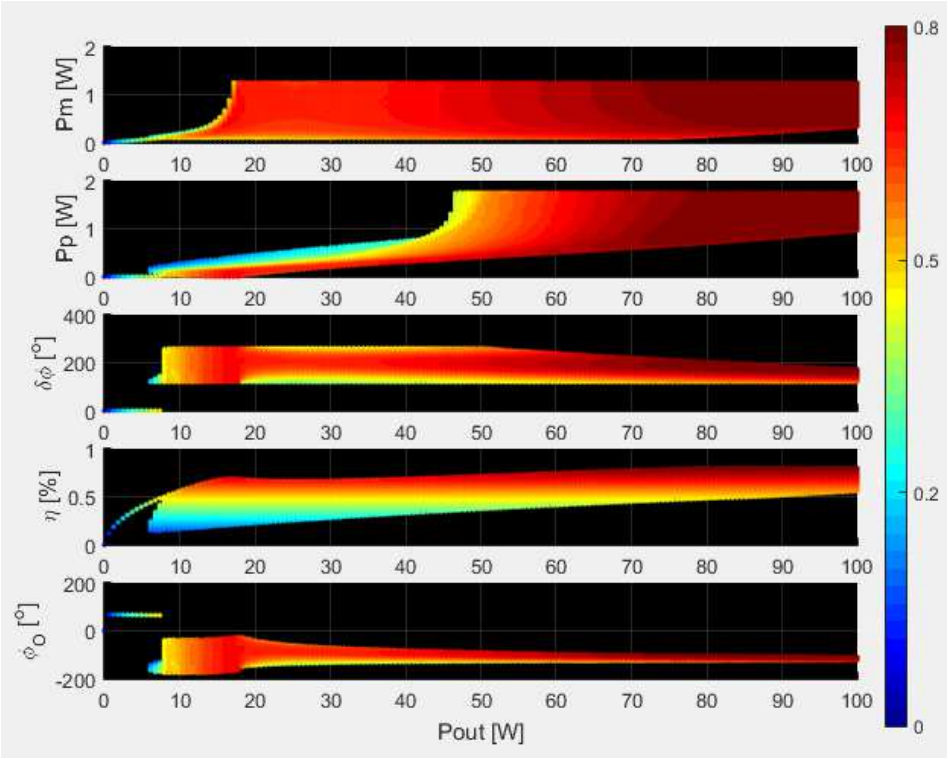

Figure 4.2: Input-output multidimensional space of the DPA.

4.2 Circuit Envelope Simulation Environment

The schematic presented in figure 4.3 was modified and extended to perform CE simulations. Of course the complexity of the schematic was then increased. The simulation was controlled by specially programmed MATLAB scripts, writing the simulation parameters inside specific configuration files, and calling ADS on the command line. Looking at figure 4.4 we can see the simulation parameters controlled by MATLAB:

- Fc : Carrier frequency of the modulated signal in GHz
- t_stop : Duration of the simulation in seconds
- t_step : Sampling period of the IQ data in seconds

The input power sources have been replaced by user defined timed data sources, loading the IQ data previously generated in MATLAB and modulating them through an IQ modulator (see figure 4.5).

The signal at the output of the PA is then fed into an IQ demodulator (figure 4.6), and all the necessary variables are exported to a MATLAB variable through an dedicated MATLAB output block.

The nonlinear effects, as in any other PA, are here due to the matching and bias networks, charge trapping, thermal effects and non-linearity of the transistors. Making use of CE simulation, we can keep track of all dynamic effects that cannot be normally appreciated when performing HB simulations, and we can go far beyond the steady state solution. We cannot separate all the nonlinear effects mentioned above, but we gain anyway more control over some important parameters such as the temperature during PA operation (see figure 4.7).

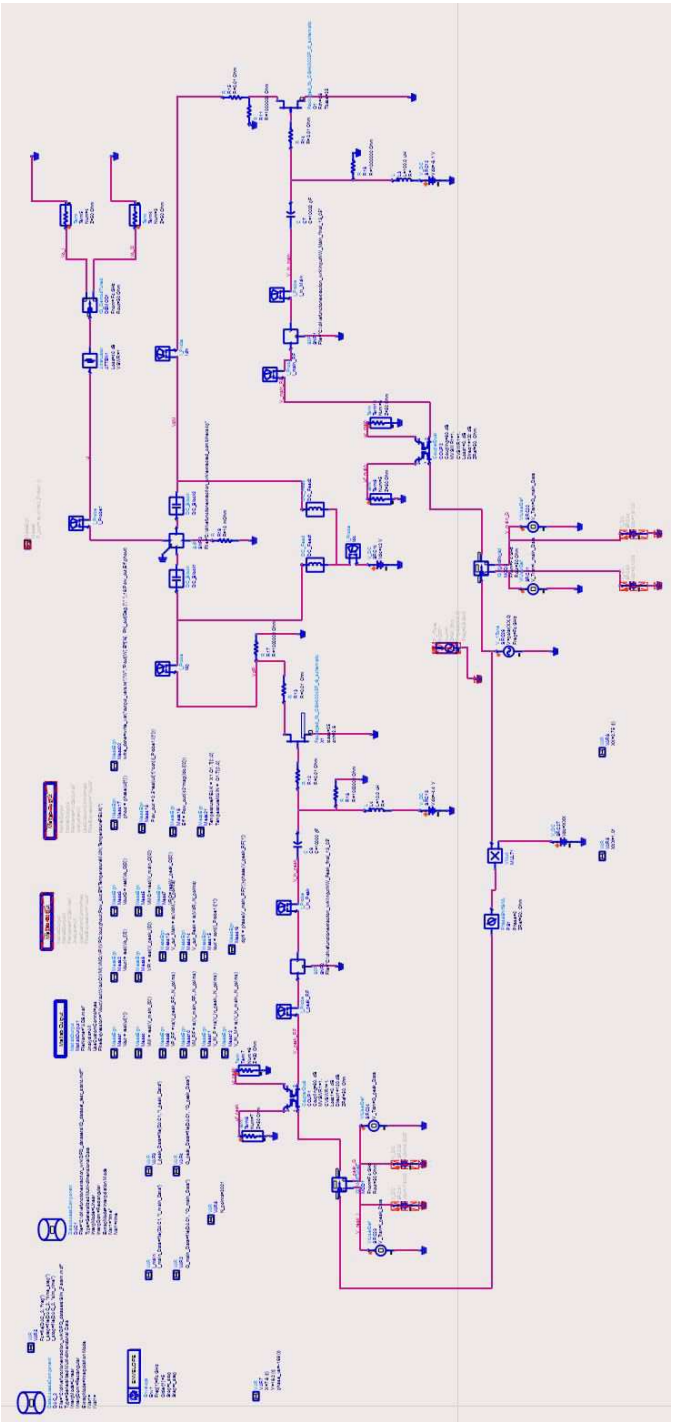

Figure 4.3: ADS model of the DPA for CE simulations.

Figure 4.4: CE Simulation controller.

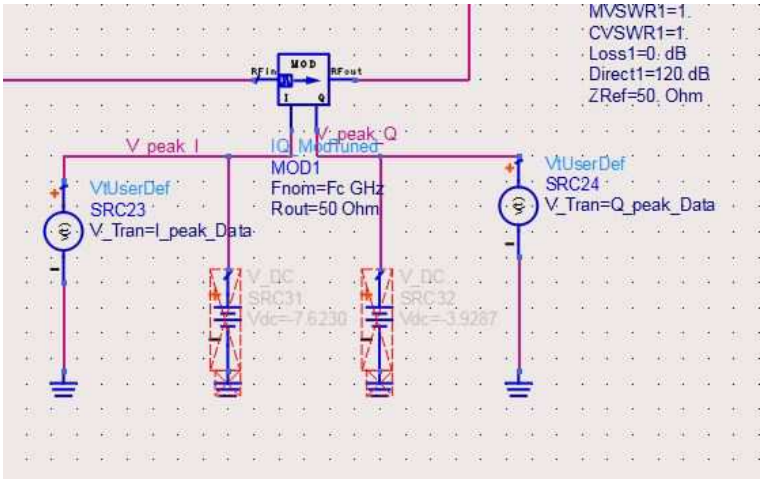

Figure 4.5: IQ modulator at the input of each DPA branch.

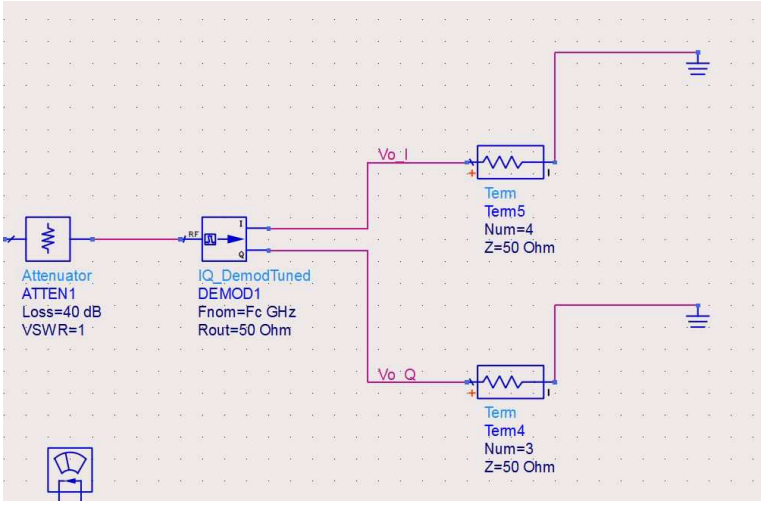

Figure 4.6: IQ demodulator at the PA output.

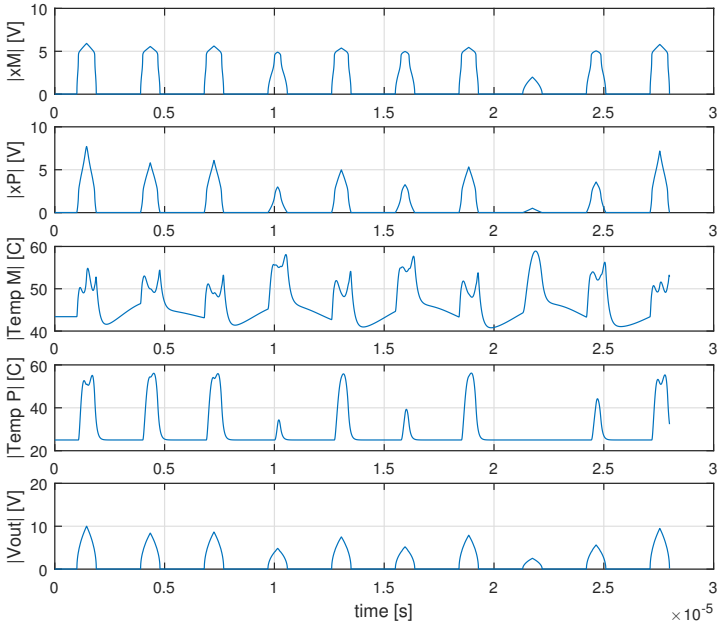

Figure 4.7: Junction temperature of MAIN and PEAK PAs obtained using CE simulation.

Chapter 5

Drive Function

In section 2.5 we have discussed the theory behind the dual-input Doherty architecture presented in [13]. Separating the input branches of the DPA, we gain a further degree of freedom in the reconfiguration of the linearity and average efficiency of this kind of PA.
Now we aim to pre-distort MAIN and PEAK PA independently by adjusting both amplitude characteristics and phase relationship between them. It was shown that using an efficiency optimized power splitter, allows a great efficiency improvement. Howerer a DPD block is still necessary in order to correct the dynamic effects due to memory of the device.
In section 4.1 we have introduced the concept of triplet. What we actually see in figure 4.2 is a multidimensional representation of the search space made of an infinite number of triplets. A very important concept that must be understood looking at this picture, is that several triplets can generate the same output power, but only some of them give the maximum efficiency. In order to better address this problem, we can zoom on a random point of the dataset (Pm vs. Pout), and see how the domain looks like.
We can appreciate the effect of the zoom in figure 5.1:

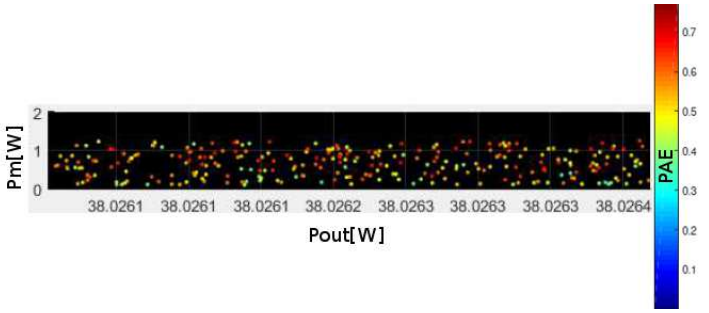

Figure 5.1: Zoom on the MAIN PA dataset at 900 MHz.

With a very small approximation, we can state that all the points included in the graph are generating the same output power, of about 38 W, but not all of them deliver maximum efficiency. This means that we must choose the right input triplets given that a very little error in positioning a triplet translates into a huge loss of performance in terms of linearity and/or efficiency.
To understand how the DF tweaks the performances, we need to revise the predistortion approach to and bring it into the DPD. We are going to analyze the physical behavior of our DPA and make use of the obtained knowledge to find an optimum DF for that specific frequency.

5.1 Maximum Input Power Ratings

The approach we are going to introduce is more based on the physics of the device than normal DPD models. Later it will be also important to know inside which range we can tweak the input power into MAIN and PEAK transistors, this can be done by consulting the datasheet of the devices.
The MAIN PA is a CREE CGH40025F, while the PEAK PA is a CREE CGH40045F. The characteristics reported from the datasheets are resumed in table 5.1:

Component	Function	Typical Small Signal Gain [dB]	Max. Pout [W]
$CGH40025F$	MAIN PA	13	30
$CGH40045F$	PEAK PA	14	55

Table 5.1: CHG40025F and CGH40045F parameters.

Starting from these values we can calculate an approximation of the maximum power levels that we can apply on the two PA input paths. The formula of the gain expressed in decibels is:

$$G_{dB} = 10 * \log_{10}\left(\frac{P_{out}}{P_{in}}\right) \tag{5.1}$$

By inverting this formula and using the parameters in table 5.1 we obtain an estimation of the maximum allowed input power as function of the maximum output power and the gain:

$$P_{in} = \frac{P_{out,max}}{10^{\frac{G_{dB}}{10}}} \tag{5.2}$$

$$\begin{aligned} PMAX_{main,IN} &= 10^{\frac{30}{13}} = 1.5\,\mathrm{W} \\ PMAX_{peak,IN} &= 10^{\frac{55}{14}} = 2.18\,\mathrm{W} \end{aligned} \tag{5.3}$$

These values are referring to the maximum ratings given by the constructor and are provided as physical limits to the operation ratings of the components. This gives a first limitation to the input power applied to the inputs of MAIN and PEAK PAs, which is also related to the aging of the components. Applying the maximum ratings during the whole operation reduces the lifetime of the component. It is therefore not recommended to drive the transistors in that regime.
In Figure 5.2 we see the result of applying a power sweep on the MAIN PA input, while keeping the PEAK PA off. In this scenario we notice that the MAIN PA reaches the 1 dB compression point already with an input power of 200 mW, delivering a maximum output power of 17.5 W. This value is 2.3 dB under the maximum value declared inside the datasheet. This effect is due to the matching networks of the dual-input DPA.
When the MAIN PA is operating alone, it cannot deliver maximum power of 30 W since the impedance of the combiner is designed to be matched to reach 18 W. For this reason it provides a lower gain.
Things are changing when the PEAK PA turns on, because the drain impedance seen by MAIN and PEAK is modified by the load modulation mechanism and both MAIN and PEAK contribute with a higher power to reach 100 W at

the output of the DPA. For this reason we have limited the maximum input power of the MAIN PA to 1 W. Unfortunately the same relationship cannot be tested on the PEAK PA because of the behavior of the output combiner that does not allow the same transparency regarding its physical effects between input and output.
In this case since we have motivated roughly one third of maximum MAIN input power due to considerations on the physics of the device, we can assume the same safety reduction factor for the PEAK input power, obtaining a maximum of 1.5 W.

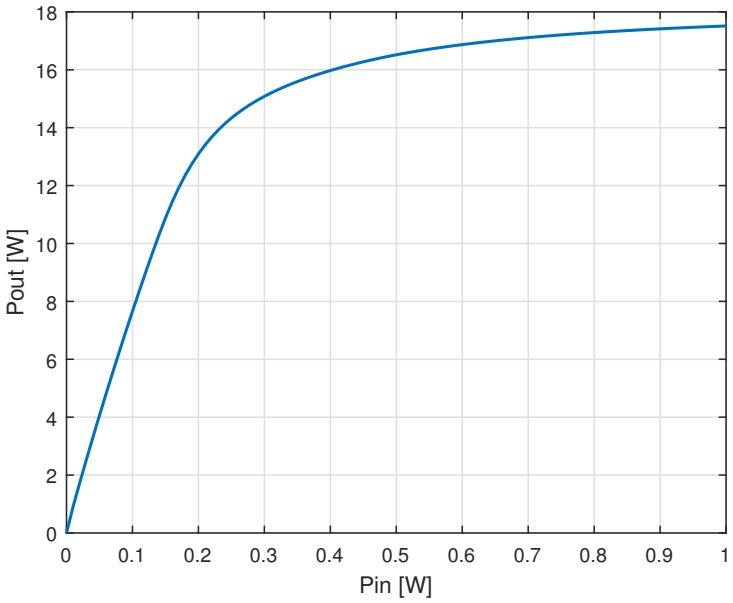

Figure 5.2: Result of a power sweep on the MAIN device only.

5.2 Static Drive Function for MAIN PA

The starting point to understand how to find an optimum DF is to analyze the behavior of the dual-input DPA. In back-off region, the characteristic of a DPA is only dependent on the MAIN PA because the PEAK PA is turned off.
If we keep the PEAK shut off and we make a power sweep on the input of the

MAIN PA, we obtain the power transfer characteristic of the device. In order to obtain a steady state behavior, every step of the power has to be held long enough, thus avoiding the excitation of memory effects in the PA structure. Iterating this process on distinct values of the carrier frequency, we can see the static behavior of the MAIN PA over the whole frequency span.
Looking at figure 5.3, the two extreme cases where the carrier frequency are respectively at the lowest and the highest, we notice that for each frequency the maximum efficiency is reached at different values of the input power. Thus we need to be able to reconfigure the efficiency according to the carrier frequency where the signal is modulated.
Figures 5.4 and 5.5 give us a better representation of the effect. If a certain signal is placed for instance at 700 MHz, at the lower edge of the frequency range allowed by the DPA, we see that the saturation power of the MAIN device is 20 W. The efficiency characteristic is dropping when feeding the MAIN with more than 150 mW, so if we want to maximize the PAE at low power levels we need to turn on the PEAK device at this point. Taking into account the whole DPA operation, this means that with a maximum output power of 100 W we want to have maximum efficiency at 8.2 dB Output Power Back-Off (OPBO).

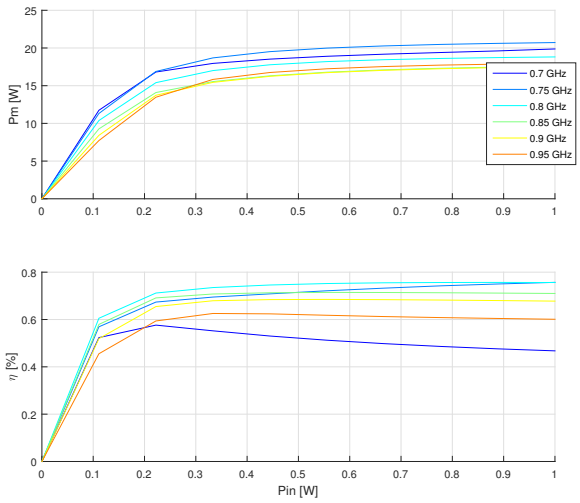

Figure 5.3: Power transfer characteristics and PAE of MAIN PA only at several frequencies.

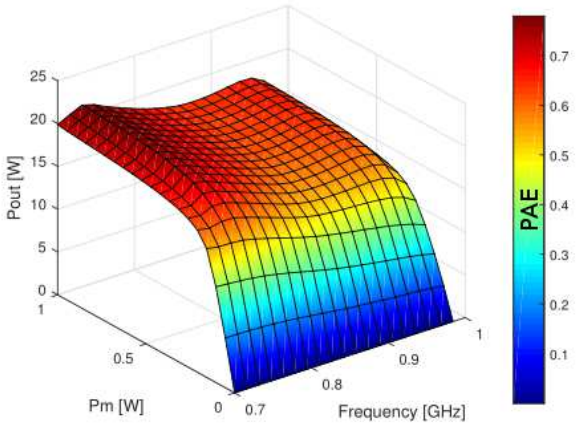

Figure 5.4: 3D output power-frequency characteristic of MAIN PA only.

Positioning the carrier frequency at 950 MHz, the maximum efficiency is reached at about 315 mW input power so the OPBO is about 2 dB higher compared to the 700 MHz carrier frequency at which the OPBO would be of 5.01 dB. Of course, this behavior depends on power-frequency characteristic of the devices involved into the design of the DPA. In our case we have 2 dB of freedom in choosing the entry point of the PEAK PA with a 300 MHz bandwidth.
The previous analysis shows that separating the inputs of the DPA allows a limited, but still present, degree of freedom configuring the efficiency at the wanted OPBO point for a certain carrier frequency. This is one of the advantages of using a dual-input DPA.
Our dual-input DPA has a MAIN device operating in class AB and a PEAK device operating in class C. Thus the linearity in the low power range is only dependent on the characteristics of a class AB PA. If we want to operate with maximum PAE we need to drive the MAIN device to the level of the maximum efficiency point.
Another important aspect shown by the previous analysis concerns the performance of the device over frequency. Close to the middle of the bandwidth we get the highest performance in terms of efficiency, and we notice a deterioration closer to the band's edge. According to this observation, we are expecting worse efficiency and linearity when the carrier is positioned in those ranges.

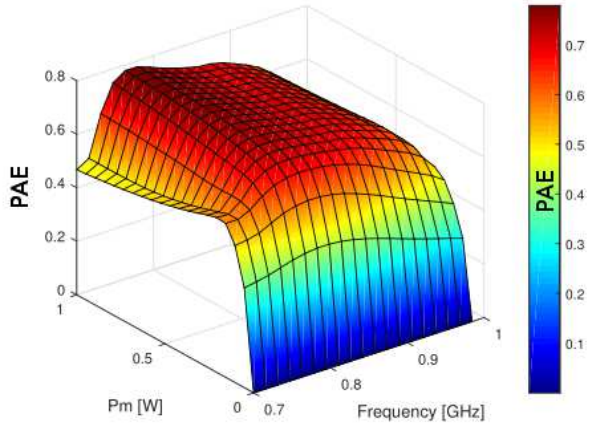

Figure 5.5: 3D PAE-frequency characteristic of MAIN PA only.

Considering a specific frequency, the static DF for the MAIN PA can be obtained simply inverting its power characteristic. Figure 5.6 shows the AM/AM curve for the MAIN PA, obtained by sweeping the input power between 0 and 1 W when the carrier frequency is at 900 MHz. From the inversion of the characteristic we obtain the AM/AM of the pre-distorter for the MAIN PA (figure 5.7).
Once we have identified the DF for the lower power range, we can choose the behavior of the pre-distorter. Using this procedure, we are gaining the ability to configure the bandwidth expansion of the pre-distorter and also optimize it according to the characteristics of the Digital to Analog Converter (DAC). To better understand how the shape of the DF is influencing the bandwidth of the pre-distorted signal we should recall the effect of a polynomial on the bandwidth of the signal. As a rule of thumb the order of the polynomial is setting the bandwidth expansion of the pre-distorted signal. For instance a polynomial of the 5^{th} order expands the bandwidth of the signal about five times. In DPD applications, polynomials are used in order to model the nonlinear effects introduced by the PA. The DPD calculates the inverse model used to pre-distort the signal and linearize the device.

Referring to Figure 5.7, the first part of the predistorter characteristics has a rather high order of non-linearity, and can be modeled by a polynomial of the 11^{th} order. Choosing the shape of the DF will then set the amount of linearization bandwidth to linearize the MAIN PA.

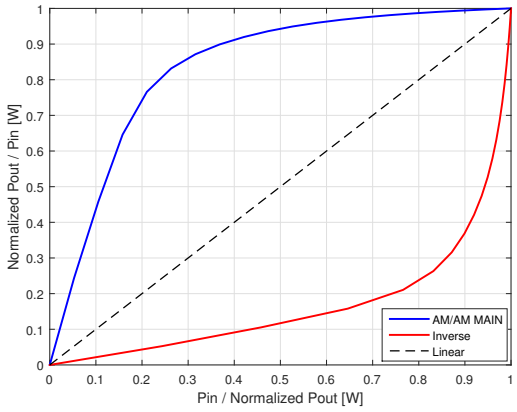

Figure 5.6: Drive function for MAIN PA at 900 MHz.

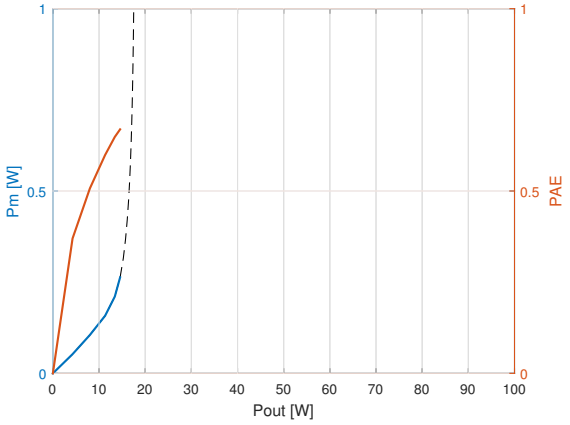

Figure 5.7: First part of Drive Function versus PAE.

5.3 Bandwidth Expansion of MAIN Drive Function

In the previous section, we have seen that the bandwidth expansion caused by the DF of the MAIN signal branch is set by the behavior of the device itself. We are therefore forced to invert the characteristic of the MAIN PA and we end up with a fixed expansion (see Figure 5.8). In our case the expansion is given by the LUT, identified by sweeping the input power of the MAIN device only and inverting the characteristic.
In order to estimate the effect of the first part of the MAIN DF, we can pick up a test signal with a maximum peak power equal to the maximum power represented by the characteristic shown in Figure 5.7, and compute the Power Spectral Density (PSD) of the resulting signal.
Let us consider a LTE sequence with 10 MHz of bandwidth and a 10 dB PAPR. The spectrum of such signal is represented in Figure 5.9.
We can model the obtained DF by using a 7^{th} order polynomial, this would limit the bandwidth expansion for this area of operation. Since we are making use of a LUT, the results are different than the ones we would expect using a polynomial. What we see is that the ACLR is about 38 dBc and the signal shoulders sink to 100 dBc within the observable bandwidth. We are observing a theoretical infinite bandwitdh expansion due to two principal effects: generation of even and odd terms because of the LUT and limited sampling frequency (Fs).
A LUT is simpler to implement in our case, but it generates both harmonics and inter-modulation products. The intermodulation products are laying next to the carrier and are responsible for the leakage into the immediate out-of-band region, while the higher harmonics, which are even multiples of the carrier frequency (Fc), are far away from the band of the signal. These intermodulation products are present, and with a limited observation bandwidth due to low Fs, are aliasing back into the observed bandwidth (see Figure 5.10). This is not the only contribution to the expansion, in fact we still need to choose the profile of the DF after the entry point of the PEAK PA. One of the most logic and easy options, according to the previous observation, is to choose a linear characteristic as it will introduce any bandwidth expansion on this operating range.

An example of complete MAIN DF is shown in Figure 5.11. Pre-distorting the same LTE signal with the LUT shown in Figure 5.11 we obtain the spectrum in Figure 5.12.
It is evident that due to the limited observation bandwidth, the highest achievable Signal to Noise Ratio (SNR) at the input of each branch of the DPA has an inferior limit.

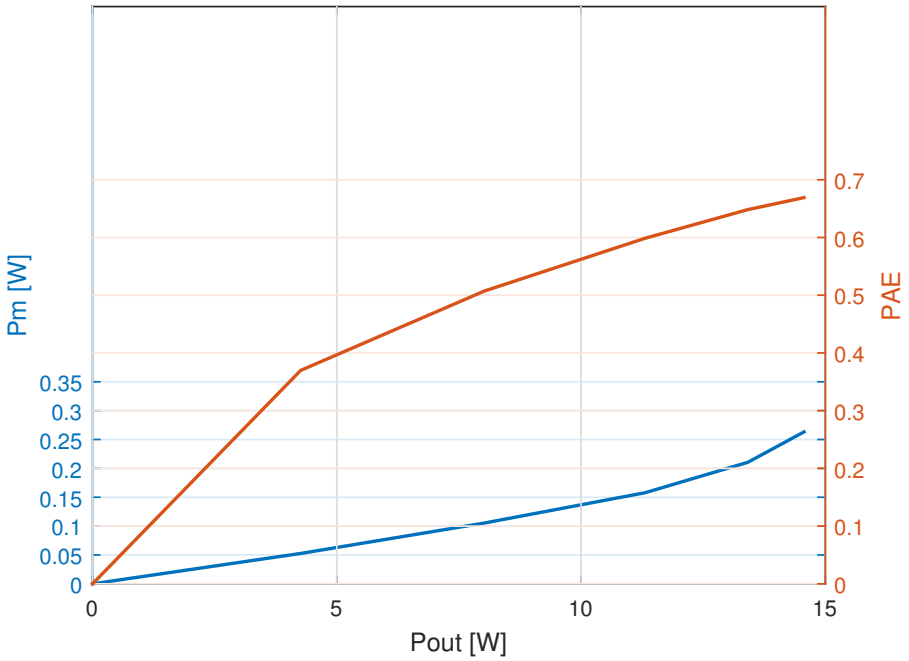

Figure 5.8: DF versus PAE for MAIN only.

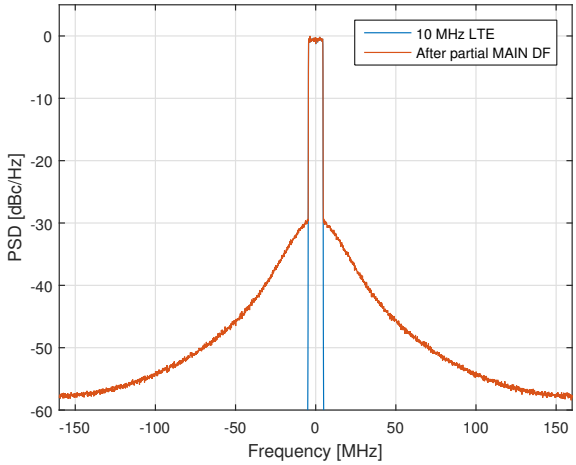

Figure 5.9: Bandwidth Expansion due to the first part of the MAIN DF.

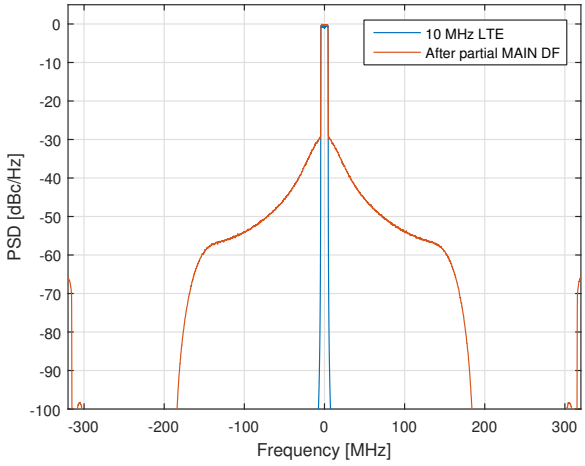

Figure 5.10: Bandwidth Expansion due to the first part of the MAIN DF with double observation bandwidth.

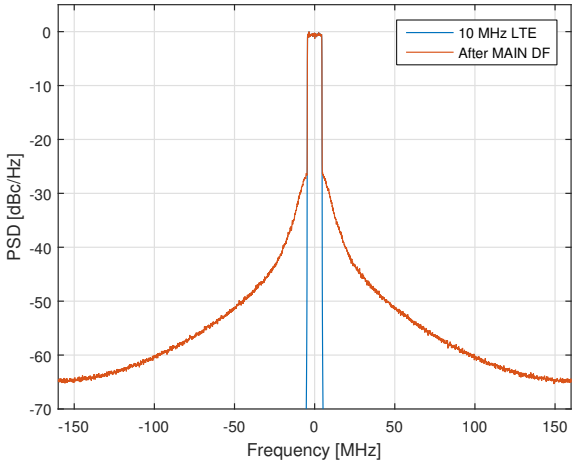

Figure 5.11: Spectrum of a signal predistorted by the MAIN DF in power back-off.

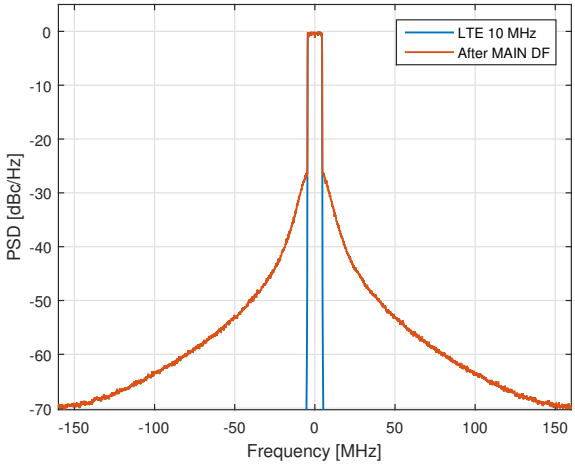

Figure 5.12: Spectrum of a signal predistorted by the complete MAIN Drive Function.

5.4 Static Drive Function for PEAK PA

In section 5.2 we investigated the static behavior of the DF for the MAIN PA, based on the physics of the device. We were able to configure the point assuring the maximum efficiency at PBO and shape the pre-distorter function in order to contain the bandwidth expansion on the MAIN input branch of the dual-input DPA. The operation of the DPA was explained in chapter 2, so at this point we can also be confident about the expected behavior of the PEAK DF. The extension of the efficiency range, in the DPA is obtained by driving the MAIN PA into the wanted compression point, and activating the PEAK PA after this point to keep high efficiency up to the maximum output power.
Using a dual-input digitally driven DPA we are able not only to configure the efficiency of the PA, we can also control the bandwidth expansion of the two device input channels and control its linearity. It is in the choice of the DF that we find the compromise between linearity, efficiency and bandwidth. Figure 5.13 shows an example of DF for the PEAK PA.

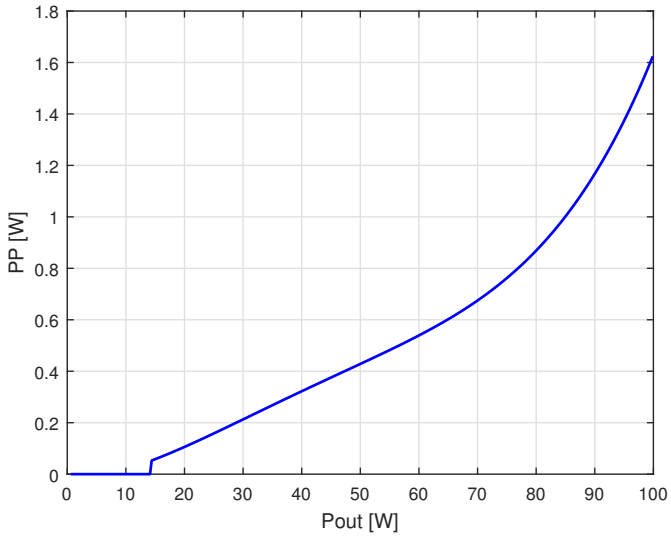

Figure 5.13: Basic Drive Function for PEAK PA only.

Such function needs to be identified by applying an identification process which we will explain in the upcoming sections. For the moment we should notice

the discontinuous behavior of the DF, in particular about the PEAK PA entry point. This discontinuity is responsible for a theoretically infinite bandwidth expansion on this branch of the DPA. We are observing a problem similar to the one generated by the knee in the MAIN DF. Due to the statistic of the input signal, the output of the pre-distorter is showing a switching behavior since the PEAK PA is switched off during a significant amount of the signal duration. We can appreciate this behavior in Figure 5.14, where the components separation between MAIN and PEAK PA is obteined using the DF.

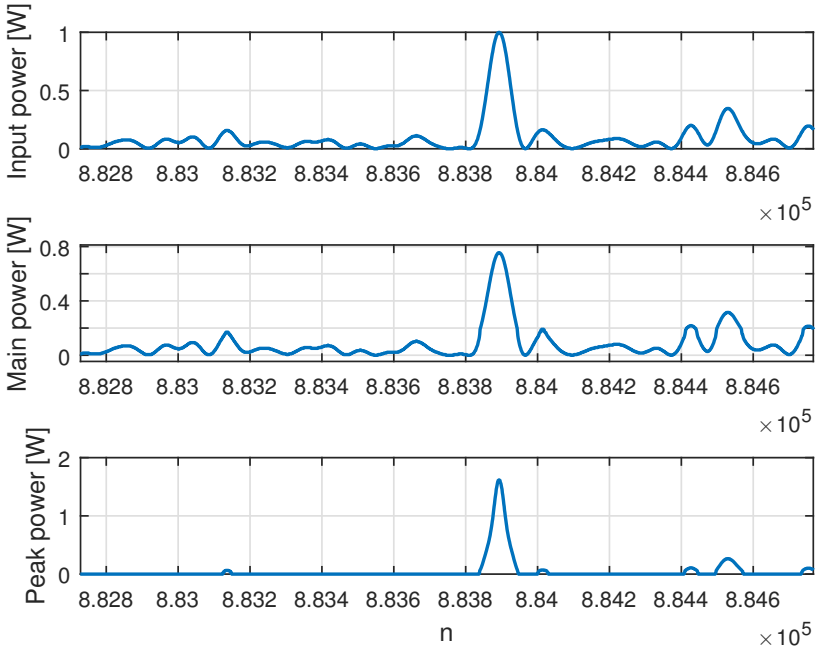

Figure 5.14: Amplitude power separation through drive function (n is the sample number in the sequence).

The signal of the PEAK pre-distorter is active as soon as the input power reaches the compression point of the MAIN PA. A fair comparison has been achieved by applying a mere amplitude correction at the PEAK signal to compensate for its AM-AM characteristic, leaving the AM-PM unchanged. By doing so, we see that the PEAK path demands a higher amount of bandwidth.

In chapter 2 we have introduced the relationship between the relative bandwidth and the drive level of the PEAK PA. In order to complete the model of the digital DF, we must also introduce the third input control parameter, the phase difference between MAIN and PEAK input signals. The simplest choice is to apply the whole phase difference on the side of the PEAK PA while maintaining a constant phase at the MAIN PA, obtaining two predistorters: a simple amplitude correction for the MAIN amplifier signal and an amplitude and phase correction on the PEAK signal path. An example of the phase relationship is shown in figure 5.16.

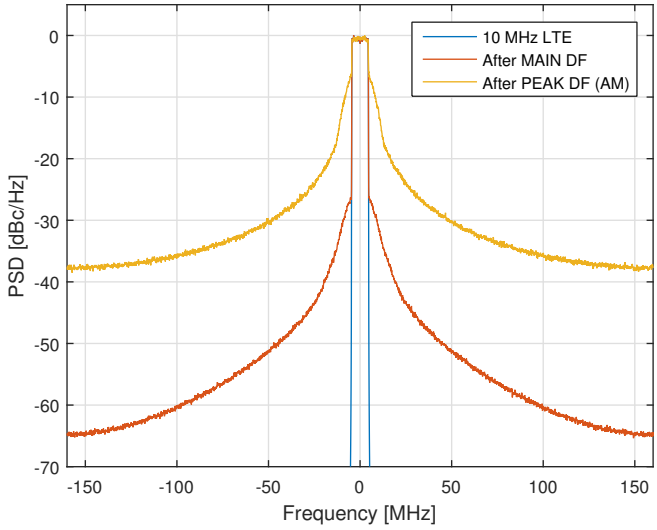

Figure 5.15: Comparison of the output spectra for amplitude DFs.

In general, we can imagine the complete DF as the union of the pre-distorters for MAIN and PEAK PAs. On the MAIN signal path we just have a pre-distorter with a simple AM/AM characteristic, while on the PEAK path the pre-distorter has both AM/AM and AM/PM. In the next section we will address the problem of detecting such functions.

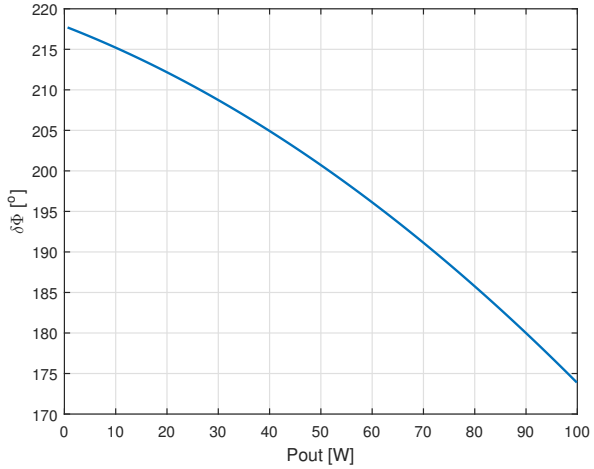

Figure 5.16: Example of phase relationship between MAIN and PEAK PA.

5.5 Identification of Static Drive Functions

In chapter 3 we have presented the various techniques used to linearize power amplifiers, we have introduced the classic techniques for PA identification and we presented an overview of the most commonly used models for devices and pre-distorters. In the previous sections, earlier in this chapter, we have shown the basic shape of the MAIN and PEAK DFs motivating their behavior according to the physics of the device operation. We have also shown that, other than polynomial models, our functions are generating a huge bandwidth expansion on their outputs. This is due to the LUT form assumed by the functions, which are presenting sudden gradient variations (on the MAIN path) and discontinuity (on the PEAK path).
Coming back to figure 5.1, we have introduced one of the most important concepts on which we have based our algorithms. The behavior of the dual-input DPA is controlled by the parameters generated by the DF, which are forming a triplet $(Pm, Pp, \delta\Phi)$. The identification of two way PA structures is then more complicated than the one used for common architectures. This was already shown in figure 4.2, where we have set a specific carrier frequency and we have obtained a database which we have used in order to study the properties of the DFs, and find a way to identify them.

We are in front of a multidimensional problem where we want to find a function mapping the tri-dimensional input space into a bi-dimensional output space. We can thus write two equations:

$$Pout = f_1\left(Pm, Pp, \delta\Phi\right); \tag{5.4}$$

$$\eta = f_2\left(Pm, Pp, \delta\Phi\right); \tag{5.5}$$

these relationship have been used to extract DFs from the huge dataset available. Please notice that for each carrier frequency, a single DF can be extracted. With being able to generate several DF (for different carrier frequencies), we acquire the ability of extending the efficiency bandwidth of the dual-input DPA during operation. We can build a wideband DPD formed by several narrow band DFs where, being able to detect the instantaneous frequency of the input signal, we can choose the DF responsible for a certain frequency range. A representation of the expected behavior of a wideband DF is shown in figures 5.17, 5.18 and 5.19; the input signal can be pre-distorded according to the specific frequency where is is modulated. An example of the PAE profile is shown in figure 5.20.
Let us now concentrate on the identification of a single DF; the identification process can be applied to each carrier frequency according to the wanted resolution. In our case the database extracted by means of ADS harmonic balance simulations at four different frequencies: 700, 800, 900, 1000 MHz.

For each possible carrier frequency we must solve a multidimensional problem which practically has an infinite number of triplets delivering the same output power, but not the maximum efficiency. Once we fixed the carrier frequency, a huge number of combinations for the input signals was fed into the ADS model of the DPA, and the output parameters ($Pout$,η, ϕ_O) were recorded. The number of combinations tested was about $9.000.000$ per frequency, thus the database for a single frequency results into a $7x9.000.000$ table. This is one of the disadvantages of this first identification method, having to deal with large databases. Another problem is represented by the discrete nature of the database. The resolution used to generate the triplets is limited and so the solutions identified within the database are affected by an error. We are trying to build a LUT of the pre-distorter, so we are going to choose a certain number of discrete points used later to apply an interpolation. The number of points used to build up the LUT of the drive function is arbitrary.

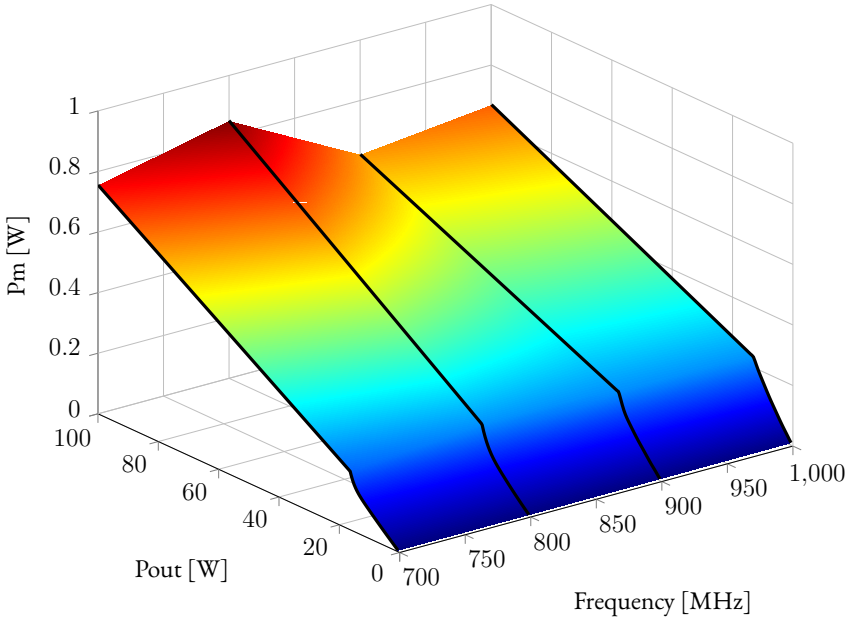

Figure 5.17: 3D Drive Function for MAIN PA.

In order to reduce the dimensionality of the problem, we can start from the identification of the MAIN DF using the process explained in section 5.2, which leads to an array of discrete values of power for the AM/AM conversion on the main path (PM_{target}). Since we want to obtain a linear AM/AM at the output, we need to define a target output vector made of linearly spaced power values (Pout). One of the requirements is for our DPA to deliver a maximum of 100 W, so we have chosen to use 200 values for the target output power vector $Pout_{target}$.
Once the MAIN DF has been identified we can use a simple euclidean distance formula to find the most suitable triplets on the database. The following formula is nothing more than the euclidean distance between the $i-th$ point in the reference array and the whole points contained in the dataset.

$$distance = \sqrt{(PM - PM_{target}(i))^2 + (Pout - Pout_{target}(i))^2 + (\eta - \eta_{target}(i))^2} \quad (5.6)$$

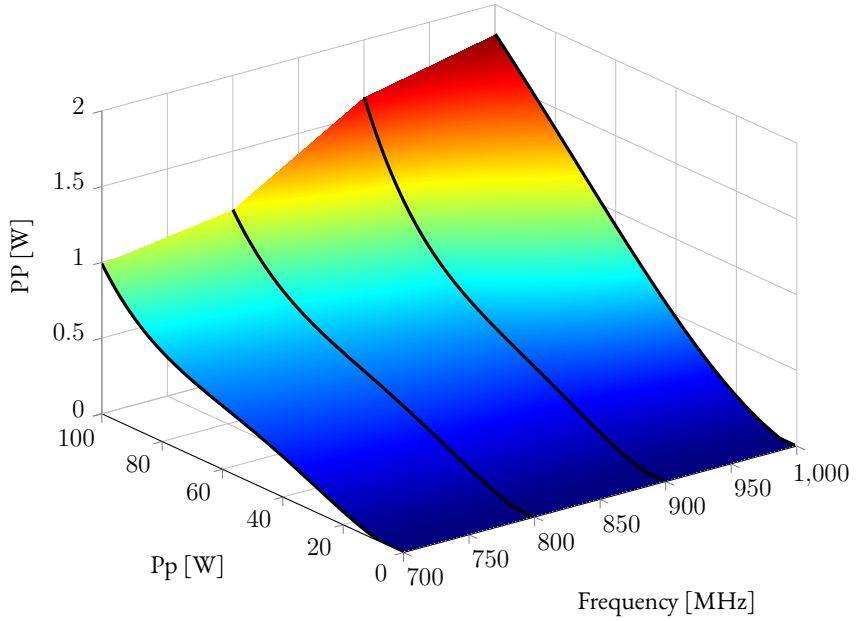

Figure 5.18: 3D Drive Function for AM of PEAK PA.

$$(Pm, Pp, \delta\Phi) => \underset{(PM,PP,\delta\Phi)}{\arg\min}\ distance(i) \tag{5.7}$$

This calculation is iterated on each point of the target vector, and every time the set of distances from the $i-th$ point is available, the point with the minimum distance is chosen.
This process allows to identify a narrow-band drive DFs for the chosen carrier frequency. The identified DF shows a very interesting characteristic. With increasing frequency the range of $\delta\Phi$ increases, realizing an irregular left handed behavior which is difficult to realize with a passive network. This explains why digital DFs are more performant than passive splitters.

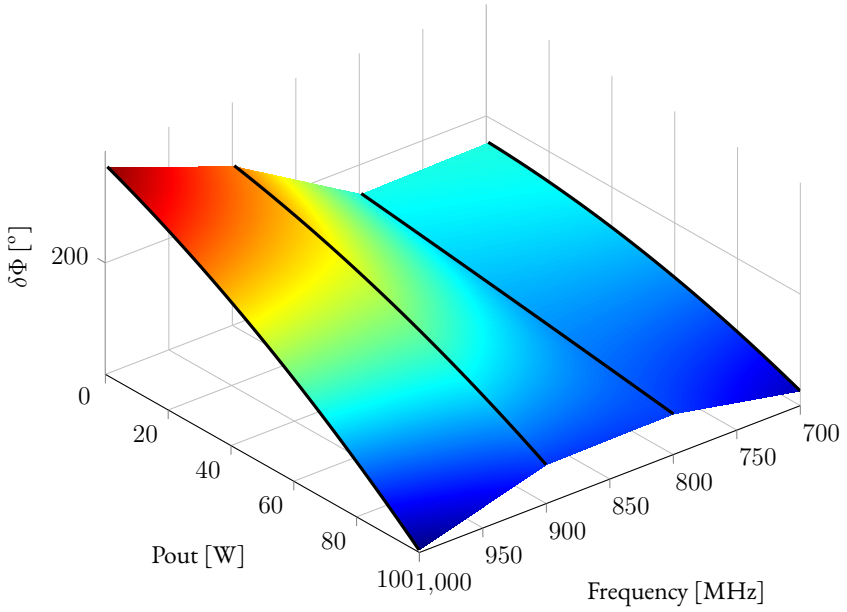

Figure 5.19: 3D Drive Function for PM of PEAK PA.

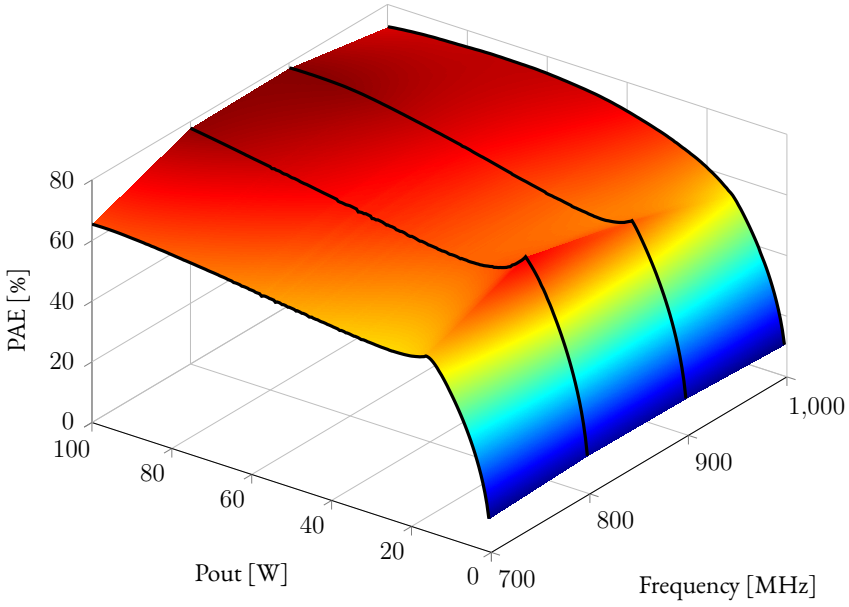

Figure 5.20: 3D profile of the PAE.

5.6 Reduction and Equalization of the Input Bandwidth Expansions

We have seen that the basic behavior expected by the digital DFs shows impulsive nature due to its discontinuities and sudden changes in their gradients. This could introduce limitations on the input side, due to the bandwidth limitations in the signal chain of the digital pre-distortion system.
Baseband complex polynomials applied to a signal are delivering a bandwidth expansion which is proportional to the order of the polynomial itself.
From the analysis of the Volterra series, we are able to study the harmonics and mixing products generated by a nonlinear static characteristic. Higher order harmonics are not influencing the adjacent channels, as they are far away from the carrier frequency. However we are normally concerned about the odd order mixing products as they are positioned in the proximity of the transmission bandwidth. For this reason, we normally account only for those terms in the polynomial models for DPD. An example of this behavior is shown in figure 5.21. With LUTs things work differently, because we have a finite number of points of the characteristic and we use them to pre-distort the original input signal by interpolation. It is easy to understand that this method is also affected by discontinuities in the derivatives. The points contained in the LUT act as blending points for the characteristic, where we have a C^0 continuity (no gaps in the characteristic) but no C^1 and C^2 continuity. As a consequence changes are introduced in the derivatives, which generate more unwanted spectral components.

Furthermore, with LUTs we generate both even and odd order nonlinear terms and we obtain a lower SNR.
In figure 5.22, we can see a comparison between a $5th$ order polynomial model and a LUT model using 50 points with polynomial cubic spline interpolation. We see that by using the LUT, the general noise level is also increased of about 40 dB. In order to mitigate the bandwidth expansion generated by the single drive functions, we need to smooth gradient variation in the DF, improving the continuity conditions of derivatives up to the second order (C^2). Starting from the MAIN DF obtained after the previous analysis, we know that the knee is responsible for the bandwidth expansion, and for the slow decay of the power density spectrum in frequency domain.

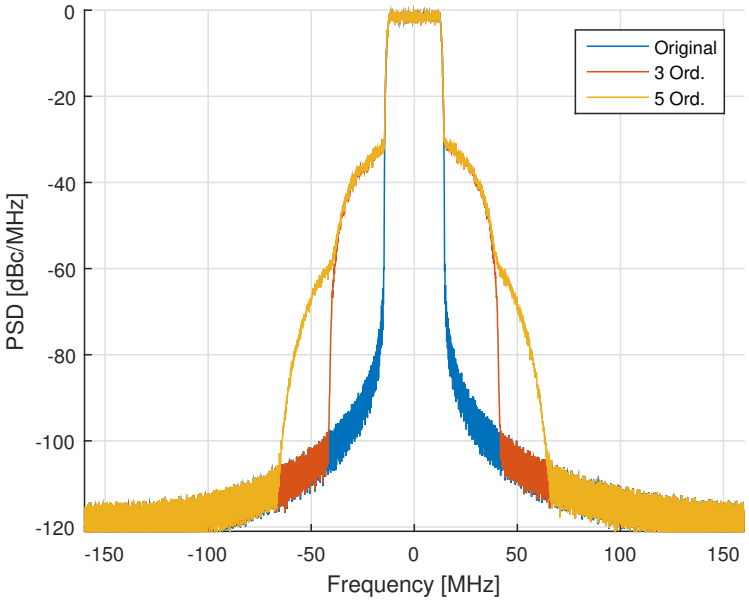

Figure 5.21: Bandwidth expansion through baseband polynomial.

The analysis of the dataset in figure 4.2 shows that we have freedom in choosing the shape of the MAIN DF, under the condition of fulfilling the wanted performance in terms of back-off and maximum efficiency.
Since in our approach we first determine the MAIN DF, we have to find a way to reduce the bandwidth expansion occurring due to the transitions of the input signal around the knee of the static characteristic. A very simple approach consists in redefining the DF as a piecewise function made of three sections:

- Inverse characteristic of the MAIN PA (1)
- Blending curve (2)
- Linear characteristic (3).

We have already seen the contribution of (1) and (3) in section 5.2, now we need to identify a blending function owning the characteristic of harmonizing the

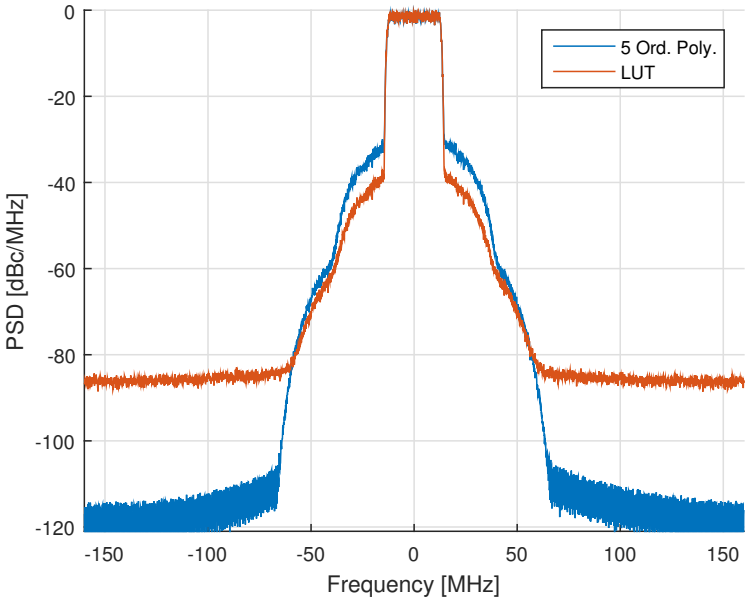

Figure 5.22: Comparisons of bandwidth expansions due to polynomials and LUTs. Far-off noise is very important as it could desensitize the own receiver.

gradient change between the principal segments. Basically we could compute the local derivative, respectively on the left and on the right side of the two junction points and then fit a monotonic function with such initial and final derivatives between those points. If we can make sure that the transitions (1)-(2) and (2)-(3) are sharing the same first derivative, then they are both C^0 and C^1 continuous. If we can verify the same hypothesis also for the second derivative, then we have also C^2 continuity, and the gradients are also changing with gradual speed, allowing for smoother changes in the spectrum of the predistorted signal. Such process would involve a lot of calculations and mathematical analysis of the problem. The problem of blending curves together smoothly is common also to other fields of application such as mechanics and computer graphics where precise and small curvatures are aimed for. The tool that we can apply to obtain this result quickly is called "Bézier Interpolant" or "Bézier Curve" [31], [32]. Those curves were invented by Dr. Pierre Bézier, a Renault engineer, about 50 years ago as a mean for curve formulation and shape design.

Given a certain number of masses, positioned at N points $(P_0, P_1, P_2, ..., P_N)$, we can calculate the position of their center of mass P as:

$$P = \frac{\sum_{n=0}^{N} m_n P_n}{\sum_{n=0}^{N} m_n} = \frac{m_0 P_0 + m_1 P_1 + m_2 P_2 + \cdots + m_N P_N}{m_0 + m_1 + m_2 + \cdots + m_N} \tag{5.8}$$

where it is assumed that the masses m_n are continuously changing as functions of a parameter $t \in [0, 1]$. The N points used to build the Bézier Curve are called control points, while the masses m_n are called blending functions and can be calculated according to the number N of control points chosen. The blending functions, also known as Bernstein polynomials are defined as:

$$B_n^N(t) = \binom{N}{n} (1-t)^{N-n} t^n \tag{5.9}$$

where $n = 0, 1, 2, ..., N$ and $\binom{N}{n}$ is the binomial coefficient. The equations of the Bézier curve as a function of the control points is instead expressed as:

$$P(t) = \sum_{n=0}^{N} \binom{N}{n} (1-t)\, t^n P_n \tag{5.10}$$

where P_n are the control points and N is the number of total control points. Bézier curves lie in C^1, but can also lie in C^2 under specific conditions [33]. Spline curves automatically offer C^2 continuity, but using such curves would not allow for the control of the curvature and so the bandwidth expansion.
Analysing our case we need to define control parameters to geometrically create a space between the two parts of the MAIN DF that we want to blend, in order to allow headroom for the progressive change of the gradients. In our case we can simply use a second order Bézier interpolant $(N = 2)$ which requires three $(N+1 = 3)$ control points. Referring to figure 5.23 we define the start and end point of the blending curve, Pa and Pb respectively. We then calculate the first derivatives on the left side of Pa and on the right side of Pb (which is a linear characteristic itself) and we use their meeting point Pj as third control point for the Bézier interpolant.

With $N = 2$ the Bernstein polynomials $B_n^N(t)$ involved in our approach are:

$$B_0^2 = (1-t)^2 \tag{5.11}$$
$$B_1^2 = 2t(1-t) \tag{5.12}$$
$$B_2^2 = t^2 \tag{5.13}$$

so the resulting formula for the Bézier interpolant P looks like:

$$P = (1-t)^2 Pa + 2t(1-t)Pj + t^2 Pb \tag{5.14}$$

where t changes in an interval between 0 and 1. By setting the granularity to subdivide the interval, we also choose the number of points to use in the LUT to describe the knee region. In figure 5.24 we can see the application of this concept to the MAIN DF, where Pa is identified by the coordinates (Pout_comp, Pm_comp) and Pb is (Pout_gap, Pm_gap).

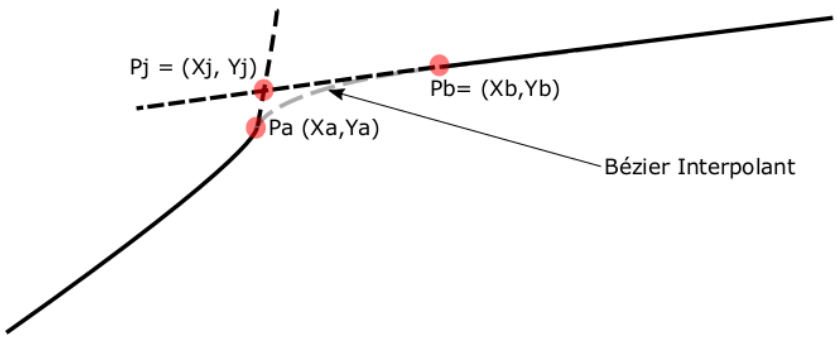

Figure 5.23: Bézier Interpolant.

Assuming this workflow, the MAIN DF is defined by a simple set of parameters:

- gap is an arbitrary value expressed in Watts to create a "spacing" for the Bézier interpolant

- Pout_comp is the output power set by choosing the compression point for the MAIN PA

- Pm_comp is the output power of the MAIN DF related to Pout_comp

- Pout_gap is an arbitrary output power at which the blending function must join the linear characteristic

- Pm_gap = $Pm\_comp + gap$ is the value of the output power of the DF for the blending point.

The defined MAIN DF is used as a starting point for the identification process presented in section 5.5 to obtain the PEAK DF. The PEAK identified DF also needs a similar smoothing process, which is suppressing the side lobes actually more than on the MAIN signal's path. In figure 5.25 we see the effect obtained by pre-distorting a 10 MHz LTE input signal using the smoothed versions of the MAIN and PEAK DFs. We have provided a C^1 continuity for the characteristic of the MAIN DF and we have also promoted the AM-AM characteristic of the PEAK DF from a discontinuity to C^1. Thus the spectrum of the signal on the PEAK signal path is now decreasing much quicker than before, meaning that the bandwidth expansion is greatly reduced.
Analyzing the resulting PSDs, we noticed that under these conditions the MAIN DF is less linear than the PEAK DF and generates slightly higher shoulders. In figure 5.24 we have also introduced Pm_target. This parameter, in conjunction with Pm_comp, influences the bandwidth expansion due to the MAIN DF. Changing these two parameters accordingly, reduces the gradient excursion between the blended curves, and decreases the spectral regrowth after the main DF is applied to the input signal. In figure 5.26 we see that changing the value of Pm_target gives an extra range of about 8 dBs to further control the linearity on the MAIN signal path. We will see later that in order to obtain high linearity at the output of the DPA, we need to apply a Static Phase Correction (SPC) to compensate for the AM-PM distortion introduced by the MAIN PA, and that this is compromising the bandwidth requirements. Changing the value of Pm_target could help in order to reduce such requirements and get closer to

the wanted specifications, depending on the application and the characteristic of the available DACs.

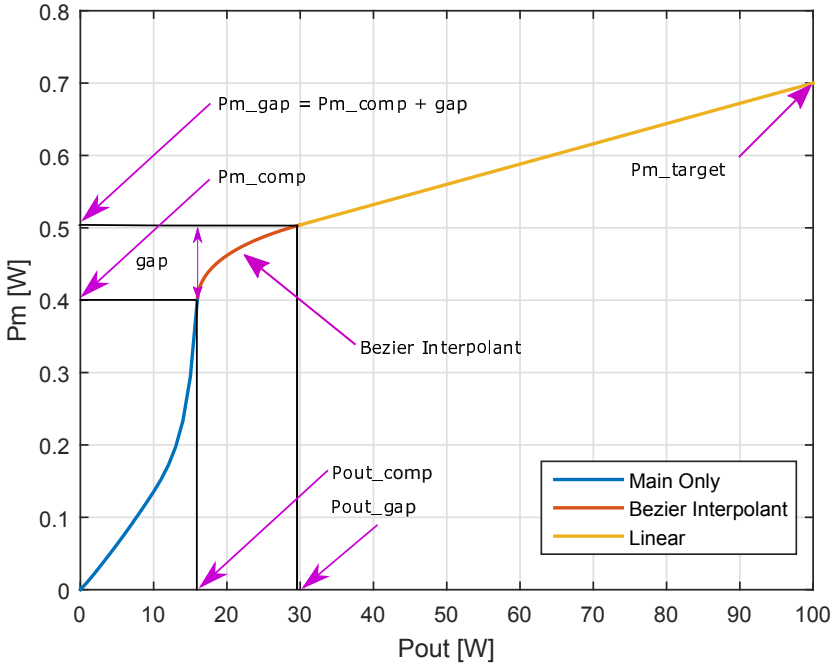

Figure 5.24: MAIN DF with mitigated gradient.

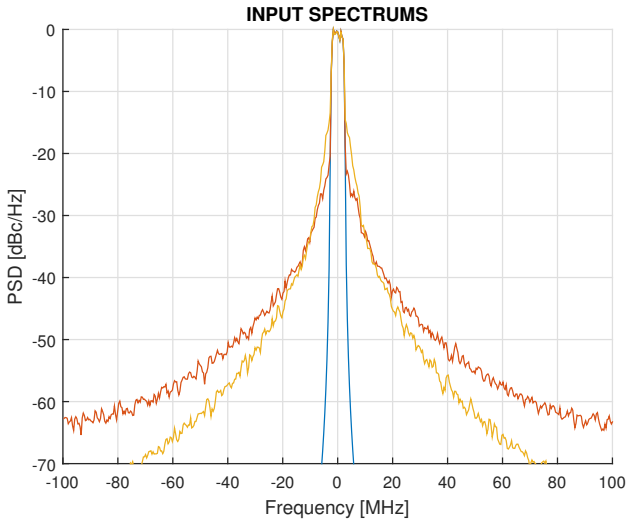

Figure 5.25: Spectra resulting from the smoothed MAIN and PEAK DFs.

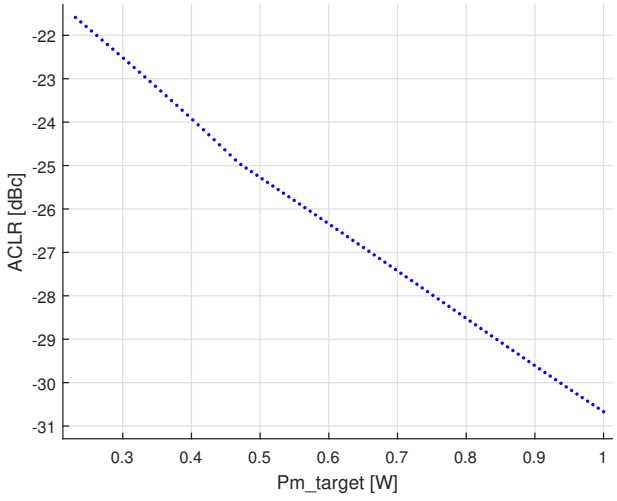

Figure 5.26: Effect of Pm_target on the linearity of MAIN DF.

5.7 Static Drive Function: Results

In the previous sections we have shown how, starting from the analysis of the device operation, it is possible to obtain a digital pre-distorter which allows full control over linearity, PAE and bandwidth expansion of the pre-distorted signals. We will now show the performance achievable using this approach in conjunction with the model of the analyzed DPA.
Let us consider a 5 MHz LTE signal with a peak power of 1 W and a PAPR of 10 dB modulated at $F_c = 900\,\mathrm{MHz}$.
Applying the static digital DF shown in figure 5.27, we correct the static nonlinearities of the DPA, obtaining the linear input-output characteristic presented in figure 5.28.

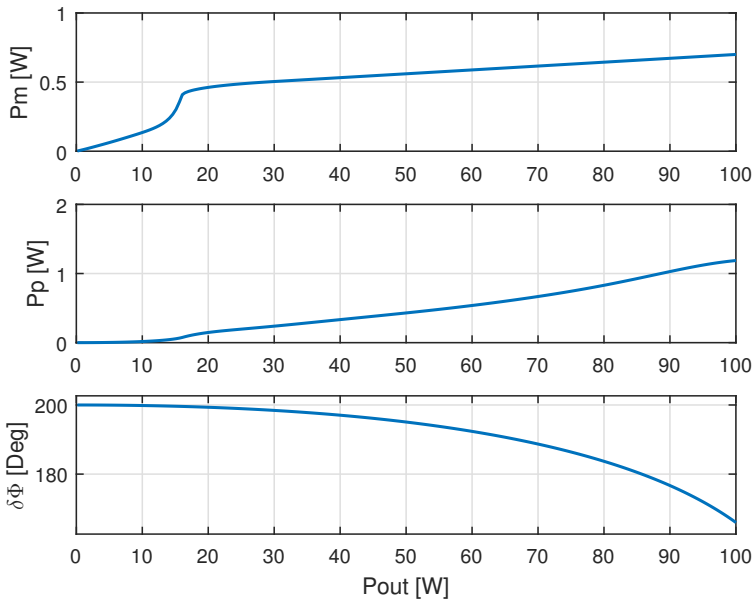

Figure 5.27: Example of DF at 900 MHz.

If we analyze the PSD of theDPA characteristic after the DF, we notice that the ACLR lies only at about 30 dBc. This is caused by the fact that the identification process considers only the system between the two independent inputs of MAIN and PEAK PAs, and does not account for the whole phase difference

between the input of the LTE signal and the output of the PA (figure 5.30). Such phase characteristic is represented in figure 5.30 and it can be corrected only after the DF is identified.
The identification can now be performed by using the LTE signal as excitation signal to extract the static phase characteristic of the DPA in series with the DF. The static phase relationship is then modeled using a simple static polynomial and it is then inverted and used to apply a SPC to the input signal. By doing so we obtain a huge improvement of the linearity which is visible on the spectrum of the output signal in figure 5.30.
As it is demonstrated, the approach leads to a huge improvement of the linearity, the ACLR dropping from 30 dBc to 52.4 dBc (22 dB better than with the DF only).

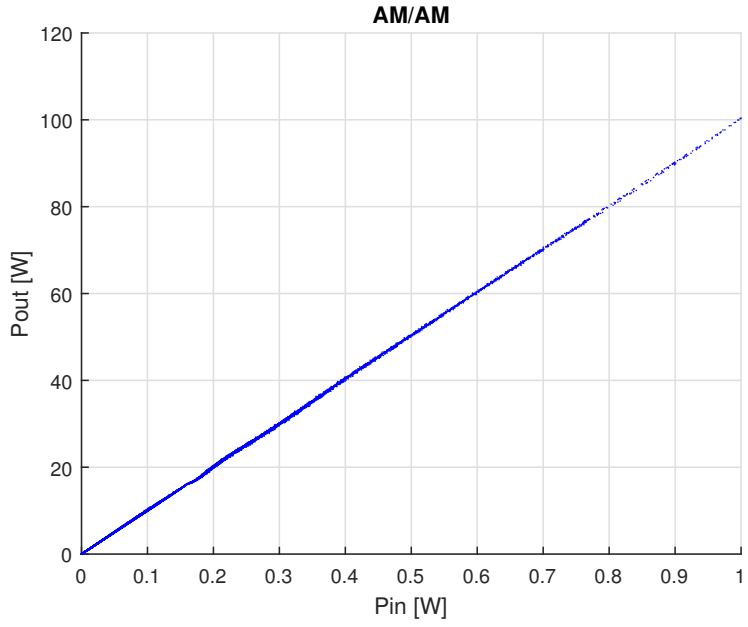

Figure 5.28: Linearized input-output characteristic of the DPA.

In figure 5.29 are presented the AM-AM and AM-PM characteristics of DPA and DF before and after the SPC. The x-axis for this characteristic is expressed in dBFS, this is because the DF is thought for an implementation in the digital domain where the available power levels are expressed in relation to the full scale provided by the digital converters.

By evaluating the AM-AM and AM-PM characteristics in dBs, we can better appreciate their dispersive nature which is due to the memory effects present inside the system. This result can be also noticed in figure 5.30; in general the presence of asymmetry in the shoulders of the signal spectrum is due to the memory of the system.
The performance, in terms of average PAE, depends on the signal's statistic. In our scenario, which is shown in figure 5.31, a signal with a PAPR of 10 dB can drive the whole system to provide a PAE of about 50%. Our simulations are showing a PAPR which is about 51%, which is a very good result compared to the previously published works and also compared to the state of the art. Looking at the state of the art, such performance can be obtained by applying CFR techniques in order to change the signal's distribution and decrease the PAPR. With our approach, we obtain very good results without making use of such techniques.Therefore, introducing into this architecture could theoretically allow to obtain even higher PAE close to, $60 - 70\%$.

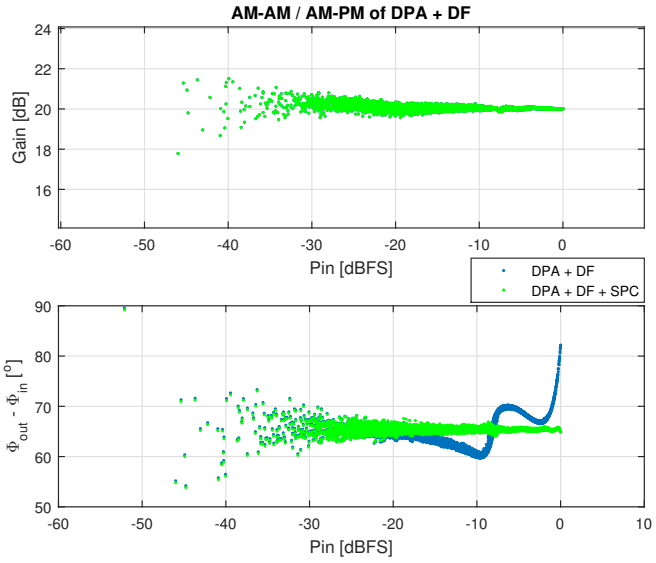

Figure 5.29: AM-AM and AM-PM characteristics of the DPA + DF + SPC.

The results obtained are valid for relatively narrowband scenarios. Results were validated applying the same DF at 900 MHz to different versions of the LTE signal (1.25, 2.5, 5, 10, 15 and 20 MHz) and tracking the value of the average PAE

obtained with such signals. Doing so, we noticed that the average PAE tends to drop when the bandwidth of the signal is increasing (figure 5.32). This is possibly due to the fact that the single static DF are dispersive in frequency and quite narrowband. A stochastic approach which brings the frequency into the model of the DF could solve this problem and remove some dependency of the obtained PAE from carrier frequency of the signal. For this scope it would be useful to implement an identification technique based on the concept of instantaneous frequency, so that every frequency component inside the bandwidth of the information signal would be pre-distorted with the right characteristic in frequency domain. Another advantage of bringing the signal statistic into the model is that it would make possible to adaptively change the shape of the DF as a function of the peak power of the input signal. This would make use of the ability to reprogram the linearity and efficiency of the dual-input DPA according to the current signal statistic, laying down the concept of a dynamic DF.
The literature about the linearization of dual-input Doherty PAs is not very rich but our approach, in relation to the currently developed techniques presented in [30], [34] is showing very good results and potential for further improvements.

Approach	Signal type	BW [MHz]	PAPR	ACPR [dB]	PAE [%]
[30]	WCDMA	5	7	45	40
[34]	LTE	5	8.5	53	43
New approach	LTE	5	10	56	51

Table 5.2: Comparison of the performances with present literature.

A comparison of our approach with the previous published methods is resumed in table 5.2. By comparing each methods the performance with similar signals, we noticed that our physically motivated approach allows to obtain much higher performance out of the DPA because it makes use of all the knowledge available to optimize the linearization at a higher level. In both the previously published works, the signals had a higher PAPR, suggesting that CFR was possibly applied. Using the optimal DF (optimal in terms of linearity, efficiency and input bandwidth expansion), we can obtain very high linearity and we can increase the average PAE of about 8 % in comparison to the other approaches. A further estimation of the improvements achievable making use of CFR can be

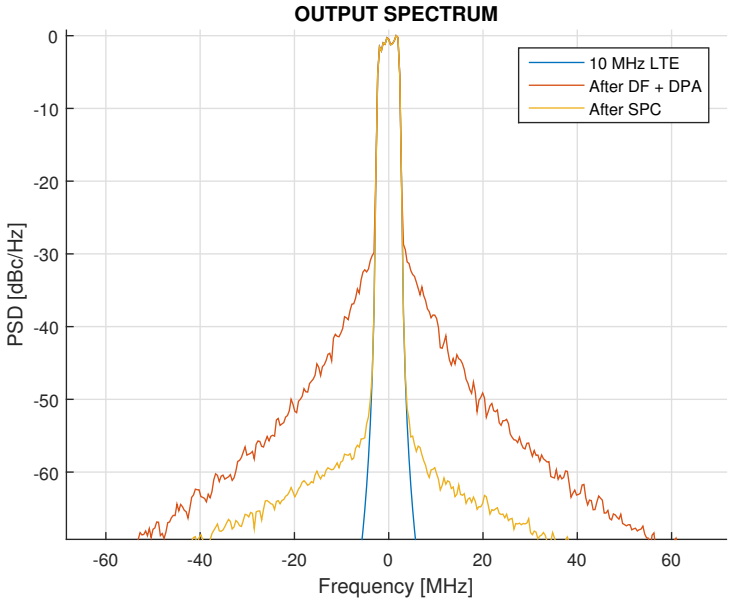

Figure 5.30: Spectrum of the linearized DPA and DF after static phase correction.

done analyzing figure 5.31. If we would also reduce the crest factor of our signal to 8.5 dB, we would obtain an average PAE of about 65 %.
The authors of the technique in [34] have identified a static signal splitter optimized only for the maximum efficiency, every further static and dynamic nonlinearity was then corrected making use of a vector switched model [35], which adds an extra level of complexity to the pre-distorter. Our approach requires only a simple static polynomial to apply the SPC to linearize the phase between the input and output of the system. As a consequence our DF is allowing good results without taking memory into account. This is visible in figure 5.30 because the spectrum shoulders, after the linearization, are not symmetric.
Until now we have analyzed the static part of the steering function. Once this has been identified, we can additionally identify the memory of the system in order to correct it if needed.

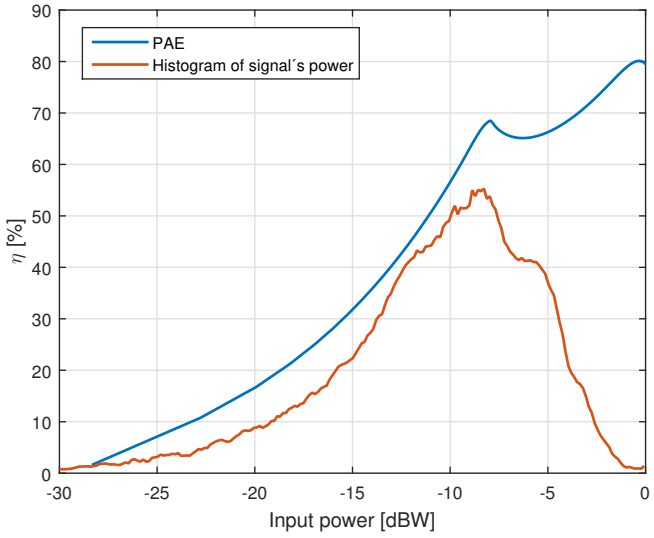

Figure 5.31: Estimation of the DPA efficiency with power histogram.

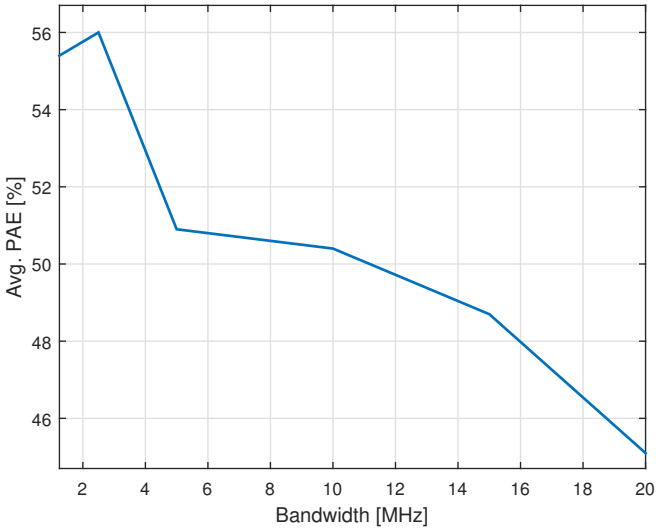

Figure 5.32: Bandwidth vs. PAE.

5.8 Drive Function with Memory

In section 5.7 we have shown the performances delivered by a DPA using our physically inspired linearization approach. By applying the digital DF to the DPA followed by a simple SPC, we can obtain both high linearity and average PAE.

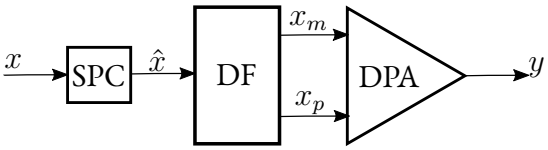

Figure 5.33: Complete scheme for static DF.

In figure 5.33 we see the block diagram of the system including the SPC to linearize the whole AM-PM characteristic, the digital DF implemented as a LUT and the dual-input DPA. For simplicity in the representation, we assume that the DPA block is also containing the IQ-modulators/demodulators, converting the complex-baseband signals to RF. The represented signals are:

- x : LTE complex-baseband input signal
- $\hat{x}$: LTE input signal with statically corrected phase
- x_m, x_p : MAIN and PEAK input signals modified by the digital DF
- y : complex-baseband output signal.

In the presence of such a signal chain, we obtain a linear power characteristic between x and y. But referring to figures 5.29 and 5.30, we see that the system still presents memory effects, because we see dispersion in the AM-AM and AM-PM characteristic and the power spectrum presents asymmetric out-of-band shoulders [36]. Memory effects are very well explained in the literature, many books ([1], [2], [3], [37], [38], [39]) and papers ([40], [41], [42], [43]) are dedicated to this topic. In [2], Steve Cripps mentioned that memory effects are

"an additional source of nonlinear behavior that is typically not accounted for in PA models". Nowadays this affirmation is not true anymore since manufacturers are able to deliver accurate models of their devices, while representing such effects. In our case for example, as we have stated in section 4.2, we have a model containing memory effects with respect to the temperature of the transitor junction and memory effects generated by the matching and bias networks. Following the definition given in [1], memory is a concept related to the dependence of the present value from the values that the signal assumed in the past time. The simplest example of such effect is the behavior of an R-C circuit, where the current flowing into it is depending on the quantity of charge previously stored inside the capacitor.
Memory gives birth to time constants, between its input and output (namely rise and fall time), that are affecting the characteristic. This is true for CW-signals but also for modulated signals with a larger bandwidth and so with several frequency components; therefore memory effects are also depending on the bandwidth of the signal. We can divide such nonlinear effects into two main categories namely short-term and long-term memory effects, depending on their time constants. Short-term memory effects are generally due to:

- Matching networks : capacitors, inductors and transmission linear
- Device capacitance : transport of charge inside the nonlinear device

while long-terms memory depends on:

- Thermal effects : flow of thermal energy, time constant related to time envelope of the signal
- Charge trapping : imperfection in the semiconductor material
- Bias circuit : re-modulation of the signal due to gain variation
- Control circuitry : time constants longer than RF cycle.

Further analyzing our system chain, we should point out the similarity with the Wiener model introduced in section 3.2; the SPC and static DF are representing the block correcting the static non-linearity introduced inside by the dual-input DPA. Thus we now need to identify a linear dynamic block correcting the memory inside the system. To detect the memory length of the system, since memory is depending on the signal bandwidth, we can analyze the system response to band limited signals with increasing bandwidth. Ideally we could use square pulses to characterize the memory but they generate a large spectrum which is theoretically infinite. Gaussian pulses offer a possibility to control the trade-off between frequency and time behavior. In general, any pulse could be used for this purpose because we can control the bandwidth by changing the pulse duration. The general relationship between minimum bandwidth and pulse duration, for Gaussian pulses is obtainable by [44]:

$$BW \cdot T > 0.44 \tag{5.15}$$

where BW is the bandwidth of the signal expressed in Hz and T its duration expressed in s. Inverting this very simple formula we obtain an inferior limit to the maximum duration of the pulse:

$$T > \frac{0.44}{BW} \tag{5.16}$$

Using this formula we just find a lower bound to the pulse width in frequency domain and we meet two technical problems: we do not have pure control on the input signal bandwidth and with the sampling frequencies we are using, we end up with very short pulses which are made of few samples in time domain. Thus we have decided to make use of ramp signals where we control the bandwidth by changing the duration of the pulses, which results in a much easier analysis.
We can appreciate the results obtained using a single triangular pulse with a 1 MHz bandwidth ($T = 4.4 \cdot 10^{-7}$ s) in figure 5.34. As we mentioned, the simulation accounts for transistor self heat. Self heating generates memory effects and leads to performance degradation. In our case, also if the junction temperatures (T_jm and T_jp) of the devices are varying , we can we can appreciate the effects of the linearization through the DF. The output looks perfectly linear in power domain (Pin, Pout). The real dual-input DPA is provided with

a liquid cooling system, so in the laboratory we can keep these junction temperatures constant, thus we can expect better performance than in the simulations.
Another, very useful representation of the nonlinear effects is obtained by plotting the complex baseband signals on the I-Q plane (figure 5.35). On the I-Q plane we can describe circular areas which represent the space where a vector has constant amplitude and is free to rotate changing its phase. Remembering this, we can discretize the space where our complex signals live, and track the effects of non-linearities as closed paths on the I-Q plane. The blue curve, for instance, represents the case where the AM-AM of the system is linear, but the phase between input and output needs a static correction. After applying the SPC we correct the whole phase difference; and as a consequence all the nonlinearities of the device are compensated (green curve). Please notice that the vector representing the original signal is not visible because it is totally covered by the linearized output.
This representation is very helpful to resume all the static and dynamic nonlinear effects at once.
Memory should provoke an hysteresis in the signal path which is usually visualized as an aperture of the I-Q diagram. In the described scenario we do not experience a visible memory effect, because we see no aperture and the signal is raising and falling on the same path.
To excite dynamic memory effects we can use the same signal and diminish the pulse duration in order to increase the pulse bandwidth. For instance, we cold take a 20 MHz signal and use it as stimulus for the system ($T = 2.2 \cdot 10^{-8}\,\mathrm{s}$).
Comparing the results in figures 5.35 and 5.36, we see can distinguish two important contributions to the linearization. First there are about 15^o of static correction to linearize the phase left uncovered by the DF. Second there is a constant phase offset to align the linear output signal to the input signal. We also see that now the I-Q path shows an hysteresis (figure 5.37), which is only due to the memory inside the system. The input signal is experiencing a lower gain on the rising edge, and higher gain on the falling edge, thus we see this aperture on the AM-AM characteristic. A similar aperture is also experienced on the AM-PM of the system.
Once we have identified this behavior, we could apply any adaptive algorithm (such as Recursive Least Squares (RLS) or LMS) to identify the filter needed in order to compensate the memory inside the system.
What we learned from the results in figures 5.28 and 5.29 is that we are dealing with a system which presents an AM-AM characteristic which is very close to a

linear characteristic one and an AM-PM which presents a dispersion of about $8 - 10^o$. The identification of such nonlinear filter would be very complicated, but with making some basic observations we could simply correct part of the memory effects by dynamically correcting the AM-PM characteristic only. Referring to figure 5.38 we have analyzed three different cases to see the effect of correcting the AM-AM and AM-PM separately in polar coordinates.
We noticed that after applying the static corrections to the system (DF and SPC), we have a system which is as close to linear as the precision involved in the identification procedure has allowed.
Memory effects are responsible for the asymmetry of the components of the inter-modulation distortion, and so of the spectrum of the output signal, therefore it is also responsible for the dispersion visible in both AM-AM and AM-PM characteristics (case [a]). If we assume that our system would have a linear AM-AM and nonlinear AM-PM (case [b]), we would obtain a 4 dB improvement of the Adjacent Channel Power Ratio (ACPR) (58 dBc meaning also better linearity) keeping a reduced spectrum asymmetry which is barely visible on the graphs.
A final study case is when we do not change the AM-AM characteristic and we apply a dynamic phase correction to the system, influencing the AM-PM only (case [c]). Doing so we obtain the same ACPR obtained after the static corrections but we remove the spectral asymmetry and partially the memory effects.
It is not possible, in general, to separate memory effects between the AM-AM and AM-PM characteristics separately. But by having control over the device physics, it is possible to identify the macro effects controlled by each parameter, and think about new ways to draw the maximum performance from the system. A further study of the memory effects correction is left to future work.

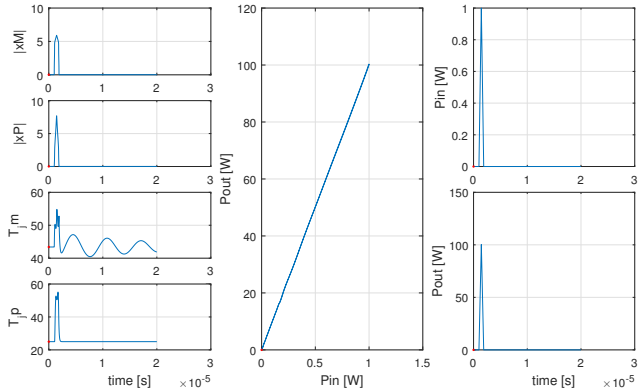

Figure 5.34: Memory effects with saw-tooth (1 MHz bandwidth).

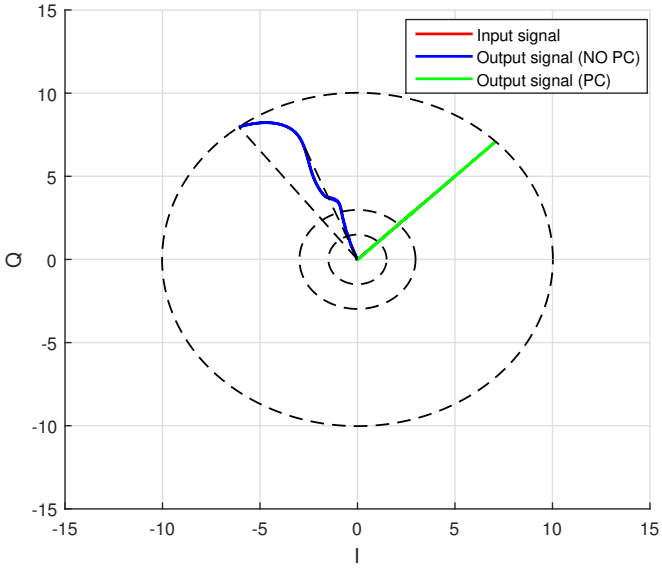

Figure 5.35: Memory effects with saw-tooth (1 MHz bandwidth) on the I-Q plane.

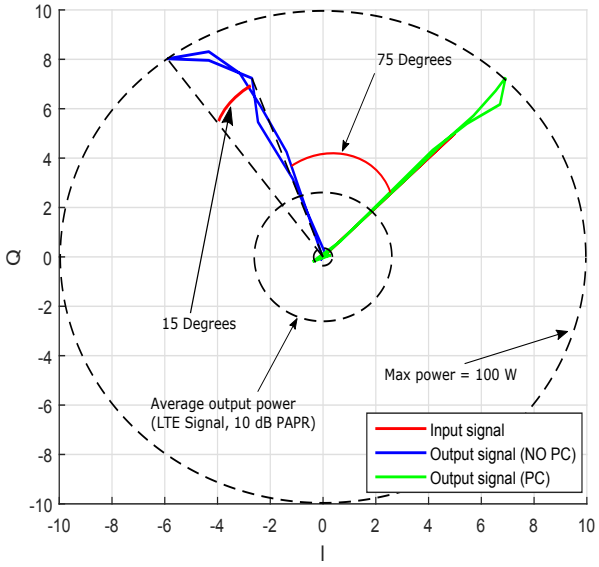

Figure 5.36: Memory effects with saw-tooth (20 MHz bandwidth) on the I-Q plane.

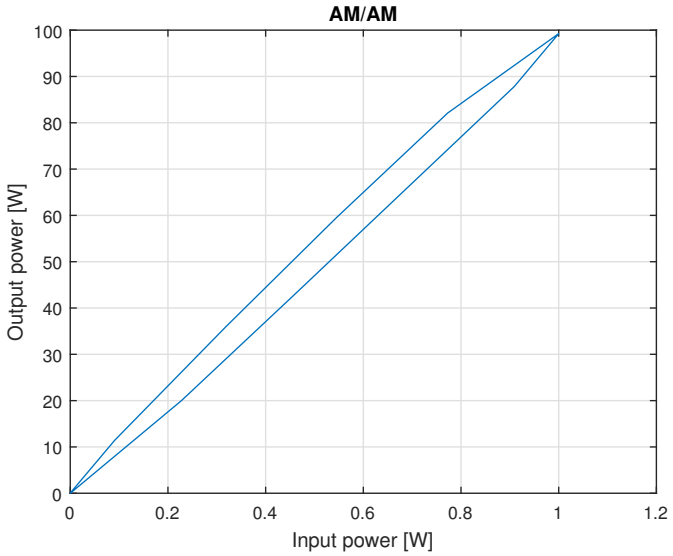

Figure 5.37: Memory effects with saw-tooth (20 MHz bandwidth) on the AMAM characteristic.

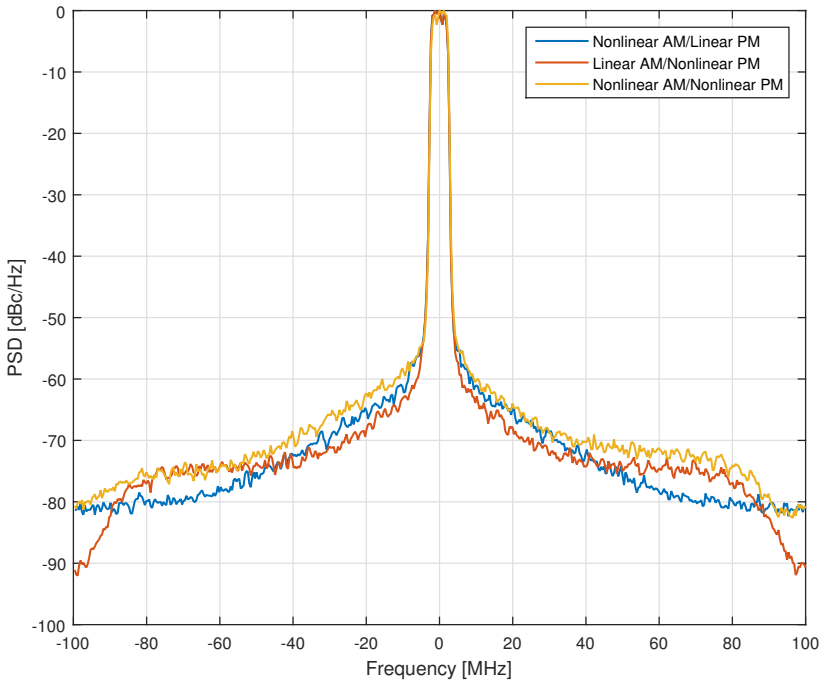

Figure 5.38: PSD comparison with [a] nonlinear AM and PM, [b] linear AM and nonlinear PM and [c] nonlinear AM and PM.

5.9 Effect of the Static Phase Correction on the MAIN Path

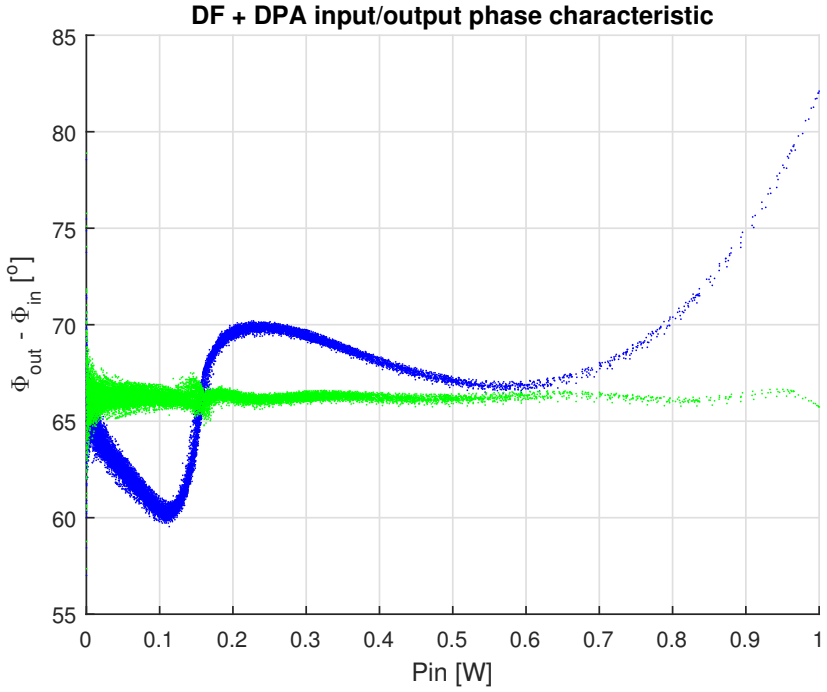

Figure 5.39: I/O phase difference as a function of the input power.

The phase difference between input and output of the system, represented in figure 5.39, is the result of the cooperation between MAIN and PEAK PAs. We have shown how the application of the SPC allows high linearity maintaining also high average PAE in presence of a dynamic input signal.
Previously in section 5.7, we have introduced the concepts enabling to control the bandwidth expansion of the input signals thanks to the static DF. Smoothing the characteristics of the DFs properly and setting the right values of the parameters, we could control the behavior of the input signals in frequency domain and find the best trade off.
Analyzing the same input spectra, after applying the SPC, we have seen that the signal on the MAIN path is subject to an extra bandwidth expansion. This

effect can be observed in figure 5.40. The shoulders of the PSD related to the MAIN input channel are rising of about 18 dB while the PEAK keeps the same behavior. This happens because before the entry point of the PEAK PA, the MAIN operates alone and the nonlinear effects inside the system are only due to it. A way to verify this is to operate the MAIN and PEAK PA modifying the static DF to split $\delta\Phi$ between the two signal paths, as depicted in 5.41. This way of operating allows the phase splitting between the MAIN and PEAK PA AM-PM characteristics, keeping the same $\delta\Phi$ between the inputs of MAIN and PEAK, with the scope of trying to improve the performance of the DFs in terms of bandwidth expansion at the inputs of the DPA. The results of this test have shown that the phase splitting does not change the bandwidth expansion of the input signals, this is because the AM-PM of the DF is a monotonic function and varies the signal's phase by a constant value at each input power level.

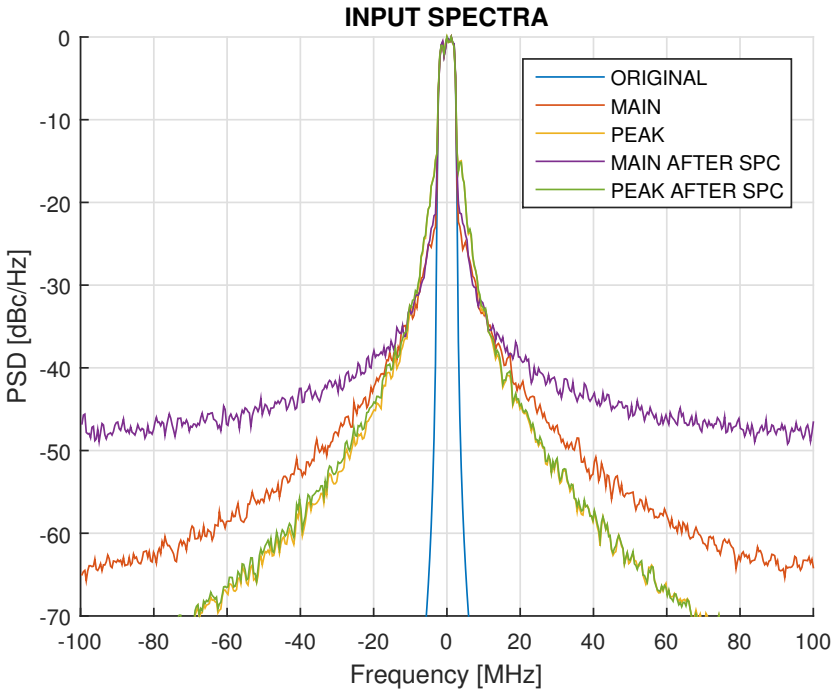

Figure 5.40: DPA input bandwidth expansion before and after SPC.

This result is remarkable because it is showing two important aspects of the linearization for dual-input DPAs. First the linearization of the MAIN PA re-

quires extremely more input bandwidth than the PEAK PA, because after correcting the discontinuity of its characteristic it becomes more linear than the AM-AM of the MAIN DF which is also continuous but with a high clipping factor. Second we obtained a further confirmation of the relationship existing between the $\delta\Phi$ and the drive level of the PEAK PA. Indeed also if the phase split keeps same phase difference between MAIN and PEAK, the linearity and efficiency obtained charging the whole $\delta\Phi$ on the MAIN are drastically reduced. This opens the discussion on the possibility to identify the DF by using four parameters instead of just three, separating $\delta\Phi$ into $\delta\Phi_m$ and $\delta\Phi_p$. Future work should concentrate on the effects that could be obtained by splitting the AM-PM between MAIN and PEAK.
The huge bandwidth expansion on the MAIN channel is then only due to the nonlinear phase characteristic of the PA since the MAIN PA operates alone in the power range under the compression point.

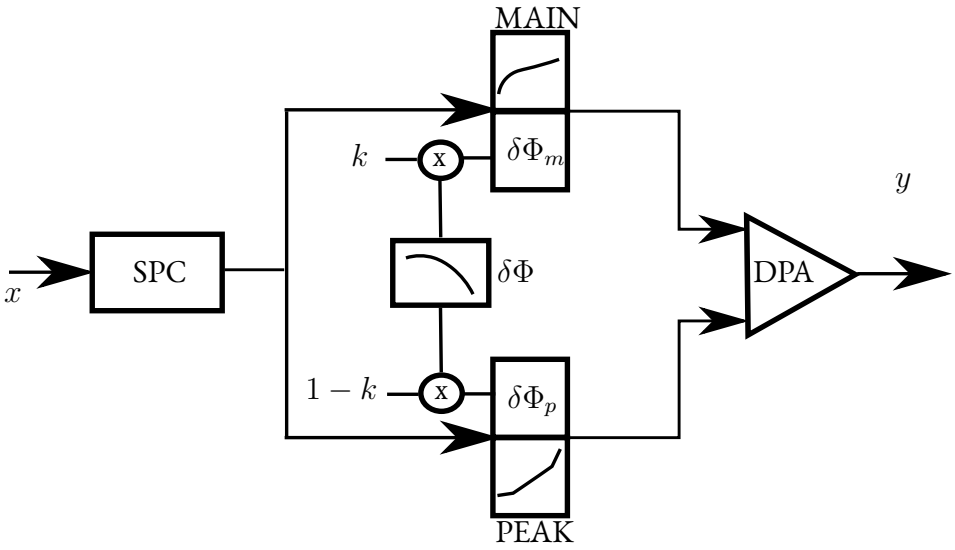

Figure 5.41: DF with phase splitting.

Making DC sweeps on V_{GS} and V_{DS}, we obtain a set of intrinsic static characteristics of the device which shows two nonlinear effects: saturation and dependency on the temperature. When the PEAK PA is completely off, the load

modulation of the combiner is not operated. When the MAIN PA is on and the PEAK PA is off, the MAIN PA sees a high ohmic impedance which stays constant until the PEAK PA turns on, allowing V_{DS} to swing over the whole available voltage range.
Under this condition, if we apply a LTE modulated signal at the input of the MAIN PA and observe the output of the combiner, we obtain the behavior shown in figure 5.42. From the dynamic loadlines of MAIN and PEAK PAs we notice that both the devices are subject to high voltage swings, but the MAIN PA is showing an hysteresis in the middle power range. Such behavior is generated by the AM-PM distortion due to the MAIN PA operating in class AB, and can be explained by means of a Volterra series expansion (of relatively low order) of the drain current, I_{DS} for the small signal model. Analyzing the resulting non-linear Volterra transfer functions in presence of a band limited signal, we are in the presence of a memoryless non-linearity for low input power, therefore we have just AM-AM conversion.
By increasing the power of the input signal, we noticed that the resulting load line is not straight, instead it is presenting an aperture. This effect is depending on the sensitivity of the circuit to envelope dynamics. This aspect is influenced by passive components such as the DC blocking capacitors and the RF choke. For a class AB amplifier, such as the MAIN PA, this is happening when the signal reaches the limits of the saturation, generating even order non-linearities which are responsible for the generated aperture, and so for the AM-PM characteristic. Pushing the device even more into compression, where the device is working in triode region, leads to a clipping of the I_{DS} current which determines a strong presence of odd order terms and an attenuation of the second order terms. This behavior, which is close to having a square wave, leads also to a negligible order of non-linearity and reduces the AM-PM distortion as the input power is increased, nullifying the hysteretic effect experienced at medium input power. This behavior is exhaustively explained in [45] where a deep analysis of the behavior of the PA is performed.

This motivates the presence of the AM-PM distortion experienced in the dual-input DPA under the PBO point. Furthermore in [15] a detailed analysis of AM-AM and AM-PM distortion generation for LDMOS and GaN HEMT devices was performed, showing that the AM-PM observed in our DPA is typical of class AB PAs. The application of the SPC correcting the AM-PM distortion introduced by a class AB amplifier allows high linearity at the output of the

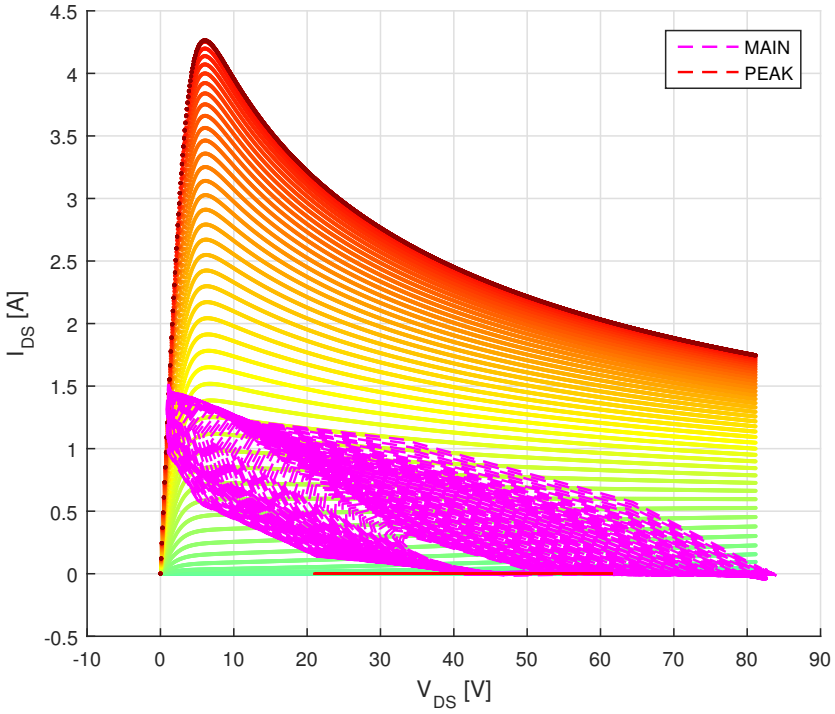

Figure 5.42: Behavior of the small signal mode with LTE modulated input signal.

DPA but causes very high bandwidth requirements for the DAC on the MAIN signal path. This requirement is much higher than the one for the PEAK PA. A possible solution would be to design the MAIN PA to be more linear, hoping to obtain a monotonic AM-PM and keep the bandwith requirements at the input of the MAIN PA as low as possible.

Chapter 6

In-situ Calibration Technique for Static Drive Function

6.1 Introducing the new technique

With the scientific work pursued in the previous chapters, we have shown what are the advantages, but also the disadvantages, of using dualinput DPAs in BS technologies. By separating the input branches of the DPA, we are able to apply physically-motivated linearization algorithms, throwing less heavy maths into the realization of the linearizer, allowing to program the PBO point of the device, obtaining both high linearity and efficiency and allowing to control the bandwidth expansion of the predistorted and output signals. Once the digital DF is identified and applied to the DPA, we can evaluate the positioning of our PA architecture in relation to the requirements. In our case, by having more degrees of freedom in the choice of the parameters, we increase also the space where we perform the trade-off of the requirements (Figure 6.1). In a classic scenario, we want to reach the best trade-off between the requirements which are, a high average power efficiency (which is also waveform specific), linearity and output power. In the new presented scenario, we are interested in setting the bandwidth expansion of the predistorted signal thus adding a new dimension to the problem and so a new degree of freedom. In [30] the authors have obtained an efficiency optimized static digital splitter, which needed an external and complex vector switched model to correct the non-linearity and the

memory. The splitter that they presented was identified by sweeping the input signals of the DPA around a specific domain where maximum efficiency was obtained. Such sweeps were performed by means of ADS HB simulations to avoid risks when operating with the true DPA.
Unfortunately not many details about the identification process have been discussed, and the optimization was performed only by taking into account the efficiency while the linearity was left to a common DPD block.
Our approach allowed us to identify the static part of the DF making use of an intelligent algorithm, based on the knowledge of the device to obtain optimum performance in both linearity and efficiency, allowing also to control the input bandwidth expansion (as much as the AM-PM distortion allows it). In chapter 4, we introduced the data set used to perform the study of our physically inspired DPD and to lay down an identification process suitable for this kind of amplifier and application.

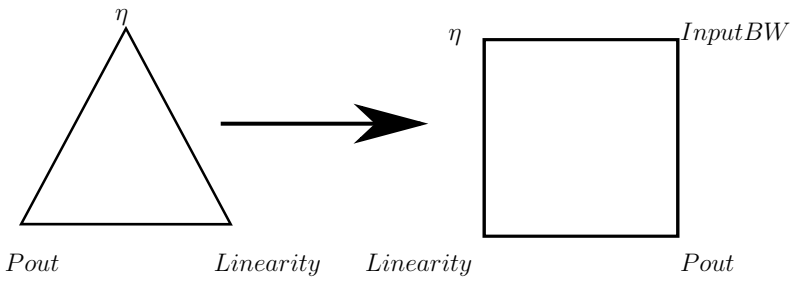

Figure 6.1: Trade-off for requirements in dual-input DPA with DF.

By means of power sweeps in HB simulations, the whole input domain of the power amplifier was swept but this was extremely time consuming and also did not take in account the limits of the DUT, risking damages to the device in a real test bench. In chapter 3 we have shown various states of the art algorithms for the identification of PAs, but their validity was restricted to SISO systems where the nonlinear effects were "well behaved" and the functions describing their nonlinear effects are depending on few parameters.
A DPD algorithm for dual-input DPA was developed in [30], but we have seen that this algorithm did not allow the performance that can be obtained by using the knowledge of the device characteristics.

Fast FPGA-based digital systems were used to identify and pre-distort PAs and as the clockrate of the technology increased, they allowed the realization of new high speed identification approaches and fulfill the requirements on the necessary bandwidth expansion for the pre-distorter.
The price to pay to reach such ambitious results was the increasing complexity of the digital hardware, because we needed to drive two separate inputs and so have two independent and similar DACs, double the logic implementing the pre-distorter and allow enough data rate to manage the required bandwidth expansion.
We developed our digital DF in form of a LUT because of its simplicity, therefore we also need to find a suitable identification process. Such work flow must allow the optimization for linearity and efficiency at the same time, be simple and must be converge fast. To do so we have to revisit the identification problem and adapt it to our dual-input DPA.

6.2 Novel Identification Approach

We can imagine the problem of the identification of a static DF, at a given carrier frequency, performed by the black box shown in Figure 6.2, where Pm, Pp and $\delta\Phi$ are reflecting the values of the input powers for MAIN and PEAK amplifier and the phase relationship between them. At the output of the model we have power (Pout) and power added efficiency (η).
Seen in this way, the identification of a single drive function can be exploited as a multidimensional nonlinear optimization problem. Specifically if we could try all the possible triplets (Pm, Pp, $\delta\Phi$), we would end up discovering that there is a theoretically infinite number of combinations leading to the same output power. The challenge relies in identifying the triplets maximizing the efficiency for a specific power level and frequency.

Referring to Figure 5.1 we recall the very important concept that several triplets allow the generation of the same output power, but only few of them allow maximum efficiency. This was already explained in chapter 5, now we can make use of the acquired knowledge on the behavior of the device and use it to implement an *in-situ* identification technique that can be applied directly on the device and under total safe conditions.

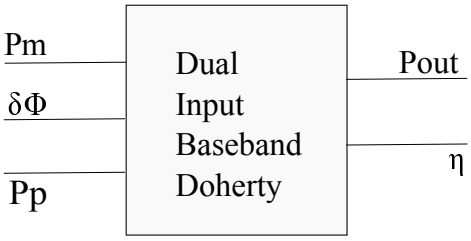

Figure 6.2: Dual-input identification concept.

In order to safely prove the concept, and in absence of an adequate measurement system, we made use of our co-simulation environment interfacing MATLAB and ADS.
We started by defining the characteristic of the MAIN DF as we explained in chapter 5. We left the PEAK PA off and we swept the MAIN input power until saturation. We then chose the compression point according to the wanted PAE. As we have demonstrated, the choice of the MAIN DF allows to control the input bandwidth requirements and to configure the efficiency at PBO.
Another important aspect, which results from the analysis of the DPA data set (Figure 4.2) is that there is a relationship between the absolute output phase (ϕ_O) and the PAE (η). Such relationship can be used to find an appropriate cost function to be used with an intelligent algorithm in order to obtain a power optimized lineazizer for the dual-input DPA.
A linear system ideally presents a linear AM-AM characteristic and a constant AM-PM characteristic. In Figure 6.3 we see a block scheme of our simulation environment. When running the identification of the MAIN DF, the simulation returns also the value of the absolute output phase which can be used to define a linearity criterion for the phase. Forcing the DPA to keep this constant value of the output phase at every output power level makes sure that we obtain a very linear AM-AM with maximum (or very close to maximum) efficiency.
We had defined the DF in the power domain but we operated on the digital baseband. In fact looking at the scheme block of the simulation environment, we noticed that the signals handled inside MATLAB are all complex baseband signals, thus we can take into account both phase and magnitude when designing an optimization algorithm to identify the linearizer. Starting from the previous considerations the pure Error Vector Magnitude (EVM) represents an appro-

priate cost function for our identification process and can be calculated as:

$$EVM = \frac{|S_r - S_i|}{|S_r|} \tag{6.1}$$

where S_r is i-th symbol of the target vector ans S_i is the current output vector. This formula is expressing the ratio between the error vector and the elements of the target vector that must be defined and fed into the algorithm. Our DPA was designed to operate with a maximum power of 100 W so we had to define a vector of linearly-spaced power values:

$$Pout\_target = 0 : \frac{100}{N\_supports - 1} : 100 \tag{6.2}$$

where $N\_supports$ is the number of power points contained in the LUT to identify. Let us call ΦO_{comp} the absolute output phase at the back-off point, we can generate a vector of complex reference symbols for the output signal:

$$Vout\_target = \sqrt{Pout\_target} \cdot e^{i\Phi_{O\_comp}} \tag{6.3}$$

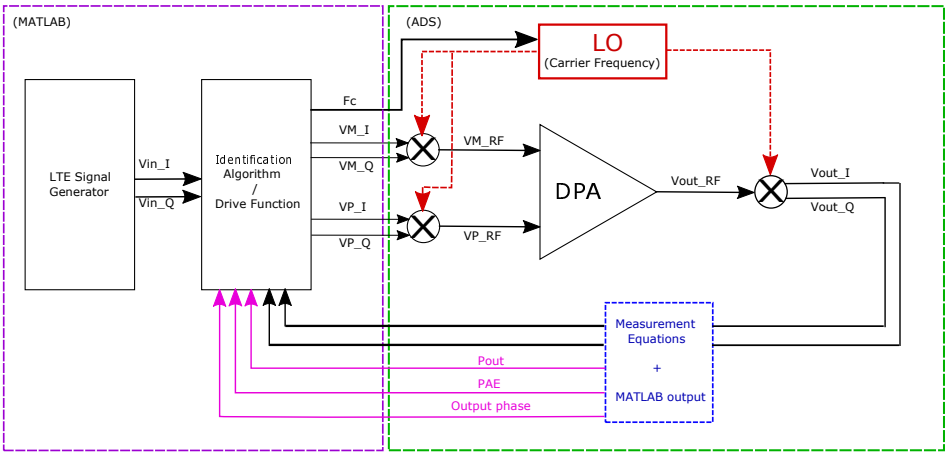

Figure 6.3: MATLAB ADS co-simulation environment for *in-situ* identification.

using them to compute the cost function at each step of the algorithm ($Vout_{target}$ is S_r). With the defined cost function we could find the correctly aligned output

complex vector, with the target power and efficiency. It should be emphasized that our minimization problem involved a single object to optimize but the final result was a bi-dimensional optimization of the linearity and efficiency. By choosing the right phase reference we optimized the efficiency.
The defined cost function was minimized making use of classic gradient based optimization algorithms such as the ones to train DPD models. A deep description of identification techniques for non-linear systems can be found in [16], in our case, gradient-based algorithms presented very slow convergence so they would not be appropriated for real applications.
Particle Swarm Optimization (PSO) [46] represents a very attractive algorithm for this sort of application because it is simple to implement, can achieve very fast convergence and allows control over the power range swept at the input of the dual-input DPA.
This algorithm was inspired by the animal world, it aims at modeling the behavior of swarms of birds or school of fishes when searching for sources of food. The idea behind PSO is very simple, a single particle is described by a set of parameters:

- Position (X): *described by the decision variables*
- Velocity (V): *velocity of the particle during its motion, defines also the direction of search*
- Local Best (L): *local best met by the particle, updated each time when the local best is improved during the search*
- Global Best (G): *global best found by the whole swarm, this information is shared between all the particles*

Each particle is moving in the 2-dimensional space updating its speed according to the social interactions with the rest of the swarm. The formulas to update the velocity and position are expressed as in 6.4 and 6.5.

$$V^{n,d} = \chi V^{n,d} + c_1 \cdot rand() \cdot (L^{n,d} - X^{n,d}) + c_2 \cdot rand() \cdot (G^d - X^{n,d}) \quad (6.4)$$

$$X^{n,d} = X^{n,d} + V^{n,d} \tag{6.5}$$

The coefficients appearing in the equation of the velocity are controlling the "memory" of the particles to lead them towards the best solution that has been found so far. Coefficient c_1 is controlling the tendency of the particle to search in the direction of its own best found solution, while c_2 manages the social interaction of the particle with the rest of the swarm members to let its position drift towards the global best found by the whole swarm.
The flow of the optimization algorithm 1 is very simple to implement and can be adapted to a large range of problems by performing a proper sensitivity study of the parameters.
To make sure that the particle swarm optimizer does not stop if no convergence is met, a maximum number of iterations can be established. This also sets the speed of the algorithm in the worst case, when no optimum is found or when the cost function does not reach the expected precision.

Algorithm 1 PSO

1: Initialize a population of particles with random position values and velocity from *D* dimensions in the search space
2: Return the global minimum G and the values of the input variables generating it
3: while Termination condition not reached do
4: for Each particle i do
5: Adapt velocity of the particle using Equation 6.4
6: Update the position of the particle using Equation 6.5
7: Evaluate the fitness $f(\overrightarrow{X}_i)$
8: if $f(\overrightarrow{X}_i) < f(\overrightarrow{P}_i)$ then
9: $\overrightarrow{P}_i \leftarrow \overrightarrow{X}_i$
10: end if
11: if $f(\overrightarrow{X}_i) < f(\overrightarrow{P}_g)$ then
12: $\overrightarrow{P}_g \leftarrow \overrightarrow{X}_i$
13: end if
14: end for
15: end while

6.3 Simulation Setup and Speed Quantification

We have tested the performance with PSO using the co-simulation scheme represented in Figure 6.3. The signal generation, baseband signal processing and analysis of results were performed in MATLAB while the whole physical part of the simulation was left to ADS configured for circuit envelope simulation.
The simulation environment is controlled by a MATLAB script which generates the MAIN DF with a number of support points defined by the user. In our case we used only 50 points, which is four times less than the ones used during the analysis with the data set of the DPA. After choosing the compression point, the algorithm starts to sweep the input power of the MAIN PA only. Once the compression point is reached, the output value of the phase is saved and is used to generate the output target as defined in the previous section. At this point the PSO starts to look for the correct PEAK input power and $\delta\Phi$ for each target symbol (namely the AM-AM and AM-PM for the PEAK DF) trying to minimize the EVM under the threshold defined by the user.
Since we want to characterize only the static correction of the DPA, we generate in MATLAB constant power points with a duration that avoids the excitation of dynamic effects and so memory. We have experimentally seen that memory effects for our DPA are visible just up to 300 ns. For this reason we have set the duration of the power pulses to 1 µs.
The speed of convergence for PSO depends on the number of particles involved. We used 20 particles as it was shown to be a good compromise between the simulation time and the precision of the results (we have chosen a tolerance of 10^{-4} for the EVM). To limit the maximum duration of the simulation we have set the number of maximum iterations to 50.
Doing so, the whole simulation takes about:

$$Tsim_{max} = N_{particles} \cdot N_{targets} \cdot N_{max-iterations} \cdot T_{cycle}. \qquad (6.6)$$

where $Tsim_{max}$ is the maximum duration of a simulation, $N_{particles}$ is the number or particles used, $N_{targets}$ is the length of the targe vector, $N_{max-iterations}$ is the number of maximum iterations of the PSO and T_{cycle} is the duration of a single cycle in ADS (which is about 2 s in our case).
A full simulation with 50 target points takes about 27 hours in the worst case, meaning that each of the 50 triplets are not met within the maximum number

of iterations. The solution, when the reference phase is defined correctly, was generally found after less than 10 iterations, so the simulation could be completed in 2 to 5 hours.
We expect that by performing the measurement *in-situ* using an appropriate FPGA system, the time to measure each point could be reduced to the limits of the memory effects, resulting in a complete identification of the drive function in 15 ms. This process can be applied around several carrier frequencies, creating a raster of DFs to obtain a wideband model.
This work flow generates a LUT, which is used to evaluate the results by running a simulation with an LTE signal.

6.4 Results with PSO-based Identification

We have simulated the identification of the drive function by setting the carrier frequency at 900 MHz, setting Pm_target at 0.9 V and the PBO at about 16 W, allowing a very little gap (0.1 V). The identified drive function is shown in Figure 6.4.

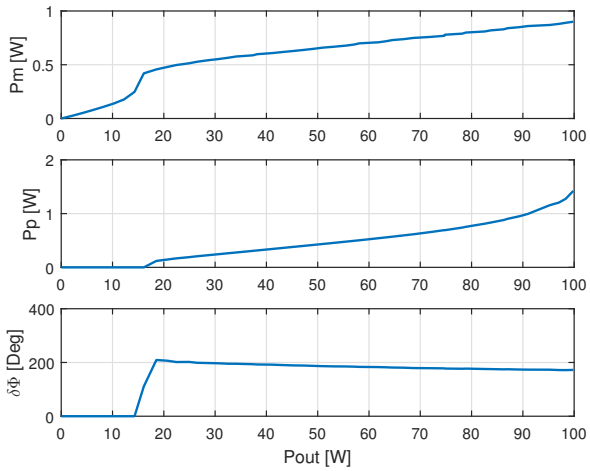

Figure 6.4: Drive function at 900 MHz identified by PSO.

Using the identified DF to predistort the DPA driven by a 5 MHz signal with a 10 dB PAPR (no CFR was applied), we obtained a very linear AM-AM charac-

teristic (Figure 6.5), where we still noticed dispersion around the static line due to memory.

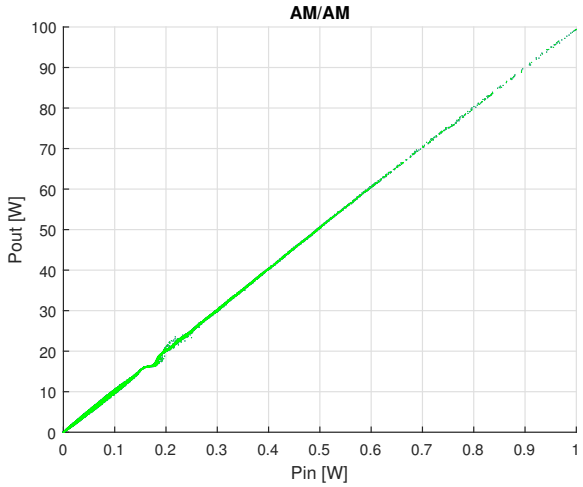

Figure 6.5: AM-AM characteristic of DPA + DF + SPC obtained by PSO.

As we can observe, the characteristic is very close to linear but there is a slight imperfection around the defined compression point. This is because the reference output phase cannot be supposed linear at all the frequencies as the impedance of the combiner changes at every frequency. In general, the combiner shows an ideal behavior around the middle of his bandwidth and drifts away from ideal while approaching the upper and lower frequency bounds.
The algorithm that we have introduced, sweeps the input power of the MAIN PA until the wanted compression point and saves the corresponding output phase. In order to find an acceptable target vector, it is important to find the value of the output phase at maximum power, and make the right assumption about the behavior of the expected output phase.
In our case we have performed a power and phase sweep at the input of the PEAK PA when the MAIN had the power value allowed by the DF at its input. The result can be seen in Figure 6.6. In our case the output phase vector varied from 112^o (at PBO) to 123^o (at 100 W). This already gives good results, but since the phase varies in a non linear fashion between PBO and steady state output there is still a source of error for the PSO in this region. A better estimation of the reference phase would allow to obtain even better results and this is left for future analysis.

If we compare the MAIN DF used during this test with the one previously identified from the data set, we see that it allows a higher maximum input power on the MAIN PA. The effect of this choice has pushed the MAIN more into compression, and has stimulated more memory effects. This is visible in Figure 6.7 where more dispersion is noticed in PBO in relation to Figure 5.39.
The oscillations presented by the AM-PM are caused by the tolerance of the identification algorithm. It appears clear that using the pure EVM allows little error at low power levels and gets bigger while approaching 100 W in the output power. Improving the cost function could attenuate or even eliminate this oscillating behavior by improving the linearity of the system.

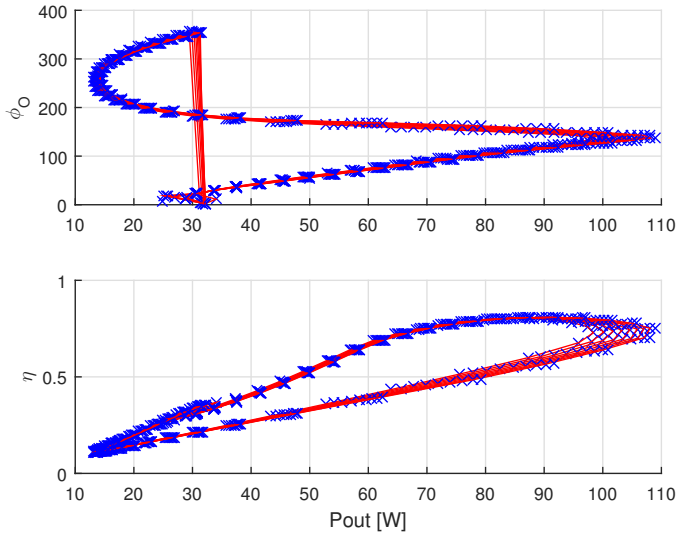

Figure 6.6: Power and phase sweep on PEAK with MAIN at maximum allowed level.

Despite the characteristics we have just mentioned, the results obtained applying such DF were still good. The average efficiency obtained with a 5 MHz bandwidth signal is still very high (about 51%) but the ACPR is deteriorated of about 6 dB (Figure 6.8). Such decrease is justified by the discontinuities of the PEAK DF: the AM-AM must still be smoothed and the AM-PM must be made continuous and monotonic in PBO. By applying this corrections we can improve the ACPR to the same level previously demonstrated.

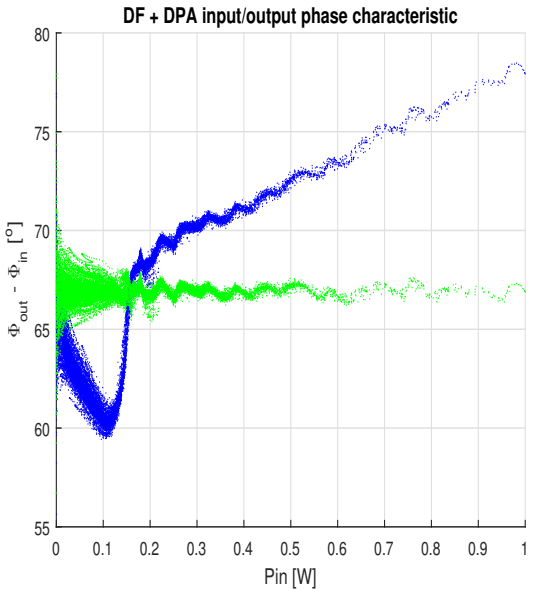

Figure 6.7: AM-PM before (blue) and after (green) SPC.

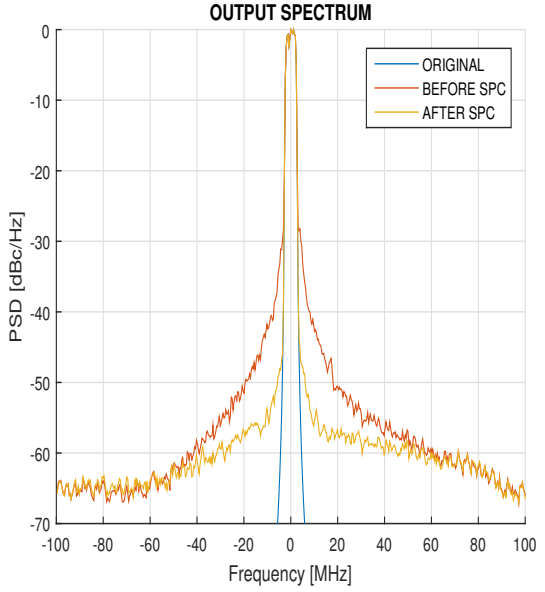

Figure 6.8: Output spectra before and after SPC with PSO.

Chapter 7

Conclusions and future work

This work was focused on the topic of DPD techniques for dual-input DPAs, based on the physics of the device instead of pure mathematical models. Starting from some considerations inspired by the knowledge of the device operation and the analysis of the device behavior, with an appropriate simulation environment, we designed and verified a workflow for the linearization of a dual-input DPA. The results led to an iterative identification approach that could be implemented in the future on an FPGA-based system, to perform an in-situ calibration of the DPD (our DF) automatically and in few seconds.

7.1 Contributions

The primary contributions of this work are listed hereafter:

- Identification of the maximum power ratings based on the physics of the components,
- Definition of a physically inspired identification workflow,
- Analysis of the pre-distorter (DF) characteristics and justification of the requirements in terms of linearization bandwidth, efficiency and spectral regrowth,

- Simplification of the DPD model in relation to the achievable performance,
- Identification of the power dependent phase relationship between MAIN and PEAK inputs,
- Identification of the tradeoffs between the choice of parameters and obtainable performance,
- Identification of the non-linear effects that could be fully compensated in future designs,
- Development of a physically-inspired identification approach for dual-input DPA based on PSO and previous acknowledgements,
- Development of a workflow for a multi-band linearization model to be developed in future research works,
- Validation of the algorithm by means of MATLAB/ADS co-simulations in circuit envelope mode, using dynamic signals and compact transistor model, thus in the presence of memory effects.

7.2 Key results

The linearization of dual-input DPA introduced new degrees of freedom in terms of the re-configuration of parameters such as:

- control of bandwidth expansion, reduction of envelope BW and absolute BW in driver stages,
- achievable PAE,
- achievable linearized output power,
- relation between compression level and memory.

The proposed method for dual input DPA linearization, physically motivated, represents a huge advantage for the utilization in BS technology, in comparison with complex identification processes and complexity of the classic mathematical models. Such complexity is normally shifted to the digital hardware performing the linearization, increasing the number of requested resources and the general complexity of the design.
It has been demonstrated that using a dual-input DPA introduces a complicated multi-dimensional optimization problem. We had here a system described by three input variables (Pm, Pp, $\delta\Phi$) that we wanted to optimize in relation to two output parameters (Pout and η). Since many of those triplets led to the same output power but to a different efficiency, we needed to find a way to reduce the complexity of the problem. Using the knowledge of the component physics we developed a workflow to first identify the DF for the MAIN PA. The knowledge of the DF helps to reduce the dimensionality of the identification problem, because we needed to identify only the DF of the PEAK PA which was only bi-dimensional.
We studied the behavior of the MAIN DF and we have defined it as a function of a set of parameters to control the implied bandwidth expansion. We also showed that the MAIN PA requires much more linearization bandwidth than the PEAK PA. Despite the fact that the PEAK PA presented a naturally strong discontinuity in its AM-AM characteristic, its correction using a blending function did not degrade the operation of the dual-input DPA. Through our analysis we observed that the MAIN PA bandwidth expansion could be reduced to the same level of the PEAK PA. Unfortunately from the analysis of the intrinsic characteristic of the MAIN PA (operating in class AB) we showed that the AM-PM correction required was too important because it demanded more bandwidth on the DAC for this amplifier stage.
We presented the achievable performance with the usa of the DF, removing the necessity of complex DPD functions in front of the static DF. Once the static part was corrected, the dynamic effects due to memory can be easily characterized and reduced by means of simple algorithms.
Based on our analysis, we developed an iterative identification technique, making use of the knowledge of the device physics and swarm intelligence to identify the static DF. Compared to the current techniques, our approach showed very good potential in terms of achieved performance, operational safety and simplicity.

7.3 Suggestions/Future Research

This work has shown both advantages and drawbacks of using dual-input DPAs in BS and also opened new questions left to further future investigations. The following list contains suggestions for the follow up work:

- More detailed analysis of memory effects and simplification of the model.
- The biasing of the MAIN PA sets the bandwidth requirements of the DF because of the typical AM-PM characteristic. An analysis of the possible bias points of the MAIN PA should be performed to find a linearization trade-off allowing a smoother PM correction and reduce such requirement.
- We have shown that the DF is dispersive in frequency, so particular attention should be dedicated to the identification of a frequency dependent model of the DF.
- Opening the input branches of the DPA allows new degrees of freedom in the reconfiguration of the device. The achievable average PAE depends on the statistic of the input signal, thus the frequency dependent model should also have a stochastic nature. Therefore the DF should be able to be dynamically reconfigured to get the best efficiency depending on the current signal properties.

List of Figures

Bibliography

[1] J. Wood, *Behavioral Modeling and Linearization of RF Power Amplifiers:* ser. Artech House Microwave Library. Artech House, 2014.

[2] S. Cripps, *RF Power Amplifiers for Wireless Communications*, ser. Artech House microwave library. Artech House, 2006.

[3] S. Cripps, *Advanced Techniques in RF Power Amplifier Design*, ser. Artech House microwave library. Artech House, 2002.

[4] J. y. Lee, J. y. Kim, J. h. Kim, K. j. Cho and S. P. Stapleton, 'A high power asymmetric doherty amplifier with improved linear dynamic range', in *Microwave Symposium Digest, 2006. IEEE MTT-S International*, Jun. 2006, pp. 1348–1351.

[5] H. Jang, P. Roblin and C. Quindroit, 'Adjustable load-modulation asymmetric doherty amplifier design using nonlinear embedding', in *Microwave Symposium (IMS), 2014 IEEE MTT-S International*, Jun. 2014, pp. 1–4.

[6] J. Son, I. Kim, J. Moon, J. Lee and B. Kim, 'A highly efficient asymmetric doherty power amplifier with a new output combining circuit', in *Microwaves, Communications, Antennas and Electronics Systems (COMCAS), 2011 IEEE International Conference on*, Nov. 2011, pp. 1–4.

[7] K. Bathich, A. Z. Markos and G. Boeck, 'A wideband gan doherty amplifier with 35 bandwidth', in *Microwave Conference (EuMC), 2010 European*, Sep. 2010, pp. 1006–1009.

[8] C. Ma, W. Pan, S. Shao, C. Qing and Y. Tang, 'A wideband doherty power amplifier with 100 mhz instantaneous bandwidth for lte-advanced applications', *IEEE Microwave and Wireless Components Letters*, vol. 23, no. 11, pp. 614–616, Nov. 2013.

[9] N. Tuffy and L. Pattison, 'A linearized, high efficiency 2.7 ghz wideband doherty power amplifier with class-j based performance enhancement', in *Microwave Conference (EuMC), 2015 European*, Sep. 2015, pp. 215–218.

[10] L. Piazzon, R. Giofre, P. Colantonio and F. Giannini, 'A wideband doherty architecture with 36bandwidth', *IEEE Microwave and Wireless Components Letters*, vol. 23, no. 11, pp. 626–628, Nov. 2013.

[11] D. Y. T. Wu, J. Annes, M. Bokatius, P. Hart, E. Krvavac and G. Tucker, 'A 350 w, 790 to 960 mhz wideband ldmos doherty amplifier using a modified combining scheme', in *Microwave Symposium (IMS), 2014 IEEE MTT-S International*, Jun. 2014, pp. 1–4.

[12] S. Gao, P. Butterworth, A. Sambell, C. Sanabria, H. Xu, S. Heikman, U. Mishra and R. A. York, 'Microwave class-f and inverse class-f power amplifiers designs using gan technology and gaas phemt', in *European Microwave Integrated Circuits Conference, 2006. The 1st*, Sep. 2006, pp. 493–496.

[13] D. Gustafsson, C. M. Andersson and C. Fager, 'A modified doherty power amplifier with extended bandwidth and reconfigurable efficiency', *IEEE Transactions on Microwave Theory and Techniques*, vol. 61, no. 1, pp. 533–542, Jan. 2013.

[14] H. S. Black, 'Inventing the negative feedback amplifier.', *IEEE Spectrum*, vol. 14, no. 12, pp. 55–60, Dec. 1977.

[15] H. S. Black, 'Stabilized feedback amplifiers', *The Bell System Technical Journal*, vol. 13, no. 1, pp. 1–18, Jan. 1934.

[16] O. Nelles, *Nonlinear System Identification: From Classical Approaches to Neural Networks and Fuzzy Models*, ser. Engineering online library. Springer, 2001.

[17] H. Paaso and A. Mammela, 'Comparison of direct learning and indirect learning predistortion architectures', in *Wireless Communication Systems. 2008. ISWCS '08. IEEE International Symposium on*, Oct. 2008, pp. 309–313.

[18] V. Volterra, *Theory of Functionals and of Integral and Integro-differential Equations*, ser. Dover Books on Mathematics Series. Dover Publications, 2005.

[19] M. Schetzen, *The Volterra and Wiener Theories of Nonlinear Systems*. Krieger Pub., 2006.

[20] V. Mathews and G. Sicuranza, *Polynomial signal processing*, ser. Wiley series in telecommunications and signal processing. Wiley, 2000.

[21] L. Ding, G. T. Zhou, D. R. Morgan, Z. Ma, J. S. Kenney, J. Kim and C. R. Giardina, 'A robust digital baseband predistorter constructed using memory polynomials', *IEEE Transactions on Communications*, vol. 52, no. 1, pp. 159–165, Jan. 2004.

[22] P. Gilabert, G. Montoro and E. Bertran, 'On the wiener and hammerstein models for power amplifier predistortion', in *Microwave Conference Proceedings, 2005. APMC 2005. Asia-Pacific Conference Proceedings*, vol. 2, Dec. 2005, 4 pp.–.

[23] D. R. Morgan, Z. Ma, J. Kim, M. G. Zierdt and J. Pastalan, 'A generalized memory polynomial model for digital predistortion of rf power amplifiers', *IEEE Transactions on Signal Processing*, vol. 54, no. 10, pp. 3852–3860, Oct. 2006.

[24] J. Zhang, Q. Wang and Q. Hao, 'Lut predistortion based on measured non-linear characteristics of power amplifier', in *Microwave and Millimeter Wave Technology, 2007. ICMMT '07. International Conference on*, Apr. 2007, pp. 1–4.

[25] K. J. Muhonen, M. Kavehrad and R. Krishnamoorthy, 'Look-up table techniques for adaptive digital predistortion: A development and comparison', *IEEE Transactions on Vehicular Technology*, vol. 49, no. 5, pp. 1995–2002, Sep. 2000.

[26] F. M. Barradas, T. R. Cunha, P. M. Lavrador and J. C. Pedro, 'Polynomials and luts in pa behavioral modeling: A fair theoretical comparison', *IEEE Transactions on Microwave Theory and Techniques*, vol. 62, no. 12, pp. 3274–3285, Dec. 2014.

[27] I. Kim, J. Moon, S. Jee and B. Kim, 'Optimized design of a highly efficient three-stage doherty pa using gate adaptation', *IEEE Transactions on Microwave Theory and Techniques*, vol. 58, no. 10, pp. 2562–2574, Oct. 2010.

[28] W. C. E. Neo, J. Qureshi, M. J. Pelk, J. R. Gajadharsing and L. C. N. de Vreede, 'A mixed-signal approach towards linear and efficient n-way doherty amplifiers', *IEEE Transactions on Microwave Theory and Techniques*, vol. 55, no. 5, pp. 866–879, May 2007.

[29] H. Cao, H. M. Nemati, A. S. Tehrani, T. Eriksson and C. Fager, 'Digital predistortion for high efficiency power amplifier architectures using a dual-input modeling approach', *IEEE Transactions on Microwave Theory and Techniques*, vol. 60, no. 2, pp. 361–369, Feb. 2012.

[30] H. Cao, J. Qureshi, T. Eriksson, C. Fager and L. de Vreede, 'Digital predistortion for dual-input doherty amplifiers', in *Power Amplifiers for Wireless and Radio Applications (PAWR), 2012 IEEE Topical Conference on*, Jan. 2012, pp. 45–48.

[31] W. H. W. Yu and H. U. Cheng, 'An efficient geometric curve fitting technique', in *TENCON '89. Fourth IEEE Region 10 International Conference*, Nov. 1989, pp. 960–963.

[32] G. Farin, J. Hoschek and M. Kim, *Handbook of Computer Aided Geometric Design*. Elsevier Science, 2002.

[33] B. Belkhatir, A. Kouibia, M. Pasadas, D. Sbibih and A. Zidna, 'Geometric continuity c1 g2 of blending curves', *Int. J. Contemp. Math. Sciences*, vol. 3, no. 30, pp. 1451–1460, Jul. 2008.

[34] J. C. Cahuana, P. N. Landin, D. Gustafsson, C. Fager and T. Eriksson, 'Linearization of dual-input doherty power amplifiers', in *Integrated Nonlinear Microwave and Millimetre-wave Circuits (INMMiC), 2014 International Workshop on*, Apr. 2014, pp. 1–3.

[35] S. Afsardoost, T. Eriksson and C. Fager, 'Digital predistortion using a vector-switched model', *IEEE Transactions on Microwave Theory and Techniques*, vol. 60, no. 4, pp. 1166–1174, Apr. 2012.

[36] N. B. D. Carvalho and J. C. Pedro, 'Large- and small-signal imd behavior of microwave power amplifiers', *IEEE Transactions on Microwave Theory and Techniques*, vol. 47, no. 12, pp. 2364–2374, Dec. 1999.

[37] K. Gharaibeh, *Nonlinear Distortion in Wireless Systems: Modeling and Simulation with MATLAB*, ser. Wiley - IEEE. Wiley, 2011.

[38] P. H. Aaen and J. A. Plá, *Modeling and characterization of RF and microwave power FETs*. Cambridge : Cambridge University Press, 2007.

[39] F. Ghannouchi, O. Hammi and M. Helaoui, *Behavioral Modeling and Predistortion of Wideband Wireless Transmitters*. Wiley, 2015.

[40] H. Ku, M. D. McKinley and J. S. Kenney, 'Quantifying memory effects in rf power amplifiers', *IEEE Transactions on Microwave Theory and Techniques*, vol. 50, no. 12, pp. 2843–2849, Dec. 2002.

[41] P. Roblin, D. E. Root, J. Verspecht, Y. Ko and J. P. Teyssier, 'New trends for the nonlinear measurement and modeling of high-power rf transistors and amplifiers with memory effects', *IEEE Transactions on Microwave Theory and Techniques*, vol. 60, no. 6, pp. 1964–1978, Jun. 2012.

[42] S. Boumaiza and F. M. Ghannouchi, 'Thermal memory effects modeling and compensation in rf power amplifiers and predistortion linearizers', *IEEE Transactions on Microwave Theory and Techniques*, vol. 51, no. 12, pp. 2427–2433, Dec. 2003.

[43] P. Draxler, I. Langmore, T. P. Hung and P. M. Asbeck, 'Time domain characterization of power amplifiers with memory effects', in *Microwave Symposium Digest, 2003 IEEE MTT-S International*, vol. 2, Jun. 2003, 803–806 vol.2.

[44] J. Diels, W. Rudolph, P. Liao and P. Kelley, *Ultrashort Laser Pulse Phenomena*, ser. Optics and photonics. Elsevier Science, 2006.

[45] P. M. Cabral, J. C. Pedro and N. B. Carvalho, 'Dynamic am-am and am-pm behavior in microwave pa circuits', in *2005 Asia-Pacific Microwave Conference Proceedings*, vol. 4, Dec. 2005, 4 pp.–.

[46] J. Kennedy and R. Eberhart, 'Particle swarm optimization', in *Neural Networks, 1995. Proceedings., IEEE International Conference on*, vol. 4, Nov. 1995, 1942–1948 vol.4.

Author's Publications

[GD1] G. Donati, C. Musolff, G. Gottardo, D. Popp and G. Fischer, 'Physically inspired digital predistortion for doherty power amplifiers and automatic in-situ identification', in *5th International Conference on Telecommunications and Remote Sensing*, Milan, Italy, Oct. 2016.

[GD2] G. Gottardo, G. Donati, C. Musolff, F. G. and T. Felgentreff, 'Hybrid recursive active filters for duplexing in rf transmitter front-ends', *Radio Science*, vol. 8, pp. 1363–1376, 2016.

[GD3] G. Gottardo, G. Donati, C. Musolff, G. Fischer and T. Felgentreff, 'Hybrid recursive active filters for high selectivity in rf transmitter front-ends', in *2nd International Scientific Symposium "Sense. Enable. SPITSE.*
, St. Petersburg, Russia, Jun. 2015, pp. 15 –18.

[GD4] G. Gottardo, G. Donati, C. Musolff, G. Fischer and T. Felgentreff, 'Hybrid recursive active filters for duplexing in rf transmitter front-ends', in *IEEE 15th Mediterranean Microwave Symposium (MMS) 2015*, Lecce, Italy, Nov. 2015, pp. 1 –4.

[GD5] G. Gottardo, G. Donati, C. Musolff, R. Weigel and G. Fischer, 'Novel hybrid recursive active filters in rf transmitter front-end', in *German Microwave Conference (GeMiC)*, Aachen, Germany, Mar. 2014, pp. 1 –4.

Modern telecommunication systems are designed to meet very high requirements, in order to support new top quality services and provide maximum power, linearity and efficiency over an ever-increasing bandwidth. The key component of the transmit chain is the power amplifier (PA), which is a non-linear component that needs to meet all the requirements introduced above. Digital pre-distortion (DPD) is the solution commonly used to achieve linearity and efficiency at the same time. Signal standards introduced in LTE systems require PAs capable of operating with wideband input signals and high Peak-to-Average-Power-Ratio. The dual-input Doherty Power Amplifier (DPA) given its/thanks to its wideband output combiner has been developed to meet such requirements. Opening the input branches of the DPA introduces new degrees of freedom in terms of linearization and reconfiguration of the PA by proper digital steering. The DPD approach presented in this book has been developed during the cognitive mobile radio (COMORA) project, supported by the German Federal Ministry of Education and Research (BMBF) and Nokia Networks. In this thesis I have investigated ways to control the trade-off between linearity, efficiency and linearization bandwidth, by separately driving the DPA inputs. Based on the physics of the device I have proposed/developed a novel linearization technique that can be applied to dual-input DPA architectures in order to: i. reduce the costs of the hardware running the DPD, ii. linearize the device and reach very high efficiency, iii. show a way to reconfigure the device according to carrier frequency and the signal condition. A method for in-situ identification of the dual-input DPD model (Digital Steering Function) is also presented and validated using system level simulations.

ISBN 978-3-96147-080-8

FAU UNIVERSITY PRESS 2017